AEDC-TR-86-34

A Post-Stall Compression System Modeling Technique

M. W. Davis, Jr.
Sverdrup Technology, Inc.

February 1987

Final Report for Period October 1, 1984 – September 30, 1986

Approved for public release; distribution unlimited.

ARNOLD ENGINEERING DEVELOPMENT CENTER
ARNOLD AIR FORCE STATION, TENNESSEE
AIR FORCE SYSTEMS COMMAND
UNITED STATES AIR FORCE

NOTICES

When U. S. Government drawings, specifications, or other data are used for any purpose other than a definitely related Government procurement operation, the Government thereby incurs no responsibility nor any obligation whatsoever, and the fact that the Government may have formulated, furnished, or in any way supplied the said drawings, specifications, or other data, is not to be regarded by implication or otherwise, or in any manner licensing the holder or any other person or corporation, or conveying any rights or permission to manufacture, use, or sell any patented invention that may in any way be related thereto.

Qualified users may obtain copies of this report from the Defense Technical Information Center.

References to named commercial products in this report are not to be considered in any sense as an endorsement of the product by the United States Air Force or the Government.

This report has been reviewed by the Office of Public Affairs (PA) and is releasable to the National Technical Information Service (NTIS). At NTIS, it will be available to the general public, including foreign nations.

APPROVAL STATEMENT

This report has been reviewed and approved.

Marjorie S. Collier

MARJORIE S. COLLIER
Directorate of Technology
Deputy For Operations

Approved for publication:

FOR THE COMMANDER

Marion L. Laster

MARION L. LASTER
Technical Director
Directorate of Technology

UNCLASSIFIED

SECURITY CLASSIFICATION OF THIS PAGE

REPORT DOCUMENTATION PAGE

1a. REPORT SECURITY CLASSIFICATION Unclassified	1b. RESTRICTIVE MARKINGS
2a. SECURITY CLASSIFICATION AUTHORITY	3. DISTRIBUTION/AVAILABILITY OF REPORT Approved for public release; distribution unlimited.
2b. DECLASSIFICATION/DOWNGRADING SCHEDULE	
4. PERFORMING ORGANIZATION REPORT NUMBER(S) AEDC-TR-86-34	5. MONITORING ORGANIZATION REPORT NUMBER(S)
6a. NAME OF PERFORMING ORGANIZATION Arnold Engineering Development Center 6b. OFFICE SYMBOL (If applicable) DOT	7a. NAME OF MONITORING ORGANIZATION
6c. ADDRESS (City, State and ZIP Code) Air Force Systems Command Arnold Air Force Station, TN 37389-5000	7b. ADDRESS (City, State and ZIP Code)
8a. NAME OF FUNDING/SPONSORING ORGANIZATION Arnold Engineering Development Center 8b. OFFICE SYMBOL (If applicable) DO	9. PROCUREMENT INSTRUMENT IDENTIFICATION NUMBER
8c. ADDRESS (City, State and ZIP Code) Air Force Systems Command Arnold Air Force Station, TN 37389-5000	10. SOURCE OF FUNDING NOS. PROGRAM ELEMENT NO: 65807F PROJECT NO. TASK NO. WORK UNIT NO
11. TITLE (Include Security Classification) A Post-Stall Compression System Modeling	
12. PERSONAL AUTHOR(S) Davis, M.W., Jr., Sverdrup Technology, Inc., AEDC Group	
13a. TYPE OF REPORT Final 13b. TIME COVERED FROM 10/1/84 TO 9/30/86	14. DATE OF REPORT (Yr., Mo., Day) February 1987 15. PAGE COUNT 99
16. SUPPLEMENTARY NOTATION Available in Defense Technical Information Center (DTIC).	

17. COSATI CODES			18. SUBJECT TERMS (Continue on reverse if necessary and identify by block number)
FIELD	GROUP	SUB. GR.	
21	05		gas turbine engines; rotating stall; compression systems; surge; component performance; mathematical modeling

19. ABSTRACT (Continue on reverse if necessary and identify by block number)

This report presents a one-dimenstional, stage-by-stage compression system modeling technique capable of exhibiting post-stall behavior such as surge and rotating stall. Included is a brief overview of previous efforts by others, their major contributions and how the present effort enhances and extends these efforts. The modeling technique, governing equations, numerical simulation, and stability criteria are all discussed. The model is validated by comparing it with a multitude of experimental test results from low-speed and high-speed compressor rigs and engine test results. The model provides an analysis tool for analyzing compression system and individual stage behavior during surge and rotating stall. Because the modeling technique is based upon stage characteristics, stage modifications can be analyzed for their affect on recoverability.

20. DISTRIBUTION/AVAILABILITY OF ABSTRACT UNCLASSIFIED/UNLIMITED ☐ SAME AS RPT ☒ DTIC USERS ☐	21 ABSTRACT SECURITY CLASSIFICATION Unclassified	
22a. NAME OF RESPONSIBLE INDIVIDUAL Mr. William O. Cole	22b. TELEPHONE NUMBER (Include Area Code) (615) 454-7813	22c. OFFICE SYMBOL DOS

DD FORM 1473, 83 APR EDITION OF 1 JAN 73 IS OBSOLETE

UNCLASSIFIED

SECURITY CLASSIFICATION OF THIS PAGE

11. TITLE. Concluded.
Technique

PREFACE

The work reported herein was conducted by the Arnold Engineering Development Center (AEDC), Air Force Systems Command (AFSC). The results were obtained by Sverdrup Technology, Inc., AEDC Group, operating contractor for the propulsion test facilities of the AEDC, AFSC, Arnold Air Force Station, Tennessee during the period of October 1, 1982 through August 1, 1986 under Project Number D185EW. The Air Force Project Manager was Ms. Marjorie S. Collier and the manuscript was submitted for publication on September 5, 1986.

CONTENTS

ILLUSTRATIONS

Figure Page

Figure | Page

1.0 INTRODUCTION

An important component of the gas turbine engine is its compression system. It is the compression system performance which strongly influences all other component performance. For most gas turbine engines, the compression system consists of one or more aerodynamically coupled axial compressors. These compressors may or may not be connected to the same shaft. An axial compressor consists of stages with a rotating component (rotor) and a stationary component (stator). The rotor is a series of airfoils which, when rotated, imparts kinetic energy to the fluid. The stator diffuses the flow and redirects it for the next row of rotors. Thus, it is the function of the compression system to increase the static pressure and density of the fluid. Without stable aerodynamic operation, the compression system cannot deliver the desired increase in static pressure and density.

During operation of axial-flow, multistage compression systems, instability phenomena known as surge and/or rotating stall have been observed. Surge is a violent planar disturbance in which the flow in the compressor reverses direction and empties the compressor and a portion of the combustor volumes. This flow reversal relieves the compression system, allowing correct pumping action to take place. If, however, the original cause of surge has not been corrected, the compression system will undergo repressurization until it reaches the instability limit, and surge will occur again. Rotating stall, on the other hand, is not as visibly violent as surge, but it is more damaging to engine operation. Rotating stall occurs when a portion of the circumferential annulus is locally stalled by some destabilizing event such as a low-pressure region. Flow separation on a portion of the blades causes the angle of attack to increase on the adjacent blades, thus stalling them. The stalled region progresses from one blade passage to the next, giving the appearance that the stalled region rotates in the direction of rotor rotation. Once rotating stall becomes completely established throughout a multistage compression system, it can set up a stable, stalled condition. In most cases the compression system cannot recover unless the engine is shut down. The "nonrecoverable" type of instability has promoted numerous experimental and analytical investigations over the last decade. Results of several of these experimental investigations can be found in Refs. 1 - 5.

In experimental cases, results are often limited because of specific test hardware and/or economic constraints. Where more information is desired, validated compressor mathematical models can be used to provide performance and stability information not obtained during experimental testing. In addition, these mathematical models also provide tools for studying the effects of external disturbances, helping to determine a cause-and-effect relationship.

Mathematical modeling of axial compression systems has been a continuous effort from the time axial compressors were first used in aircraft applications through present-day high-

performance military turbine engines. The modeling process has been evolutionary, with periods of revolutionary insight providing stimulus for significant advances. Axial compressor instability problems have been the driver for better and more sophisticated models. System surge was the first problem to be addressed in the 40's and 50's. Rotating stall was a known phenomenon in the 50's, but significant compression system modeling was not undertaken until the late 60's and early 70's. Inlet pressure and temperature distortion effects on compressor stability spawned a multitude of parallel compressor modeling studies and techniques. Then, with the "stagnation" problem, first associated with the F100 engine in the 70's, there was and continues to be much emphasis on understanding surge and rotating stall phenomena on an engine system level, as well as a component level. Stagnation, or as it has now become known, "nonrecoverable stall," has been the biggest driver for the understanding of compression system instability. The associated test programs have produced revolutionary insight into the problem and have also produced many mathematical models. Before the current work is described, it may be helpful to review previous works briefly to obtain an understanding of how this effort complements and extends the concepts presented by others.

1.1 PRESTALL COMPRESSION SYSTEM MODELS

The first compression system models that were written for the digital computer used one-dimensional, lumped volume numerical techniques. The time-dependent conservation laws of mass, momentum, and energy were applied separately or in combination to the lumped volumes, thus accounting for the dynamic behavior of the system. The conservation laws were expressed with one-dimensional mathematics allowing for only spatially uniform flow. The stage or group of stages was replaced by an actuator disc followed by a lumped volume equal to the stage, or group of stages. The required pressure and temperature rise across the actuator disc was supplied by a set of stage characteristics. One-dimensional models have been generally used to predict system instability for either undistorted flow or time-variant inflow distortions. These early one-dimensional compression system models did not solve the full non-linear set of conservation Euler equations but were simplified by solving only the mass equation (Ref. 6), combination of the mass and momentum (Ref. 7), or all three conservation equations but without momentum flux (Ref. 8).

Kimzey (Ref. 9) developed a one-dimensional technique which solved the full nonlinear form of all three inviscid conservation equations. His model divided the compressor into a series of elemental control volumes representing a stage (rotor-stator) and solved the governing equations with a fourth-order Runge-Kutta numerical technique. Compressor stage force and shaft work were determined from empirical stage characteristics and applied as distributed functions within the control volume. Three different single-spool compressors were modeled with the one-dimensional formulation. These models were validated against experimental data,

and they generally computed compression system stability within 1 to 2 percent of that observed experimentally. Studies were conducted with these one-dimensional models to determine the effects of time-variant planar pressure oscillations and rapid inlet temperature ramps. The computations generally compared favorably to those results observed experimentally.

Davis, using Kimzey's modeling concepts, reformulated the numerical solution technique and extended the model to dual-spool compression systems (Ref. 10). Model reformulation, which used the MacCormack explicit differencing scheme successfully, reduced most numerical instability problems associated with Kimzey's model. In the dual-spool configuration, this modeling technique used a pseudo-splitter near the exit of the fan to allow transmission of fan duct perturbations which are felt by the fan and ingested by the high-pressure compressor. The model was validated against experimental results for a current-day military axial compression system. The model indicated correct component behavior during surge-inducing external disturbances representing combustor fuel pulses, augmentor rumble, augmentor hardlights, ingested gas products from armament firings, and time-dependent inlet pressure disturbances. In addition to the correct component behavior, the model correctly predicted the stage where the instability began.

Extensions of the one-dimensional modeling techniques have produced a compression system model which can determine the effects of inlet spatial distortion on the stability limit. This type of extension is known as "parallel compressor theory." In its simplest form, the parallel compressor theory divides the distorted compressor into sections, each section treated as an individual compressor working in parallel with the other sections. The theory works with the following assumptions: (1) all parallel compressor sections discharge to the same static pressure; (2) there is no fluid dynamic connection between sections, i.e., crossflows are ignored; and (3) each section uses the undistorted stage characteristics. In its simplest form, the entire compressor is assumed to have reached instability when any one of the sectors reaches the stability limit. In more complicated forms, provisions for approximating crossflows and determining the effect of unsteady aerodynamics on compressor behavior have been incorporated. Examples of several parallel compressor models can be found in Refs. 11 and 12.

The major deficiency of these modeling techniques is that results beyond stall/surge inception are not valid. This is attributable in part to incorrect or nonexistent stage characteristic definition in the post-stall regions.

1.2 POST-STALL COMPRESSION SYSTEM MODELS

Prior to the mid-1970's most compression system modeling had been directed at determining the surge boundary and what external disturbances might influence the limits of that boundary. With the advent of the "stall stagnation" problems occurring in the F100 system, new emphasis was placed on understanding compression system behavior during post-stall events - surge and rotating stall. This emphasis spawned several experimental and analytical investigations which have produced theories and models capable of reproducing post-stall behavior.

In general, there have been two types of analytical modeling of post-stall compression system behavior pursued. One is the study of the overall compression system behavior, usually from a one-dimensional viewpoint. The other type of study deals with rotating stall development and general properties of the fluid within the stall cell. Several investigations have produced models that are capable of reproducing some aspects observed experimentally; these models are briefly summarized in the following sections.

1.2.1 One-Dimensional Lumped Compressor Models

Greitzer developed a one-dimensional time-dependent, nonlinear mathematical model (Ref. 13) of an axial compression system to predict the transient response of that system while undergoing a perturbation from steady operating conditions. His model was designed to investigate the phenomena of compressor surge and/or the compressor's response while rotating stall is present.

The system model consists of a compressor operating in a circular duct connected to an exit plenum which includes a throttling device (Fig. 1). The compressor is represented by an actuator disc, thus providing the pressure rise across the compressor, and a section of constant area pipe to account for the fluid dynamics within the compressor. The throttle is modeled by an actuator disc, across which the pressure drops, which is also attached to a constant area duct.

For the type of oscillations (low frequency) expected to be calculated with this model, the flows in the ducts can be considered to be incompressible. This imposes "slug" flow in which the fluid in any one of the equivalent ducts will have the same axial velocity throughout that duct. Since incompressible flow was assumed, Greitzer described his model with the momentum and continuity equations.

In the momentum equation, the pressure rise across the compressor must be known for the mass flow rate to be calculated. In previous analyses, it was assumed that the pressure

rise-mass flow relationship is the same transiently as it is in rotating stall. The stall cell takes some time to develop, up to 10 rotor revolutions. These times are long enough to introduce significant changes to the compressor mass flow during such processes. Thus, since quasi-steady approximations would not be adequate, a first-order time lag was imposed on the compressor pressure rise.

If the governing equations are nondimensionalized, some interesting parameters are created. One such parameter is the "B Parameter" which is defined as

$$B = \frac{U}{2a}\sqrt{\frac{V_p}{A_c L_c}} \tag{1}$$

This parameter becomes quite significant in describing the type of instability encountered.

Greitzer exercised his model to determine the effect of the B parameter on compressor instability. The compression system model was set with the throttle adjusted such that a uniform flow equilibrium point was no longer possible. With a low value of B (0.45), the compressor went directly to an operating point on the stalled portion of the compressor operating curve (Fig. 2). Operation along this stalled curve has been associated with behavior of a machine in rotating stall. With a slight increase in B to a value of 0.6, the final compressor operating point becomes the same as before but now takes some time to finally reach that point through a series of decaying amplitude oscillations (Fig. 3). At a value of B of 0.70, the compression system exhibits an entirely different behavior. The oscillations grow in amplitude and exhibit a limit cycle behavior (Fig. 4). Beyond a value of B of 0.70, the compression system response is similar in nature, but the shape of the limit cycle changes (Fig. 5). With very large values of B, the compressor post-stall behavior is characterized by: (1) a very long scale in which the plenum is slowly built up or discharged and (2) a much shorter scale in which the flow changes rapidly almost at constant pressure. This latter type of instability, typically seen in high-pressure ratio, high-speed machines, is controlled by the resistance elements of the system. The longer scale is set by the balance between resistance and restoring forces, or in other words, the rate that the plenum can empty through the throttle and the compressor.

These values of the B parameter are associated with the particular compression system that Greitzer modeled and later verified experimentally (Ref. 1). Therefore, the quantitative results cannot be used as exact measures to determine what type of instability any compressor will exhibit but should be looked upon as a qualitative measure through which one could speak about compressor behavior in general.

Gamache (Ref. 5) modified Grietzer's model to investigate the effects of a forced excitation on the recoverability of a compression system during post-stall events. Gamache found that, depending upon the timing and/or the strength of the excitation, this forced excitation could cause the compression system to stagnate upon the termination of the external excitation. In his dissertation he also concluded that the predicted forced or free response behavior is heavily dependent upon the form or shape of the compressor post-stall characteristic.

Wenzel developed a compression system model of the TF34 axial compression system to study "nonrecoverable" stall (Ref. 14). He performed a parametric study to determine which compressor or engine parameters were most important to compression system recovery. His model used quasi-steady compressor and fan maps to generate component performance. Lagging of the compressor characteristic was not performed to simulate dynamic behavior. All volume dynamics were computed using the technique of Seldner, Mihaloew, and Blaka (Ref. 15). This method is a one-dimensional technique using simplified forms of continuity, momentum, and energy. The fuel control was a simple fuel flow/compressor discharge pressure relationship with no dynamics modeled. For all events, mechanical speed and variable geometries were held constant at the initial settings. Neither the turbine nor any downstream component was explicitly modeled. Each speed line characteristic was defined for unstalled flow and for stalled flow, including reverse flow. The unstalled portions were based upon experimental data, whereas the form and shape of the stalled curves were postulated based upon Greitzer's experimental results (Ref. 1). These stalled characteristics were modeled such that they could be adjusted parametrically to determine the effect of shape and level of recoverability. Temperature performance for stalled operation was calculated based upon pressure rise and a postulated efficiency which was also programmed as a variable.

The fan performance characteristics were constructed in a similar manner but with temperature ratio assumed constant. Radial crossflow between the hub and tip was allowed and was proportional to the pressure difference between the radial segments. Flow impedance between hub and tip was also programmed for variability.

The model was exercised to determine the importance of various parameters on compression system recovery. Compressor instability was initiated by a fuel pulse in the combustor which rapidly increased the compressor discharge pressure. The fuel pulse then was ramped back down to a minimum after instability was initiated.

To quantify the effect of a certain parameter on system recoverability, turbine area was used as a stability rating criterion. At the time of instability the nominal turbine area was changed by some delta area which could be positive or negative. This increment was then adjusted until recovery was obtained. Thus, if the turbine area was increased to affect recovery,

the parameter change had a detrimental effect on recovery. (Note: an increase in turbine area relieves downstream resistance and thus relieves compressor backpressure). A set of nominal parameters was chosen as an initial (standard) set. Some parameters which were unknown were set at an arbitrary value.

Wenzel performed a parametric study varying only the shape of the stalled characteristic. For a positive or negative 10 percent change in turbine area, a very small change in the parabolic nature of the positive characteristic is noted. However, the same recovery results in a very large change in the negative stall characteristic. Wenzel concluded that compression system recovery is very sensitive to the shape of the curve in the rotating stall region and not so sensitive to the shape in the negative flow region.

Wenzel performed other parametric studies in which he was able to quantitize the relative importance of some factors governing compression system instability. Some parameters not well known (such as reverse flow characteristics and compressor stall/recovery hysteresis) were relatively unimportant to the recovery process. He noted that compressor discharge volume and inertance (positive flow between fan hub and tip regions) were important and highly sensitive parameters. These sensitive parameters may be difficult to measure experimentally, but they are the heart of any meaningful post-stall modeling effort.

1.2.2 Multi-Dimensional Rotating Stall Models

Takata and Nagano (Ref. 16) developed a model to describe rotating stall in axial-flow compressors. The flow was assumed inviscid and rotational with a compressor/blade row being replaced by a semi-actuator disk (i.e., a cascade of flat plates at some stagger angle with finite length). The model was basically concerned with two-dimensional flow (axial, circumferential) but had the capability to be expanded to a third dimension by adding spanwise variation. The modeling technique can be expressed for a single blade row and converted to multiple blade rows with and without axial spacing.

A model for the analysis of rotating stall in axial compressors was also developed by Sexton and O'Brien (Ref. 17). Much like the Takata/Nagano model, the Sexton model used a semi-actuator disc to represent the compressor rotor. The flow fields upstream of the rotor row were calculated using two-dimensional, incompressible flow equations. The blade row interaction with the flow field was modeled by specifying the dynamic pressure loss coefficient and turning angle. The major difference presented in this modeling technique was the application of an improved dynamic loss response model.

F. K. Moore developed a theory with a corresponding analytical model for the analysis of rotating stall in axial compressors (Ref. 18). In development of his theory, a small disturbance was postulated to exist in the compressor which was steady in a circumferential moving frame. When rotating stall occurred the static pressure rise across each blade row was calculated from a lagged characteristic much like what was done in Grietzer's model.

Through the study of the overall characteristic, Moore concluded that recovery from rotating stall depends first upon the compressor's steady characteristic "tallness" (height of the drop in stall compared to its width) and, secondly, the slope of the unstalled characteristic. He also concluded that the slope of the reverse-flow resistance is not nearly as significant as is the slope of the deep stall line (if that slope is positive). In addition, Moore concluded recovery did not depend on compressor lag (dynamic hysteresis) but was affected by the external lags introduced in the entrance and exit geometries. Sudden changes in exit volume would favor recovery.

In 1983, F. K. Moore and E. M. Greitzer teamed together to produce a two-dimensional theory for post-stall events in multi-stage axial compression systems (Refs. 19 and 20). The theory included a two-dimensional unsteady treatment of the compressor flow field, coupled with dynamic response of the overall system. System dynamics were modeled by a lumped parameter method which gave satisfactory results as long as compressibility did not become a factor. Compressor performance was represented by an axisymmetric characteristic with unsteady blade row response modeled as in Grietzer's previous theory. System hysteresis was provided for within the theory itself.

Some significant conclusions drawn by this investigation can be stated as follows: surge and rotating stall can each exist in a pure form, but rotating stall cannot have evolved without having induced surge-like unsteadiness into the system; the instantaneous rotating stall cell amplitude has a significant effect on the instantaneous compressor characteristic, and other parameters such as length-to-radius ratio can also have a significant effect on system response.

Variations of Grietzer's 1976 modeling techniques have been applied to complete engine models (Refs. 4, 21, and 22). In general, the compression systems were represented by a single actuator disk followed by a lumped volume. At best, a fourteen-stage high-pressure compressor was represented by three actuator disk-lumped volume combinations (Ref. 21). Prestall compressor characteristics were obtained from experimental results while post-stall characteristics were estimated based upon low-speed compressor rig results. The primary value of these models is their continued use in analysis of engine performance before and during post-stall events such as surge and rotating stall. They are used to determine what actions might be effective to affect engine recovery or prevent rotating stall. These engine models

are limited to overall compression system behavior and thus only overall compressor recovery actions can be investigated. Interstage changes and/or recovery actions cannot be evaluated. This can only be accomplished by a stage-by-stage model.

1.3 PURPOSE AND APPROACH OF PRESENT INVESTIGATION

The purpose of this investigation is to provide a compression system model capable of exhibiting observed system behavior during post-stall events (surge and rotating stall). In addition the model should provide information on a stage-by-stage basis for detailed analysis during surge and/or rotating stall.

To provide the type of post-stall compression system model desired, an existing one-dimensional, time-dependent, stage-by-stage compression system model (Ref. 10) was modified to handle post-stall events. The philosophy of the modification was to incorporate the basic concepts presented by Greitzer (Ref. 13) into the existing stage-by-stage modeling techniques. Because of the uncertainty in synthesizing post-stall stage characteristics and the lack of experimental stage data, the model is validated against experimental overall compression system behavior for similar compression systems as well as general behavior from low-speed research compression systems.

This report reviews the previous efforts by others to put the present effort in perspective and to show how it enhances and extends those efforts. The modeling technique is described in detail by describing the governing equations, modifications necessary for post-stall capability, and the numerical solution techniques. The model is validated against experimental results and some observations are made as to the nature of the post-stall events of surge and rotating stall.

2.0 ONE-DIMENSIONAL, TIME-DEPENDENT COMPRESSOR MODELING TECHNIQUE

The one-dimensional, time-dependent compressor modeling technique solves the nonlinear form of the conservation laws. The models constructed from this technique can be used for analysis of planar, transient, and dynamic effects on compressor operation and stability. A review of the governing equations, stage characteristic development, numerical techniques, and method of solution is presented in this section.

2.1 GOVERNING EQUATIONS

Illustrated in Fig. 6a is a representative single-spool compressor and ducting system which has been modeled. Included in this system is a portion of the compressor inlet and the combustor volume. The compressor and ducting system is modeled by an overall control volume shown in Fig. 6b. Acting on this fluid control volume is an axial-force distribution, F, due to the effects of the compressor blading and wall of the system. In addition, the rate of heat added to the fluid and shaft work done on the fluid are represented by distributions, Q and SW, respectively. Mass transfer rate across boundaries other than the inlet or exit (such as the case of interstage bleed) is represented by the distribution, W_B. The time-dependent inlet boundary condition is the specification of total pressure and temperature. The exit boundary condition is either the specification of static pressure or unity Mach number(choked flow).

The overall control volume of Fig. 6b is broken up into a set of elemental control volumes illustrated in Fig. 6c. In the compressor section, an elemental control volume consists of a rotor followed by a stator and associated volume representing a complete stage. The entrance and exit ducting sections of the overall control volume are divided into elemental control volumes to assure a frequency response as good as that in the compressor section (i.e., duct control volume lengths no longer than the longest compressor elemental control volume). The governing equations are derived by the application of mass, momentum, and energy conservation principles to the elemental control volume in Fig. 6c.

Applying the continuity principle to the elemental control volume yields

Continuity

$$W + \frac{\partial W}{\partial x}\,dx + W_B\,dx + \frac{\partial(\rho A dx)}{\partial t} = W \quad , \qquad (2)$$

mass leaving control volume per unit time	time rate of increase of mass within the control volume	mass entering control volume per unit time

which may be reduced to

$$\frac{\partial(\rho A)}{\partial t} = -\frac{\partial W}{\partial x} - W_B \, , \qquad (3)$$

where W_B is the interstage bleed flow per distributed length.

Applying the conservation of momentum gives

Momentum

$$Fdx + P_S A - \left[P_S A + \frac{\partial(P_S A)}{\partial x} dx\right] + P_S \left[A + \frac{\partial A}{\partial x} Dx - A\right]$$

axial forces acting upon the control volume

$$= \left[Wu + \frac{\partial(Wu)}{\partial x} dx\right] - Wu + \frac{\partial}{\partial t}[\rho u A dx] \quad . \qquad (4)$$

momentum leaving control volume per unit time

momentum entering control volume per unit time

time rate of increase of momentum within the control volume

total time rate of change of momentum

Equation (4) may be reduced to

$$\frac{\partial W}{\partial t} = -\frac{\partial(IMP)}{\partial x} + F \qquad (5)$$

where

$$IMP = Wu + P_S A \, , \qquad (6)$$

a momentum impulse term, and

$$F = F_B + P_S \frac{\partial A}{\partial x} \, , \qquad (7)$$

an axial-force distribution consisting of blade force (F_B) and the force produced by the walls of the system.

Energy conservation yields

Energy

$$\underbrace{H + \frac{\partial H}{\partial x}\,dx}_{\text{enthalpy leaving control volume per unit time}} + \underbrace{\frac{\partial}{\partial t}\left[\varrho A\left(e + \frac{u^2}{2}\right)dx\right]}_{\text{time rate of increase or energy within control volume}}$$

$$= \underbrace{H}_{\text{enthalpy entering control volume per unit time}} + \underbrace{SWdx}_{\text{rate of shaft work done on fluid in volume}} + \underbrace{Qdx}_{\text{rate of heat added to fluid in control volume}}, \qquad (8)$$

which may be reduced to

$$\frac{\partial(EA)}{\partial t} = -\frac{\partial H}{\partial x} + SW + Q\,, \qquad (9)$$

where

$$E = \varrho\left(e + \frac{u^2}{2}\right) \qquad (10)$$

and

$$H = c_p \bullet W \bullet T_T \qquad (11)$$

Equations (3), (5), and (9) represent the form of the nonlinear conservation equations used in the modeling technique.

Additional equations required include:

Equation of State

$$P_S = \varrho R T_S \qquad (12)$$

Ratio of Specific Heats

$$\gamma = \frac{c_p}{c_v} \tag{13}$$

Definition of Mach Number

$$M = \frac{u}{a}, \tag{14}$$

where a is the acoustic velocity,

$$a = \sqrt{\gamma R T_S} \tag{15}$$

Definition of Total Temperature

$$T_T = T_S \left[1 + \frac{\gamma - 1}{2} M^2\right] \tag{16}$$

Definition of Total Pressure

$$P_T = P_S \left[1 + \frac{\gamma - 1}{2} M^2\right]^{\frac{\gamma}{\gamma - 1}} \tag{17}$$

2.2 STAGE CHARACTERISTIC DEFINITION

To provide the momentum and energy equations with stage forces and shaft work, respectively, a set of stage characteristics must be provided as input to the model. A stage flow coefficient (ϕ) is defined as

$$\phi = \frac{u}{U} \tag{18}$$

where u is the axial velocity and U is the wheel speed at the mean blade radius. The flow coefficient is related to the blade angle of attack, α, through the stagger angle, λ, defined by the relationship

$$\phi = \cot(\lambda + \alpha). \tag{19}$$

A decreasing flow coefficient means that the angle of attack is increasing, thus increasing the possibility of flow separation on the blade rows. A stage temperature coefficient (ψ^T) is defined as

$$\psi^T = TR - 1 \tag{20}$$

where TR is the stagnation or total temperature ratio.

Similarly, a stage pressure coefficient (ψ^P) is defined as

$$\psi^P = PR \tag{21}$$

where PR is the stagnation or total pressure ratio. The stage adiabatic efficiency can be defined as

$$\eta_{ad} = \frac{\Delta h_{ISEN}}{\Delta h_{actual}} = \frac{(PR)^{\frac{\gamma-1}{\gamma}} - 1}{TR - 1} \tag{22}$$

$$\eta_{ad} = \frac{(\psi^P)^{\frac{\gamma-1}{\gamma}} - 1}{\psi^T}. \tag{23}$$

A set of curves

$$\psi^T = \psi^T(\phi),\ \psi^P = \psi^P(\phi),\ \text{and}\ \eta_{ad} = \eta_{ad}(\phi) \tag{24}$$

is a set of stage characteristics which fully define a compressor's stage performance. The set of equations represented by Eq. (24) is redundant; any two of the three variables are sufficient to compute the third.

A typical set of steady-state stage characteristics for both pre- and post-stall operation is presented in Fig. 7. The stage characteristics are divided into three distinct regions: prestall, rotating stall, and reverse flow. The prestall region is based upon the performance of a normal operating blade row where the flow is attached to each individual blade. The rotating stall region is based upon a flow weighted average of a fully developed rotating stall cell. The pressure and temperature ratio in this region represents the average pressure and temperature rise across the stage for both stalled flow and unstalled flow. The reverse flow characteristic region represents the pressure loss and temperature rise associated with full annulus reverse flow.

At the flow shutoff point (zero flow) there exists a discontinuity in the stage pressure and temperature coefficient. This phenomenon was first observed by Gamache (Ref. 5) on a three-stage low-speed compressor rig. Since in most cases experimental results are not available to synthesize complete stage characteristics, a discussion on stage characteristic development is appropriate.

2.3 STAGE CHARACTERISTIC DEVELOPMENT

In previous modeling efforts (Refs. 9 and 10), prestall stage characteristics have been experimentally based. If, however, experimental results are not available, a method for predicting stage performance is available. A method currently in use at AEDC for predicting overall as well as stage performance utilizes the COmbined COmpressor Design and Evaluation Code (COCODEC).

COCODEC (Ref. 23) is a computer program capable of calculating overall compressor performance. It provides a steady-state axisymmetric solution in determining both individual stage and overall compressor performance. Stage performance is determined from both total pressure loss coefficients and relative outlet flow angles estimated from the blade geometry.

The blade geometry required to execute the program is summarized in Fig. 8. Blade inlet and outlet angles may be substituted for camber and stagger angles as the indicator for the amount of turning imposed on the airstream. In addition to the blading geometry, both the flowpath boundaries and the position of the individual blade rows within that boundary must be specified.

COCODEC determines a solution to a radial equilibrium equation using the streamline curvature method of solution at a series of radially extending computing stations spaced axially in the flowpath. A computational mesh (Fig. 9) is defined by the intersection of these computing stations with a number of streamlines whose radial positions are determined by the program. A number of data items are calculated at each of these mesh points. Considering a computing station that immediately follows a blade row, mesh point output items would include flow properties, blade performance, blade loading, both pressure and temperature rise across the blade row, and overall compressor performance up to the current computing station. This detail permits the extraction of steady-state stage characteristics.

COCODEC can calculate a complete set of speed characteristics for a compressor, but it provides no indication of the point on a speed characteristic at which the compressor stalls. The point at which the overall compressor experiences surge must be based upon experimental results. This also provides the limiting flow rate for the distinction between prestall and post-stall stage characteristics.

Determination of steady-state stage performance in the post-stall regions (rotating stall and reverse flow) is not as well defined as in the prestall case. First, steady-state performance in the rotating stall region must be looked upon in a global sense. Even though the flow is not steady in a one-dimensional sense at any stage, its overall averaged performance can be said to be steady if the rotating stall cell is completely formed. Secondly, not many measurements have been taken on a stage-by-stage basis for high-speed compression systems. Many experimental investigations have been carried out on low-speed compressors which were designed to determine the size and extent of the rotating stall cell development. Steady-state characteristics have been synthesized from some of this unsteady data. The best set of characteristics was synthesized on a three-stage low-speed rig at Massachusetts Institute of Technology and is reported in Ref. 5.

Since experimental data do not exist for the high-speed/high performance compression systems typical of today's military engines, estimates of stage performance in the post-stall region must be made. In addition to the very limited experimental results, there does not exist any complete design tool such as COCODEC to predict post-stall behavior from blade geometry. Studies are currently in progress on the research level at selected universities that will provide this basic design tool (Refs. 19 and 24). Therefore, post-stall characteristics in the rotating stall and reverse flow regions are currently estimated by using the overall shape suggested by low-speed compressor rig studies and matching overall transient performance during surge and/or rotating stall.

2.4 DYNAMIC STAGE CHARACTERISTIC TREATMENT

In the preceding section, the discussion of the stage characteristic centered around the prestall and reverse flow steady-state performance and the globally steady rotating stall average performance. In a dynamic event such as rotating stall or surge, steady characteristics are not necessarily correct. For the prestall and post-stall reverse flow characteristic steady characteristics can be used as they exist. The transient events in the prestall and reverse flow regions occur within 20 revolutions. However, in the rotating stall region, rotating stall may develop in 2 to 8 revolutions (Ref. 25) and the globally steady characteristic is no longer applicable. To provide the stage with a dynamic characteristic, a first-order time lag on the stage forces has been incorporated into the modeling technique in the rotating stall region only. The first-order lag equation

$$\tau \frac{dF}{dt} + F = F_{ss} \tag{25}$$

where

F = blade force and pressure area force of the casing,

F_{ss} = steady-state force,

τ = time constant

was used by Grietzer in his 1976 work (Ref. 1). It has been later applied by others (Refs. 16, 19, and 20) and has been successfully applied to models of the overall compression system characteristic.

2.5 COMBUSTOR REPRESENTATION

Because combustor performance can greatly influence compression system stability, the combustor volume with heat addition capability has been included in the post-stall modeling technique. A representative schematic of the computational grid of the compression/combustion system is presented in Fig. 10. The overall control volume is subdivided into elemental control volumes with each elemental control volume in the compressor representing a stage. However, in the combustor no such relationship exists and each elemental control volume size was chosen to give adequate frequency response. The combustor is one-dimensional, with heat release taking place within the whole control volume. In an actual combustor there is a primary zone of combustion where the chemical reaction takes place near stoichiometric conditions. Secondary air is mixed with the products to lower the flame temperature to levels which can be handled by the turbine blades. The one-dimensional modeling technique chosen approximates the final combustion state and does not model the mixing process explicitly. Overall fuel flow rate is input into the code which then solves for a total heat release by the equation

$$Q_{total} = LHV \left[\frac{far}{1 + far}\right] \cdot W_{comb}. \tag{26}$$

This total heat release is then evenly distributed across the combustor control volumes.

During post-stall events, the proper fuel/air ratio may not occur (as in the reverse flow situation). When this happens combustion is assumed to cease with the heat release immediately going to zero. When conditions are again right for combustion in each control volume, heat release is assumed to take place. In the case of reignition, there is an ignition delay.

The combustion process occurs as long as the fuel/air ratio is within a flammability zone. Represented in Fig. 11 are the flammability characteristics for a kerosene-type fuel in air at atmospheric pressure (Ref. 26). In this figure, equivalence ratio is defined as the ratio of the actual fuel/air ratio to that at stoichiometric conditions. Using these data as a basis, the rich fuel/air ratio for blowout occurs around an equivalence ratio of 3.0 (fuel/air ratio approximately 0.17). When reignition occurs it takes place near stoichiometric conditions with an ignition delay. Ignition delay is exponentially related to initial temperature, thus causing an exponential increase in heat release. A first-order lag equation of the form

$$\tau_{comb} \frac{dQ}{dt} + Q = Q_{ss} \tag{27}$$

was used to approximate the exponential ignition delay. The ignition delay time constant is based upon the ignition delay characteristics presented in Fig. 12.

2.6 NUMERICAL TECHNIQUE

The governing equations [Eqs. (3), (5), and (9)] of the compressor modeling technique are hyperbolic in nature. Thus, a numerical technique that has been applied successfully to hyperbolic equations was used in the model formulation. A predictor/corrector method was chosen which was first employed by R. W. MacCormack in 1969 on work dealing with hypervelocity impact cratering (Ref. 27). It was an explicit numerical method that is second-order accurate both in time and space when applied to the time-dependent, compressible Navier-Stokes equations. This method has since become known as the MacCormack second-order finite-difference scheme.

The compressor model is not only an initial value problem but a boundary problem as well. Because the treatment of the boundaries can be a cause of stability problems, method-of-characteristics boundary formulations were employed. The numerical computational volume was divided into three areas: inlet, exit, and interior. MacCormack's scheme was applied at the interior, a method of characteristics (MOC) scheme was applied at the inlet, and either an MOC scheme for unchoked flow or an isentropic sonic nozzle scheme for choked flow was applied at the exit.

2.6.1 MacCormack's Scheme and Application to the Modeling Technique

MacCormack's differencing scheme has in the past been typically applied to the viscous form of the conservation equations. The basic concept will be presented using these equations, but will be specialized to the terms describing the compressor model [Eqs. (3), (5), and (9)].

The unsteady compressible form of the conservation equations for one-dimensional flow, neglecting body forces and heat sources, may be written in conservative form as

$$\frac{\partial U}{\partial t} + \frac{\partial V}{\partial x} = 0 , \tag{28}$$

where

$$U = \begin{Bmatrix} \varrho \\ \varrho u \\ e \end{Bmatrix} \text{ and } V = \begin{Bmatrix} \varrho u \\ \varrho u^2 + \sigma_x \\ (e + \sigma_x)u - k \dfrac{\partial \epsilon}{\partial x} \end{Bmatrix},$$

$$\sigma_x = P_S - (\lambda - 2\mu) \frac{\partial u}{\partial x}, \; \epsilon = \frac{e}{\varrho} - \frac{u^2}{2},$$

k = coefficient of heat conductivity,

λ and μ = coefficients of viscosity.

Applying the predictor portion of MacCormack's technique to Eq. (28) gives

$$U_i^{(P)} = U_i - \frac{\Delta t}{\Delta x_{i-1}} (V_i - V_{i-1}), \tag{29}$$

where subscript i denotes a spatial location and superscript P denotes the predicted value. Correcting the predicted value then gives

$$U_i^{(C)} = 1/2 \left\{ U_i + U_i^{(P)} - \frac{\Delta t}{\Delta x_i} V_{i+1}^{(P)} - V_i^{(P)} \right\}. \tag{30}$$

The corrected value (denoted by superscript C) then becomes the value of the dependent variable for the next instant in time. Backward differences are used in the predictor step and forward differences in the corrector step. To avoid biasing the solution because of the order of differencing in the predictor/corrector steps, the method was modified to reverse the order or differencing every other time step. At the completion of the two-step process, first derivatives are approximated effectively by central differences.

Applying this method to the governing equations of the compressor model gives

Mass

Predictor:

$$\varrho A_i^{(P)} = \varrho A_i - \frac{\Delta t}{\Delta x_{i-1}} \left[W_i - W_{i-1} - W_{B_{i-1}} \right] \tag{31}$$

Corrector:

$$\varrho A_i^{(C)} = 1/2 \left\{ \varrho A_i + \varrho A_i^{(P)} - \frac{\Delta t}{\Delta x_i} \left[W_{i+1}^{(P)} - W_i^{(P)} - W_{B_i}^{(P)} \right] \right\} \tag{32}$$

Momentum

Predictor:

$$W_i^{(P)} = W_i - \frac{\Delta t}{\Delta x_{i-1}} \left[IMP_i - IMP_{i-1} + F_{i-1} \right] \tag{33}$$

Corrector:

$$W_i^{(C)} = 1/2 \left\{ W_i + W_i^{(P)} - \frac{\Delta t}{\Delta x_i} \left[IMP_{i+1}^{(P)} - IMP_i^{(P)} + F_i^{(P)} \right] \right\} \tag{34}$$

Energy

Predictor:

$$EA_i^{(P)} = EA_i - \frac{\Delta t}{\Delta x_{i-1}} \left[H_i - H_{i-1} + SW_{i-1} + Q_{i-1} \right] \tag{35}$$

Corrector:

$$EA_i^{(C)} = 1/2 \left\{ EA_i + EA_i^{(P)} - \frac{\Delta t}{\Delta x_i} \left[H_{i+1}^{(P)} - H_i^{(P)} + SW_i^{(P)} + Q_i^{(P)} \right] \right\} \tag{36}$$

The bleed flow, the force of the compressor blading and casing, and the shaft work and heat-transfer terms are distributions over a particular axial length. These distributed terms have to be consistent with the differencing equations for the equations to account for the correct mass, momentum, and energy transfer across each elemental control volume. When backward differencing is employed, the distributed term should then be associated with the upstream

calculating station. When forward differencing is employed, the term is associated with the calculating station of interest.

In most previous works, the MacCormack method has been applied to computational fluid dynamic-type problems (i.e., internal or external flow without source terms). The compression system model not only adds source terms to the governing equations but also uses nonuniform radial spacing. The addition of source terms did not cause any instabilities in the compression system model. However, the nonuniform radial spacing resulting in large axial area changes can and does cause numerical instabilities if the area change is too large. This causes a problem in the combustor representation limiting the computational representation of the actual combustor.

2.6.2 Boundary Treatment

In all numerical solutions to boundary value problems, the way the boundaries are treated can influence the stability and accuracy of the solution. As indicated by Moretti (Ref. 28), a boundary value problem in which the permeable subsonic boundary has constant properties is an ill-posed problem. Moretti suggests that a stretching of the permeable boundary to infinity, where the velocity vanishes and other properties take on their stagnation values, is one way of having constant properties at the boundaries. Since one is limited to some finite domain, this approach has to be modified to some extent. Also, while working with numerical solutions to the Navier-Stokes equations in inlet regions, Olson et al. (Ref. 29) found it necessary to allow the boundary conditions to become functions of time.

Abbett has performed a comparative study (Ref. 30) of numerical techniques for computing the boundary flow conditions at solid walls and shock boundary points in supersonic, inviscid flow. This effort investigated 30 different calculation procedures for determining boundary flow conditions for four sample problems. The type of calculation procedures included reflection, explicit one-sided difference, extrapolation, method of characteristics (at boundary points only), combined equations, and Euler predictor/simple wave corrector. The conclusions of the study were based on comparisons of each method with a pure method of characteristics (MOC) solution (i.e., all points, interior as well as boundary points, were calculated using MOC). When a full MOC was not utilized, Abbett concluded that the MOC boundary solution, coupled with some high-order differencing scheme for the interior points (such as MacCormack's method) gave the best results in calculating steady flow in supersonic flow fields. Abbett's conclusion is also valid for the compressor modeling technique, since both it and supersonic flow fields use hyperbolic equations to describe the fluid flow.

Using the unsteady compressible form of the Navier-Stokes equations for one-dimensional flow without body forces and heat sources, the following set of equations can be derived using the method of characteristics:

$$\underbrace{\frac{dP_S}{dt} - \varrho a \frac{du}{dt} = a^2\psi_1 - \varrho a\psi_2 + \psi_3}_{\text{compatibility equation}} \quad \text{for} \quad \underbrace{\frac{dx}{dt} = u - a}_{\text{characteristic equation}} \tag{37}$$

$$\underbrace{\frac{dP_S}{dt} + \varrho a \frac{du}{dt} = a^2\psi_1 - \varrho a\psi_2 + \psi_3}_{\text{compatibility equation}} \quad \text{for} \quad \underbrace{\frac{dx}{dt} = u + a}_{\text{characteristic equation}} \tag{38}$$

where

$$\psi_1 = 0 ,$$

$$\psi_2 = \frac{1}{\varrho}\frac{\partial}{\partial x}\left[(\lambda + 2\mu)\frac{\partial u}{\partial x}\right] \text{ (momentum viscous damping terms) ,}$$

$$\psi_3 = (\gamma - 1)\left[(\lambda + 2\mu)\left(\frac{\partial u}{\partial x}\right)^2 + \frac{\partial}{\partial x}\left(k\frac{\partial T_S}{\partial x}\right)\right] \text{ (energy dissipation and conduction terms).}$$

In the absence of any viscous forces or conduction heat transfer along the characteristic curves, the compatibility equations reduce to the following set of relationships:

$$dP_S - \varrho a du = 0 \text{ for } \frac{dx}{dt} = u - a, \tag{39}$$

$$dP_S + \varrho a du = 0 \text{ for } \frac{dx}{dt} = u + a. \tag{40}$$

2.6.2.1 Inlet Boundary Solution

The inlet boundary thermodynamic properties for any time can be calculated by specifying certain boundary conditions (P_T and T_T) and using the characteristic relationships of

Eq. (39). The characteristic equation is first solved by approximating the total derivatives by differences

$$X_{new} - X_I = (u - a)\,\Delta t\ . \tag{41}$$

Illustrated in Fig. 13 is the determination of the intersection of the characteristic curve (Point X_i) with the geometry of the previous time step (Line AB). The slope of the characteristic curve runs through the point of interest (i.e., Point C of Line CD) and a point which lies along the geometry of the previous time step, where all thermodynamic properties are known at the calculation stations. The thermodynamic relationships at Point X_I can be determined by linear interpolation of the properties between Points A and B. Once this point is known, the compatibility equation [Eq. (39)] can be approximated by differences

$$P_{S_{X_{new}}} - P_{S_{X_I}} = \varrho a\,(u_{X_{new}} - u_{X_I}). \tag{42}$$

An iterative technique is employed since there are two unknowns, $P_{S_{X_{new}}}$ and $u_{X_{new}}$, and one equation.

A guess at inlet Mach number is made, and along with the thermodynamic relationships

$$P_T = P_S \left[1 + \frac{\gamma-1}{2} M^2\right]^{\frac{\lambda}{\lambda-1}} \tag{43}$$

and

$$T_T = T_S \left[1 + \frac{\gamma-1}{2} M^2\right], \tag{44}$$

Eq. (42) is solved using the interpolated values of density and acoustic velocity in the previous time frame. With P_T, T_T, and P_S known, a new value for inlet Mach number can be obtained and the process continued until Mach number does not change within a specified tolerance. To obtain a more accurate value of P_S, the above iterative technique is applied to Eq. (42), with density and acoustic velocity now being an average between the interpolated value in the old time frame and the previous iterated value at the new time step. All thermodynamic properties are calculated using these relationships and the equation of state.

During post-stall events, flow reversal may occur at the inlet boundary. In this case, specification of constant total conditions at the inlet is inappropriate. Therefore, when flow reversal is sensed at the inlet boundary, the inlet boundary acts like an exit boundary and

the specification of static pressure becomes the proper boundary condition. Thus, reverse flow inlet boundary conditions are calculated using the method-of-characteristics exit boundary solution technique described below.

2.6.2.2 Exit Boundary Solution

For subsonic exit conditions, static pressure can be specified as the exit boundary condition. A characteristic scheme, such as that used in the inlet boundary scheme, can then be employed. In addition to using the characteristic relationships of Eq. (40), a set of streamline equations is used:

$$dP_S - a^2 d\varrho = 0 \text{ for } \frac{dx}{dt} = u \, . \tag{45}$$

A procedure similar to the inlet solution procedure is used with each compatibility equation solved along its characteristic curve or streamline curve, as illustrated in Fig. 14. With the specification of static pressure and the two compatibility equations, an iterative procedure is not needed. This type of boundary specification is used when exit static pressure variation is known (such as an exit pressure ramp leading to compressor surge).

For the case when an exit sonic condition is used simulating choking in the turbines, an imaginary, zero length convergent nozzle is employed as presented in Fig. 15. Flow within this nozzle has been assumed to be steady (i.e., at any time the steady-state flow equations govern the flow within the nozzle) and isentropic. Using the concept of mass flow function, $\dot{M}_T$, based on total conditions,

$$\dot{M}_T = \frac{W\sqrt{T_T}}{P_T A} \, , \tag{46}$$

the thermodynamic properties at the nozzle exit and inlet can be calculated. At sonic conditions the mass flow function has a constant value. This implies that the mass flow function at the nozzle inlet (Station N + 1) also remains constant since the nozzle flow is governed by isentropic, steady-state equations. It is further assumed that isentropic flow exists in the preceding elemental control volume, thus specifying total pressure and temperature (P_T and T_T at Station N + 1) to be equal to that at the previous calculating station (Station N). Boundary flow rate can then be calculated if the flow function at Station N + 1 is specified based on the given area. This type of boundary condition allows compressor transients (such as inlet pressure and temperature perturbations) to take place without having to know how exit static pressure varies during those transients.

2.6.3 Model Solution Procedure

Figure 16 outlines the overall digital computer simulation procedure. At time zero (Step A), initial values of the dependent variables (ρA, W, and EA) are specified for every control volume. The solution is started from a steady, uniform flow condition. With the specification of boundary conditions, all thermodynamic variables can be calculated (Step B) at the inlet, interior, and exit planes. Using the method of characteristics scheme or sonic exit condition scheme, the inlet and exit conditions for the next step in time can be calculated (Step C).

Knowing all the interior thermodynamic properties from Step B, the force and work terms (Step D) necessary for the momentum and energy equations [Eqs. (5) and (9)] can be calculated for input into the predictor step of MacCormack's method (Step E). New values for force and work can be determined from the predicted solution (Step F) and then used in the corrector step of MacCormack's method (Step G). The new values of the dependent variables determined in Step G are then used to compute the thermodynamic properties (Step B) for that time step. The sequence is repeated with boundary conditions changing in accordance with the specified event being simulated.

The momentum and energy equations [Eqs. (5) and (9)] require axial force and shaft work distributions representing the force of the compressor blading and casing on the fluid and the shaft work input per stage. These functions are constructed from the steady-state stage characteristics as described in Sections 2.2 through 2.4.

2.7 STABILITY CRITERIA AND FREQUENCY DISTURBANCE LIMITATIONS

With any explicit differencing scheme which approximates partial differential equations, some stability criteria must be set. The system of equations used by the model is hyperbolic in nature and represents the one-dimensional compressible flow equations with source terms. A stability criterion that has been used in the past with these equations is the Courant, Friedricks, and Lewey (CFL) stability restriction (Ref. 31). The restriction states that the finite-difference domain of influence must be at least as large as the physical domain of influence (i.e., a sound wave cannot travel more than one elemental control volume length in one time increment). Expressing this mathematically gives

$$\frac{(|u| + a)\,\Delta t}{\Delta x} \leq 1. \tag{47}$$

For the maximum time step, Eq. (47) can be written as

$$\Delta t_{max} = \frac{\Delta x_{min}}{a + |u|_{max}} . \tag{48}$$

For the high-pressure compressor with combustor model the maximum time was based on $\Delta x_{min} = 0.1$, $a = 2{,}683$ ft/sec (static temperature of 3,000°R), and $u = 75$ ft/sec (conditions in a typical combustor control volume). This gave a maximum time step of

$$\Delta t_{max} = 3.63 \times 10^{-5} \text{ seconds.}$$

The time step used for the high-pressure compressor, single-spool model was 3×10^{-5} seconds.

The model's response to some disturbance is dependent upon the elemental control volume length. Disturbance propagation through a control volume must be accomplished in a relatively short period of time to allow all the fluid to respond to the disturbance. According to Kimzey (Ref. 9), maximum frequency response is limited by minimum disturbance wavelengths of $10\ \Delta x_{max}$. Thus, using Kimzey's definition,

$$f_{max} = \frac{(u + a)_{min}}{10\ \Delta x_{max}}, \tag{49}$$

the maximum frequency response for the high-pressure compressor, single-spool compressor model was estimated to be 630 Hz based on velocities encountered in the inlet ducting system and nominal duct lengths of 0.25 ft. According to Ward (Ref. 32) a criterion for maximum frequency is that the propagation time through the control volume must be less than one-third the period of disturbance. Expressed mathematically this becomes

$$f_{max} \leq \frac{a}{6\pi\Delta x} , \tag{50}$$

where a and Δx are average quantities. Using this definition, the maximum frequency for the single-spool compressor model was estimated to be 385 Hz. Therefore, the maximum frequency probably lies somewhere in between these frequencies.

3.0 MODEL VALIDATION

The modeling techniques described in the previous section were applied to a single-spool high-pressure compressor of a current-day military turbofan engine. To validate the modeling

technique completely, interstage and overall compressor experimental data would be necessary for that compression system. The turbofan engine was tested at AEDC to investigate the engine's performance characteristics during post-stall events. However, complete compression system performance either overall or interstage was not obtained because of the instrumentation set utilized. Of major importance for compression system performance is a measurement of airflow. For the turbofan engine utilizing the compression system modeled there were no measurements made for compression system airflow during the post-stall events. Thus, model validation will consist of comparing the model results with experimental data from compressor rig tests and other engine tests where compression system performance was available. This will broaden the limited amount of direct experimental results and thereby validate the modeling technique, although indirectly, more completely.

3.1 COMPRESSOR RIG RESULTS

One of the first experimental studies to investigate the behavior of compression systems undergoing surge or rotating stall was performed by Greitzer (Ref. 1). His experimental results were obtained on a three-stage axial compressor having constant annular area and a hub-to-tip radius ratio of 0.7. A schematic of the test rig is presented in Fig. 17. A variable size plenum with sufficient volume was chosen such that surge could take place. A throttle was used to backpressure the machine to produce a system instability. Instrumentation consisted of total and static pressure, total temperature, hot wire, and high response pressure measurements upstream and downstream of the compression section. Interstage measurements were not obtained.

Greitzer's main intent of his experimental investigation was to describe a boundary between the inception of surge and rotating stall. In Ref. 13, Greitzer laid the foundations for the "B parameter" which was previously described in Section 1.0. Since the "B" parameter is dependent upon the individual compression system, it cannot be used for comparing results from one compression system to that of another. But, it is convenient to review Greitzer's post-stall experimental results in light of that parameter.

At a low value of "B", low rotor speed, and small volume, the compression system moved from a point at the stability limit to a new but globally stable point at lower flow and pressure rise (Fig. 18). At this new operating point the three-stage compressor is in rotating stall. At the same corrected speed but with a somewhat larger exit plenum volume (B = 1.00), the compressor exhibits oscillations characteristic of surge (Fig. 19). This type of behavior can also be achieved with high speed and small volume (Fig. 20) as is the configuration of most current-day turbofan engines. With a larger increase in either speed or plenum volume (in effect increases "B"), the compression system will exhibit larger oscillations characteristic

of a deep surge with flow reversal (Fig. 21). Once the compressor exhibits deep surge, the decrease in mass flow takes place so quickly that it precludes the formation of any rotating stall cell pattern that might develop during classic surge (Fig. 22).

Deep surge is characterized by change in compressor mass flow that is quite rapid over part of its trajectory and rather slow over the rest. At the initiation of surge, mass flow decreases to negative values at a fairly constant pressure ratio. Once reverse flow has become established, a slow blowdown process occurs where the compressor acts as a very high loss throttling device. A large pressure drop occurs because of the high angle of attack on the blades during reverse flow. Once the pressure has dropped, the mass flow reaccelerates back to a positive flow because conditions are now correct for pumping to occur. Slow repressurization takes place in the plenum during which the compressor moves back to its original operating point along the steady-state characteristic.

The results presented by Greitzer are based upon a low-speed/low-pressure ratio compressor rig. Because today's turbine engine employs high-speed/high-pressure ratio systems, one considers how appropriate low speed results are to phenomena observed in the high speed systems. Pratt and Whitney has addressed this issue in Ref. 4.

Presented in Fig. 23 is a schematic of the High Speed Research (HSR) compressor rig designed for post-stall testing. The compressor consists of three stages capable of producing an overall pressure ratio of 2.8 at an operational rotor speed of 22,000 rpm. Compressor discharge volume could be changed to allow different post-stall events to occur. Presented in Fig. 24 is the overall system response to throttle closure at a corrected speed of 56 percent. The compression system experienced surge at a frequency of 18 Hz. When the corrected speed was reduced to 54 percent, the compressor experienced rotating stall as indicated in Fig. 25. Presentation of overall performance in this form can only show the average performance of the system without presenting any of the details of the rotating stall cell itself. However, what is of interest is the apparent boundary between surge behavior and rotating stall. Since the geometry is identical in each case, a "B" parameter could be defined which would describe that boundary for effects other than rotational speed. These results are very similar to that observed in low speed rig tests.

Another high-pressure compressor rig test was conducted by General Electric (Ref. 33) under the NASA-sponsored Energy Efficient Engine program. The compressor is an advanced technology 10-stage compressor capable of high speed and high pressure ratio. It was instrumented with inlet and exit transient airflow rakes (total and static pressure measurements) as well as inlet, exit, and interstage pressures and temperatures. The compressor was driven by a steam turbine capable of speeds up to 15,000 rpm and throttled by a metered discharge valve.

At a corrected speed of 70 percent, the throttle was adjusted to allow the compressor to experience rotating stall. Presented in Fig. 26 is the average overall compressor performance unstalled and in rotating stall at several throttle settings. Although the transients to these final states are not shown, their effective final operating points are indicated along the in-stall characteristics.

At 98.5-percent speed, the compressor was throttled to instability, producing high-speed surge cycles. Indicated on Fig. 27 is the response of the compressor beyond instability inception. The compressor did not come back to its initial unstalled operating point during the surge transients because the initial reverse flow mixed with the inlet flow, which caused an increase in inlet pressure and temperature. Since the mechanical speed was held constant, this reduced the corrected speed to near 70 percent. However, as was the case in the low-speed rig tests (Ref. 1), the surge trajectories are similar in nature with periods of full reverse flow and subsequent recovery and repressurization. Presented in Fig. 28 are key compressor performance parameters as a function of time during the surge cycles near 70-percent corrected speed. At the initiation of the surge cycle the exit pressure and flow rate drop significantly with flow reversal taking place. This causes a flow blockage at the inlet which can be evidenced by the rapid increase in inlet pressure followed by a sharp drop. Following flow breakdown, there is a period where the system remains at a low flow rate and low pressure ratio. Subsequent analysis of interstage measurements indicated that rotating stall was present. During this phase inlet temperature increases because of the mechanical work being input to the flow. The system then begins to recover with an increase in exit pressure and flow rate and a decrease in temperature. The system continues to surge since the throttle is held in the same position.

3.2 POST-STALL ENGINE RESULTS

Compressor rig experiments provide ample information about the performance and stability of the compressor itself and allow the examination in detail of certain aspects of its operation. However, the problem of nonrecoverable stall is an engine system related problem with the interaction of the combustor, augmentor, fan, and controls playing an important part in the compression system's post-stall behavior.

An engine test program was conducted at AEDC over a five-year period to investigate and evaluate the phenomena of nonrecoverable stall. Testing occurred with four modern-day turbofan engines for various flight conditions, control variations, stall inducement techniques, and potential stall clearing techniques (Ref. 3). An engine was installed in an altitude test cell capable of simulating the flight conditions of interest (i.e., setting inlet total pressure and temperature and maintaining exit static pressure). A schematic of a typical engine installation is presented in Fig. 29. Instrumentation included steady-state pressure and temperature

measurements for engine performance and dynamic pressure measurements for events such as surge and rotating stall. In addition, in some of the engine tests, compression system dynamic airflow was calculated from dynamic total and static pressure measurements at the inlet and in the middle of the high-pressure compressor.

Presented in Fig. 30 are the time histories of the compressor inlet, interstage, and bypass inlet pressures during a mainburner fuel pulse-initiated system instability. The high-pressure compressor experiences surge cycles of approximately 7 Hz for about 1 sec, then moves into rotating stall where it becomes nonrecoverable. During the instabilities, whether it is surge or rotating stall, the rotor speed decreases because the energy available from the fuel is not being released at high efficiency because of the compression system instability. In fact, there may be fuel that is not burned until it passes to the low-pressure turbine. This is suggested by the increase in low-pressure turbine exit temperature while the high-pressure turbine experiences a decrease in temperature (Fig. 31). The reduction in rotor speed attributable to inefficient energy release results in the compression system moving toward a more favorable condition for rotating stall (i.e., low "B" value). Thus, if the surge cycles are not interrupted with the compression system moving toward complete recovery, the system tends to move to a region where rotating stall will develop. Presented in Fig. 32 is a typical trajectory (i.e., conventional compressor performance map) of a high-pressure ratio compressor during rotating stall. Since the pressure probes are located at only one circumferential position, the flow calculations reflect the rotating stall cell nature with positive flow in the unstalled regions and reverse flow in the stall cell region. An averaging technique would be necessary on this performance data for the performance trajectories to appear as they do in Fig. 27. Typical compression system surge cycles are presented in Fig. 33. The high-pressure compressor in this case experienced "deep surge" as previously described by Greitzer.

Another aspect of compression system performance is the interaction of other components during post-stall events. The combustor can have a profound effect on the compression system as shown in Fig. 34. Indicated in Fig. 34a is the compression system in surge initially with the combustor partially lit, then completely blown out as evidenced by the combustor ultraviolet detector. When the combustor reignited, the rotor speed had dropped to a level where rotating stall could be and was established. Even when combustion was sustained with the use of a high rate ignitor (Fig. 34b), rotating stall was the terminal condition as a result of low speed and continuous high pressure in the combustor.

Thus, a high-pressure compressor installed in a turbine engine exhibits similar performance signatures as has been observed in low- and high-speed compressor rigs. Engine data not only gives us compression system performance but also allows us to see the interaction of other components during post-stall events.

3.3 COMPRESSOR MODEL RESULTS

Since model validation is of a qualitative nature instead of a one-on-one analysis of individual cases, model results will be analyzed by comparing general characteristics observed in the experimental data that has been presented in the previous sections. All comparisons will be made for a model configuration of a nine-stage high-pressure compressor with a representative combustor which may or may not involve combustion. High speed and low speed regions will be analyzed for their general characteristics which will encompass both types of post-stall events (surge and rotating stall). The effect the combustor has on compression system stability will be discussed for both cases.

At this point, it is appropiate to comment on the application of Greitzer's "B" parameter. Since it is system dependent, to validate the nine-stage compression system model in terms of that parameter, it would require that experimental values be generated for the same system modeled. However, because a representative combustor and not the actual combustor was modeled (i.e., a different plenum volume), comparisons with experimental results using the "B" parameter cannot be made.

For all cases the model was given a set of initial conditions and allowed to come to a steady solution (usually within 0.05 sec). The compressor was then throttled to instability by either decreasing the exit mass flow function, $\dot{M}_T$, (i.e., closing the isentropic, imaginary nozzle) or fuel pulsing the combustor when combustion was present. The throttle was held constant during the post-stall events at a level that was just sufficient to cause the compressor to go into system instability. The time constant, τ, in association with the dynamic forces [Eq. (25)] was set at a predetermined level to allow either surge or rotating stall to be the dominant post-stall event. This time constant controlled the amount of lag in the steady-state stage forces, thereby providing a dynamic stage force during post-stall events (see Section 2.4).

3.3.1 High Speed Results

For the high speed case, the model was run at an initial corrected speed of 100 percent of design at sea-level standard day inlet conditions (P_T = 14.696 psia and T_T = 518.67°R). Mechanical speed was held constant but corrected speed would vary with inlet temperature during post-stall events. The first case at this condition is without burning in the combustor. This case would be analogous to the compressor rig data presented in Section 3.1. The dynamic stage force time constant was set at 0.02 which would allow surge to be the dominant post-stall event. Presented in Fig. 35 are the model surge trajectories as they appear on a compressor map. Because the throttle was held constant after initiating the post-stall event, the compressor went through a series of surges as the combustor volume repressurized. A very rapid flow

reversal process occurred at the initiation of the event. After reversal has taken place, pressure throughout the machine begins to drop as evidenced by the dropping pressure ratio. Once the combustor and compressor volumes empty, the compressor can begin to pump, causing the flow to accelerate toward positive flow. As was the case with flow reversal, this process is fairly rapid. Once positive flow has been established, the compression system is able to increase the pressure and move the machine back to the demanded pressure ratio.

Presented in Fig. 36 are time histories of the major compressor performance parameters. These model results are similar to those experimental results obtained with the G.E. energy-efficient high-pressure compressor (Fig. 28). Comparison of several of the time history plots reveals a one-to-one correspondence in the sequence of events. At the time of the initial instability, the inlet total pressure and temperature increase rapidly, indicating a flow blockage. When flow reversal occurs, inlet total pressure and temperature initially drop. Inlet pressure recovers first to near its initial value, but temperature increases because of additional energy added by the compression system during the reverse flow process. Inlet temperature then decreases to its original value when recovery occurs. The exit total pressure also is very similar to that observed experimentally (Fig. 28) with a rapid increase at surge initiation indicating blockage, then a rapid drop indicating compressor/combustor dumpage. Repressurization takes place after the flow has been reestablished. As can be seen in Fig. 36f, corrected speed varies with the varying inlet temperature.

Surge frequency as predicted by the model is of the order of 10 to 12 Hz, which is typical of engine surge frequencies observed experimentally. This does not compare well with some of the rig experimental results because of the size of the combustor attached to the compressor. Combustor volumes of typical turbine engines are usually much smaller than the plenum volumes used behind compressor rigs. Thus, one would expect the surge frequency of the compressor rigs to be much lower than turbine engine results. This is the case for Greitzer's experimental results and the G.E. energy-efficient compressor rig. The P&WA High Speed Research (HSR) rig surge frequency was somewhat higher (approximately 17 to 18 Hz) but its plenum volume was near what a typical combustor would be. Surge frequency for the engines tested at AEDC (Figs. 29 through 34) were of the order of 9 to 11 Hz. Thus, model surge frequencies agree well with actual engine results.

Although rotating stall at high engine speeds is not common among today's compression systems, the model could successfully be used to indicate that rotating stall is sometimes present. Increasing the stage force time constant, τ, will increase the lag on the stage forces and retard the flow reversal process. If flow reversal does not take place, forces necessary for recovery may not be generated. In this case, the model will "zero in" on the steady-state compressor characteristic which represents a one-dimensional average of the rotating stall performance.

Presented in Fig. 37 are the overall compression system performance trajectories on the compressor map. The flow reversal process begins like it does in the surge event, but the average flow does not completely reverse. In this case the stage forces are quite heavily lagged (τ = 0.06), generating the scenerio outlined above. The trajectories to the final state did not appear to "spiral in" like the rig results presented in Fig. 25. In the case of the rig results, there was a facility inlet which created a high resistance to reverse flow. This did not allow restoring forces to be generated, resulting in rotating stall. In the case of the model, rotating stall was created by lagging the steady-state pressure characteristics (increasing) such that restoring forces were also not generated but in such a manner that only a partial surge cycle was generated. However, the model does finally come to steady-state performance at a pressure ratio of approximately 3.5 and a flow rate of 20 percent of design. This state represents the development of a completely formed rotating stall.

Presented in Fig. 38 are the time histories of the major performance parameters during the rotating stall event. Airflow oscillates until it finds the new operating point and compressor exit pressure settles into the new low value, both of which are similar in nature to that experienced with the P&WA HSR rig (see Fig. 25) and the G.E. energy-efficient compressor (Fig. 26). Inlet pressure and temperature oscillate about the initial condition, indicating the unsteady nature of the initial process and causing corrected speed to oscillate.

The third case to examine at high speed is the effect of heat release in the combustor on the compression system. Heat release was modeled by Eq. (26) and was initially set at a level to allow an exit temperature of approximately 3000°R (typical of today's engines at sea-level-static conditions). To cause a compression system instability, the fuel was pulsed to a new level just high enough to initiate the instability. It was then held at this level during the post-stall event. Presented in Fig. 39 are the fuel flow and heat release per combustor control volume. If, during the surge cycles, the fuel-air ratio reached a value of 0.06 the combustor heat release was shut off immediately, simulating a blowout. This generally occurred during the flow reversal process. During the blowdown phase the combustor would not generate heat and would not relight until the fuel-air ratio reached a level of 0.05, which occurred during the flow reacceleration phase. The reignition process simulated an ignition delay by using Eq. (27). The value of the time constant τ_{comb} = 0.02 sec was chosen using the characteristics presented in Fig. 12.

Presented in Fig. 40 are the overall compression system performance trajectories as presented on a compressor map. As in the first high speed case, the dynamic stage force time constant was set at 0.02. The trajectories are very similar to what was generated in the noncombustion case except that the surge frequency is tied to the combustor blowout/reignition process. This phenomenon was observed experimentally (Fig. 34b) and indicates that the reignition/blowout

of the combustor keeps the compression system in surge until the combustion process can be sustained. At this time the compression system may be at a low enough speed to allow rotating stall to develop. Because of the way the combustion process is modeled, continuous combustion during post-stall events could not be obtained for the high speed cases. This limited the high speed post-stall phenomena to surge cycles when combustion was present. This is not the case for the low speed region which will be discussed in the next section.

3.3.2 Low Speed Results

For the low speed case, the model was run at an initial corrected speed of 70 percent of design at sea-level standard day conditions. As in the high speed case, the mechanical speed was held constant but corrected speed would vary during the post-stall events. The dynamic force time constant was set at 0.03 to allow surge to be the predominant post-stall event. Initial fuel flow was set such that combustor exit temperature was in the neighborhood of 1400°R. To initiate the post-stall event the fuel was pulsed to a higher level and kept at that level throughout the event. Presented in Fig. 41 are the surge trajectories at an initial corrected speed of 70 percent. They appear much like those generated in the high speed case, with the exception that flow reversal is not quite as much. This surge event can be classified as a "deep surge" and is much like what Greitzer observed in his low speed rig (Fig. 21). In this case the combustor was allowed to experience blowout and reignition. This component interaction drove the surge frequency at approximately 12 Hz, as can be seen in Fig. 42.

At the lower speed and combustor energy levels surge events could be produced by the model without combustor blowout and reignition. Heat release drops off slightly during the surge events, as illustrated in Fig. 43. The dynamic force time constant was increased to 0.05, which prevented reverse flow and kept the combustor lit. The surge trajectories are presented in Fig. 44 and are characteristic of "deep surge" without the flow reversal. Surge frequency was approximately 12 Hz which is similar to the low speed case previously presented.

Since rotating stall in today's compression systems occurs at low speed, it is of primary interest whether the model can produce the rotating stall post-stall event. By increasing the dynamic force time constant to 0.055, the model produced a rotating stall, stagnated condition (Fig. 45). As in the previous case, the combustor heat release dropped a little during the initial surge event but remained near the initial level during the post-stall event. The compression system experienced a complete surge cycle, then "zeroed in" on the steady rotating stall value which indicates the final rotating stall state. This process can be seen clearly in Fig. 46. Further increase in the dynamic force time constant only quickened the onset of rotating stall. This model post-stall behavior is similar to that observed with the HSR rig (Fig. 25).

By obtaining good model general behavior in the two speed regions with comparison to experimental data from several compression systems, the modeling technique has been proven to be a useful tool for the analysis of compression system post-stall events.

4.0 OBSERVATIONS

In the previous section, model results were compared to existing experimental results from several different sources to provide a basis for validating the model. In general, experimental results on a stage-by-stage basis were not obtained. However, since the model was constructed on a stage-by-stage basis, one can analyze stage interaction during the post-stall events and when the results compare favorably with overall experimental results, one can have some confidence in the qualitative nature of the stage interaction.

Of interest is the flow through the compressor during the post-stall event. Presented in Fig. 47 is a time history of stage flow coefficients ($\phi = u/U_{mean}$) during a typical surge event. The flow reversal process can be seen as the execursion into the negative flow regions. The reacceleration phase is of primary interest because there exists a flow overshoot region that affects the rearward stages the most. Flow overshoot has been observed experimentally and can be seen in Figs. 21, 27, and 33. The overshoot is a result of the restoring forces generated within the compressor with the rear stages providing much of that restoring force and thus accelerating the flow more in that area than anywhere else. In the case where the model indicates that rotating stall is present, a flow overshoot is not present (Fig. 48). This indicates that forces in the compressor were not high enough to allow surge cycles to develop. This suggests that if the rear stage performance can be enhanced during the reacceleration process, rotating stall might be averted. Using a lumped compression system model, Gamache discovered that there are "windows" in the surge event where the application of an external force might affect the post-stall performance of a compression system (Ref. 5). A corollary to Gamache's conclusions might be that if a reasonable strength and proper force can be generated near the stall onset or near the reacceleration process (near zero non-flow), flow stagnation can be averted. The stall overshoot observed in the model and experimental results is a result of that force being generated.

Another observation about stage interaction can be made by analyzing the stage dynamic forces during post-stall events. Presented in Fig. 49 are the stage forces during surge cycles at 100-percent speed. Of particular interest is the low level of performance of the sixth stage, even in steady-state conditions before the surge event. The force generated by the stage is near zero, suggesting that between the fifth and sixth stage is where post-stall events will likely begin in the high-speed region. Examining the dynamic stage forces in the low-speed region implies a different region for rotating stall onset. Presented in Fig. 50 are the stage forces

during a low-speed (70-percent) rotating stall event. The front stages have values less than zero, suggesting that rotating stall will likely begin in these stages. This has been observed experimentally with this particular compression system.

These two observations demonstrate why a stage-by-stage compression system model is preferred over a lumped parameter model. The lumped parameter models can analyze only overall compression system behavior during these events and cannot answer questions about stage interaction or suggest possible solutions that may require changes within the compressor itself. The stage-by-stage model can be used to formulate possible changes or enhancements to a particular stage or group of stages within the compression system that may make the system more tolerant to the stagnated condition.

5.0 SUMMARY

An existing one-dimensional stage-by-stage compression system modeling technique has been enhanced and modified to incorporate post-stall dynamic events. This model provides a tool for analyzing surge and rotating stall on a stage-by-stage basis as well as on the overall system level. The following significant results and observations have been drawn from this effort:

1. The model solves the nonlinear form of the conservation laws using the second-order accurate MacCormack finite-difference scheme.

2. The solution of the momentum and energy equations requires the modeling of stage forces and shaft work not only in the prestall cases but also during the post-stall events of surge and rotating stall. Stage forces and shaft work are obtained from a set of steady-state stage characteristics (pressure and temperature rise as a function of mass flow rate) that are lagged by a first-order lag equation to provide dynamic characteristics during surge and rotating stall. The steady characteristics were synthesized using a compressor design code (COCODEC) for the prestall portion, and estimates of post-stall stage characteristics were based upon previous experimental results.

3. A representative combustor with dynamic blowout/relight capability was attached to the compression system model to allow component interaction to occur during post-stall events.

4. The model was validated by comparing overall model results with compression system experimental results from low speed rigs, high speed rigs, and engine test data whenever compression system performance was avaliable.

a. The model was exercised in high- and low-speed regions to analyze its general characteristics encompassing both types of post-stall events (surge and rotating stall).

b. In general, the model produced surge cycles of the "deep surge" type as classified by Greitzer (Ref. 1) with a frequency consistent with that observed during engine tests.

c. Rotating stall from a one-dimensional viewpoint can be observed on a compressor map by averaging the flow on the nonstalled region with that of the stalled rotating cell region. Model results as depicted on the average compressor map behave much like the experimental data when viewed in a similar manner. The final end state can be depicted as globally stable but of low performance.

d. Combustor interaction during post-stall events was investigated by exercising the model with combustion present in both speed regions. In the high speed region, combustor blowout and reignition kept the compression system in surge cycles. This phenomenon has also been observed experimentally. Rotating stall with burning in the combustor could not be modeled at high speed. However, at low speed, continous combustion could be sustained both during surge cycles and rotating stall. This confirms some engine experimental results, in which continous combustion at low speeds is concurrent with the onset of rotating stall.

5. Since the model is constructed on a stage-by-stage basis, analysis of stage interaction can be performed during the post-stall events. Stage performance can be analyzed to determine where post-stall events are likely to occur and whether there is enough restoring force present to prevent the onset of rotating stall. This modeling technique offers an advantage over the lumped parameter overall compression system models by being able to analyze stage interaction and suggest possible solutions on a stage-by-stage basis.

6.0 RECOMMENDATIONS

The post-stall compression system model has been constructed using an existing prestall code as a basis. That code was modified and validated against experimental results. In the course of construction certain limitations were imposed because of deficiencies in the numerical

simulation. These limitations should be removed and further improvements made to facilitate applications to future compression systems. Therefore, the following recommendations are offered:

1. **Stage Characteristics** — Stage characteristics are the heart of this modeling technique. Future experimental efforts should be directed to obtain high fidelity stage performance characteristics in the rotating stall and reverse flow regions as well as the unstalled region. Theoretical methods for obtaining characteristics should be enhanced, developed, and validated to augment the experimental information.

2. **Numerical Simulation** — During the course of model construction it was discovered that the MacCormack explicit numerical technique would not handle large changes in area from one calculating station to another. This type of area change occurs in the combustor. Satisfactory model results during surge or rotating stall simulation could not be obtained. To overcome this limitation radical changes in combustor area were not allowed, thus allowing only a representative combustor to be modeled instead of the actual geometry. Therefore, to remove this limitation another numerical technique more tolerant of area changes should be explored and adapted for turbomachinery application.

3. **Combustor Modeling** — Modeling of the combustion process in the combustor is handled by a simple heat release equation based upon fuel-air ratio and the lower heating value of the fuel. Combustion efficiency degradations are not modeled during post-stall events. Blowout and reignition are based upon limited experimental results and may not always occur at the proper combustor conditions. A more vigorous model of the combustion process should be developed and utilized to provide more accurate component interactions during post-stall events.

4. **Dynamic Engine Model** — The principles behind the dynamic compression system model should be incorporated into a dynamic engine model which can handle post-stall events. This will provide an engine analysis tool for purposes of analyzing test results and understanding their meaning. It will also provide a predictive tool to be used for streamlining future engine test programs.

REFERENCES

1. Greitzer, E. M. "Surge and Rotating Stall in Axial Flow Compressors—Part II: Experimental Results and Comparison With Theory." *ASME Journal of Engineering for Power*, Vol. 98, No. 2, April 1976, pp. 199 - 217.

2. Day, I. J. "Axial Compressor Stall." Ph.D Dissertation, Christ's College (Cambridge University), 1976.

3. Burwell, A. E. and Patterson, G. T. "Dynamic Engine Behavior During Post Surge Operation of a Turbofan Engine." AIAA Paper No. AIAA-85-1430. Presented at AIAA/SAE/ ASME/ASEE 21st Joint Propulsion Conference, Monterey, CA, July 8 - 10, 1985.

4. French, J. V. "Modeling Post-Stall Operation of Aircraft Gas Turbine Engines." AIAA Paper No. AIAA-85-1431. Presented at AIAA/SAE/ASME/ASEE 21st Joint Conference, Monterey, CA, July 8 - 10, 1985.

5. Gamache, R. N., "Axial Compressor Reversal Flow Performance." Ph.D. Dissertation, Massachusetts Institute of Technology, May 1985.

6. Gabriel, David S., Wallner, Lewis E., and Lubick, Robert J. "Some Effects of Transients in Inlet Pressure and Temperature on Turbojet Engines." Paper presented at the Twenty-Fifth Annual Meeting of the Institute of the Aeronautical Sciences, New York, January 28-31, 1957.

7. Kuhlberg, J. F., Sheppard, D. E., and King, E. O. "The Dynamic Simulation of Turbine Engine Compressors." American Institute of Aeronautics and Astronautics Paper No. 69-486, presented at the AIAA/SAE Joint Propulsion Specialist Conference, Cleveland, OH, June 1969.

8. Willoh, Ross G. and Seldner, Kurt. "Multistage Compressor Simulation Applied to the Prediction of Axial Flow Instabilities." National Aeronautics and Space Administration TMX-1880, Lewis Research Center, Cleveland, OH, September 1969.

9. Kimzey, W. F. "An Analysis of the Influence of Some External Disturbances on the Aerodynamic Stability of Turbine Engine Axial Flow Fans and Compressors." AEDC-TR-77-80 (AD-A043543), August 1977.

10. Davis, M. W., Jr. "A Stage-by-Stage Dual-Spool Compression System Modeling Technique." ASME Paper No. 82-GT-189, Presented at ASME Gas Turbine Conference, London, England, March 1982.

11. Mazzawy, R. S., Fulkerson, D. A., Haddad, D. E., and Clark, T. A. "F100(3) Parallel Compressor Computer Code and User's Manual Final Report." National Aeronautics and Space Administration CR-135388, Lewis Research Center, Cleveland, OH, May 1978.

12. Tesch, W. A. and Steenken, W. G. "Blade Row Dynamic Digital Compressor Program, Volume I, J85 Clean Inlet Row and Parallel Compressor Models." National Aeronautics and Space Administration CR-134978, Lewis Research Center, Cleveland, OH, March 1976.

13. Greitzer, E. M. "Surge and Rotating Stall in Axial Flow Compressors—Part I: Theoretical Compression System Model." *ASME Journal of Engineering for Power*, Vol. 98, No. 2, April 1976, pp. 190 - 198.

14. Wenzel, L. M. and Bruton, W. M., "Analytical Investigation of Nonrecoverable Stall." NASA Technical Memorandum 82792, February 1982.

15. Seldner, K., Mihaloew, J. R., and Blaha, R. J., "Generalized Simulation Technique for Turbojet Engine System Analysis." NASA-TND-6610, February 1972.

16. Takata, H. and Nagano, S., "Nonlinear Analysis of Rotating Stall." *Journal of Engineering for Power*, October 1972.

17. Sexton, M. R. and O'Brien, W. F. "A Model for Dynamic Loss Response in Axial-Flow Compressors." ASME Paper 81-GT-154, March 1981.

18. Moore, F. K. "A Theory of Rotating Stall of Multistage Axial Compressors." NASA CR-3685, July 1983.

19. Moore, F. K. and Greitzer, E. M. "A Theory of Post-Stall Transients in Axial Compression Systems: Part I — Development of Equations." ASME Paper No. 85-GT-171, March 1985.

20. Greitzer, E. M. and Moore, F. K. "A Theory of Post-Stall Transients in Axial Compression Systems: Part II — Application." ASME Paper No. 85-GT-172, March 1985.

21. Chung, K., Leamy, K. R., and Collins, T. P. "A Turbine Engine Aerodynamic Model for In-Stall Transient Simulation." AIAA Paper No. AIAA-85-1429, Presented at AIAA/SAE/ASME/ASEE 21st Joint Propulsion Conference, Monterey, CA, July 8 - 10, 1985.

22. Hosny, W. M., Bitter, S. J., and Steenken, W. G. "Turbofan Engine Nonrecoverable Stall Computer—Simulation Development and Validation." AIAA Paper No. AIAA-85-1432, Presented at AIAA/SAE/ASME/ASEE 21st Joint Propulsion Conference, Monterey, CA, July 8 - 10, 1985.

23. Browell, R. W., Reynolds, L. D., and Core, W. P. "COCODEC: Combined Compressor Design and Evaluation Code." Union Carbide Corporation, Nuclear Division, CTC-INF-1039, May 1972.

24. Cousins, W. T. and O'Brien, W. F. "Axial-Flow Compressor Stage Post-Stall Analysis." AIAA Paper No. AIAA-85-1349. Presented at AIAA/SAE/ASME/ASEE 21st Joint Propulsion Conference, Monterey, CA, July 8 - 10, 1985.

25. Greitzer, E. M. "Review—Axial Compressor Stall Phenomena." *Journal of Fluids Engineering*, Vol. 102, June 1980, pp. 134 - 151.

26. Oates, G. C., Editor. "The Aerothermodynamics of Aircraft Gas Turbine Engines." AFAPL-TR-78-52, July 1978.

27. MacCormack, R. W. "The Effect of Viscosity in Hypervelocity Impact Cratering." American Institute of Aeronautics and Astronautics Paper No. 69-354. Presented at the AIAA Hypervelocity Impact Conference, Cincinnati, OH, April 30 - May 2, 1969.

28. Moretti, G. "Importance of Boundary Conditions in the Numerical Treatment of Hyperbolic Equations." *The Physics of Fluids, Supplement II* (1969), pp. 13 - 20.

29. Olson, L. E., McGowan, P. R., and MacCormack, R. W. "Numerical Solution of the Time-Dependent Compressible Navier-Stokes Equations in Inlet Regions." National Aeronautics and Space Administration TM-X-62338, Ames Research Center, Moffett Field, CA, March 1974.

30. Abbett, M. J. "Boundary Condition Calculation Procedures for Inviscid Supersonic Flow Fields." American Institute of Aeronautics and Astronautics paper presented at the AIAA Computational Fluid Dynamics Conference, Palm Springs, CA, July 19 - 20, 1973.

31. Courant, R., Friedricks, K. O., and Levy, H. Translated from German to: "On the Partial Differential Equations of Mathematical Physics." *IBM Journal of Research and Development,* Vol. II, pp. 215 - 234, 1967.

32. Ward, G. G. "Compressor Stability Assessment Program (Techniques for Constructing Mathematical Models of Compression Systems and Propulsion Systems)." Air Force Aero Propulsion Laboratory TR-74-107, Volume II, Wright-Patterson Air Force Base, OH, December 1974.

33. Hosney, W. M. and Steenken, W. B. "Aerodynamic Instability Performance of an Advanced High Pressure-Ratio Compression Component." AIAA Paper No. AIAA-86-1619, presented at AIAA/ASME/SAE/ASEE 22nd Joint Propulsion Conference, Huntsville, AL, June 16-18, 1986.

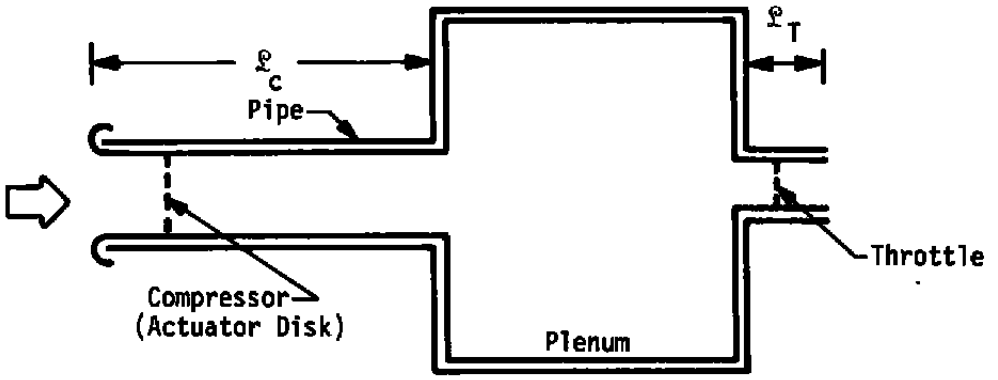

Figure 1. Greitzer's equivalent compression system used in analysis (Ref. 13).

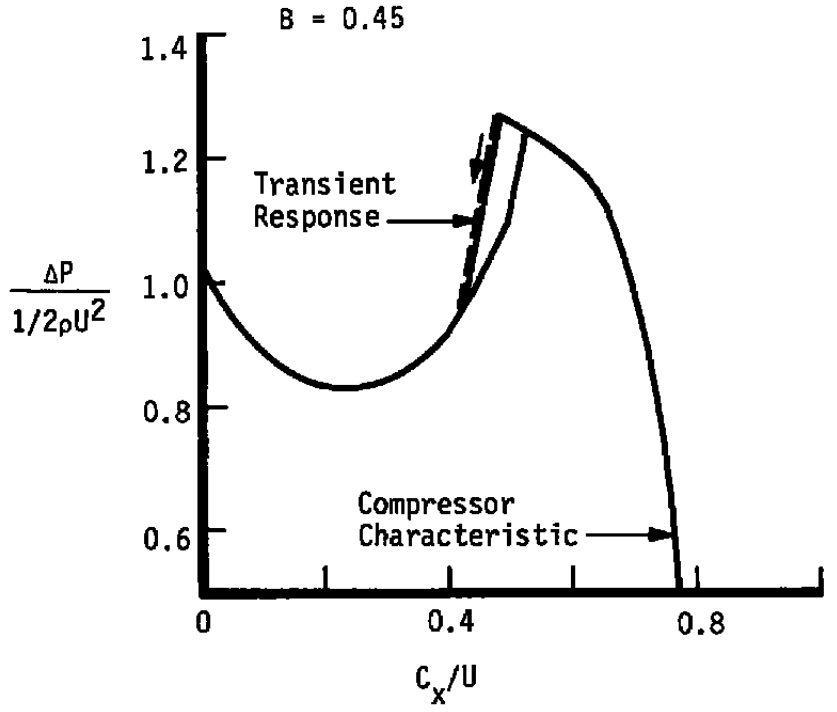

Figure 2. Theoretical transient compression system behavior, B = 0.45 (Ref. 13).

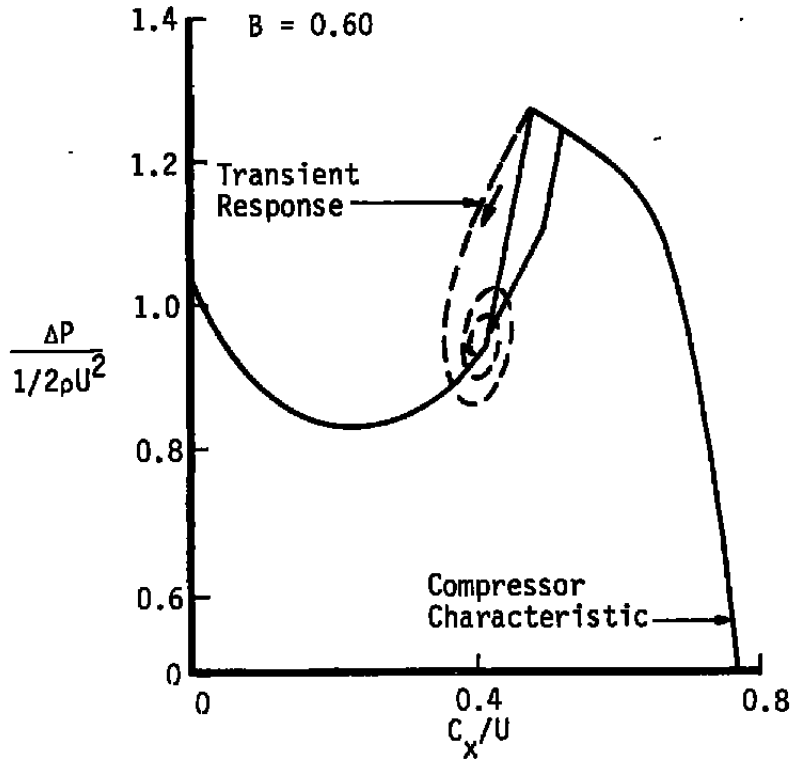

Figure 3. Theoretical transient compression system behavior, B = 0.60 (Ref. 13).

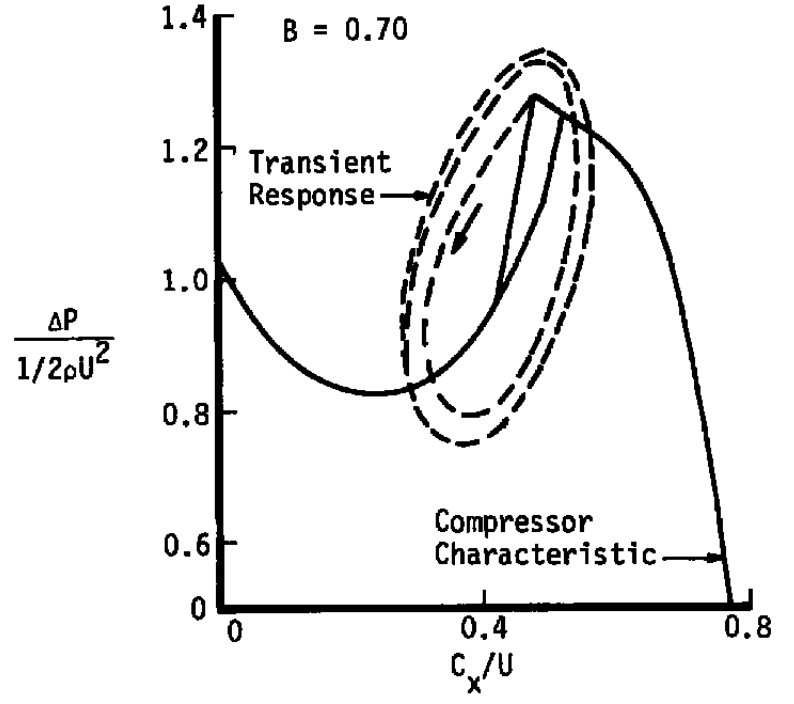

Figure 4. Theoretical transient compression system behavior, B = 0.70 (Ref. 13).

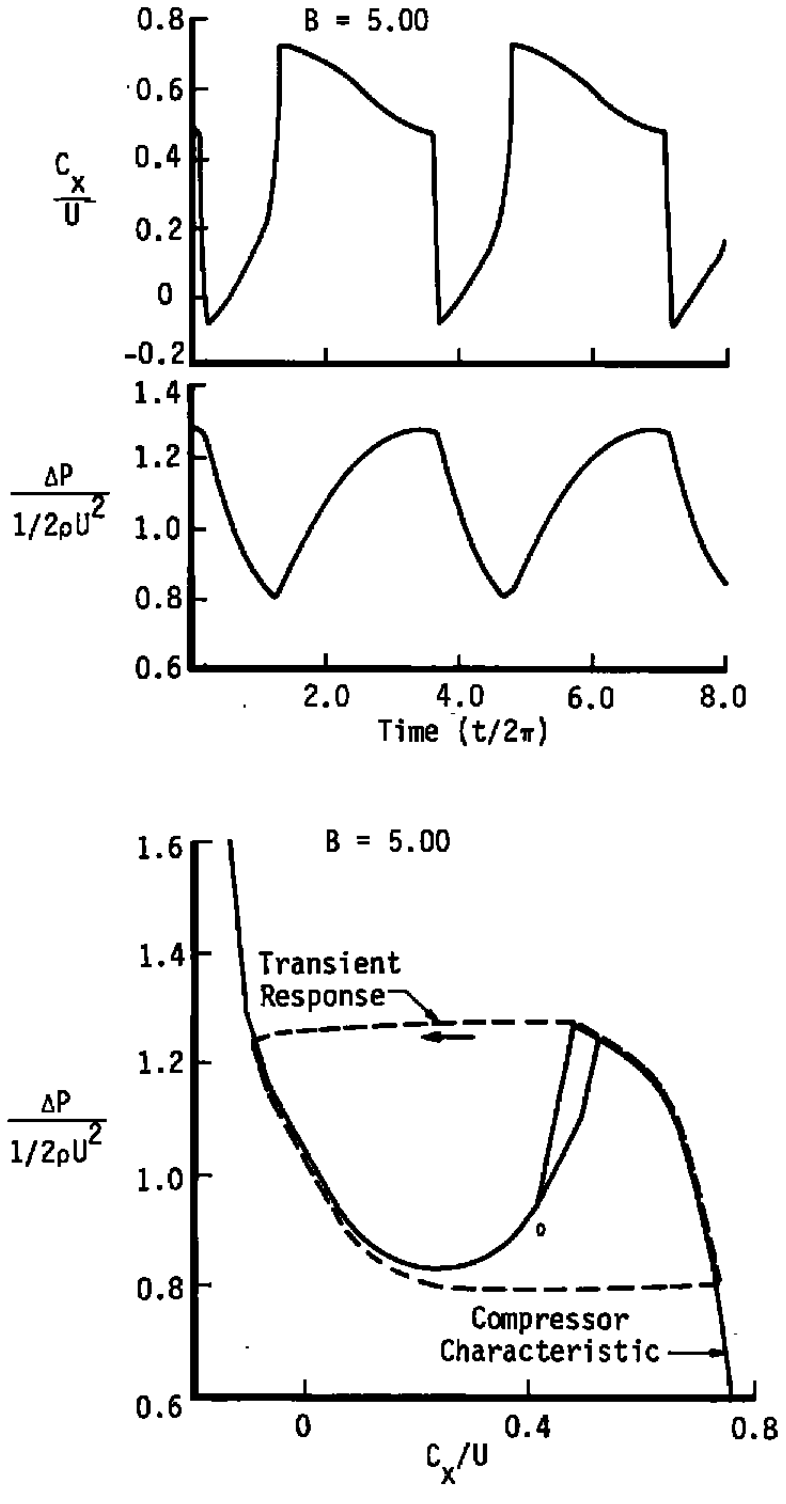

Figure 5. Theoretical transient compression system behavior, B = 5.00 (Ref. 13).

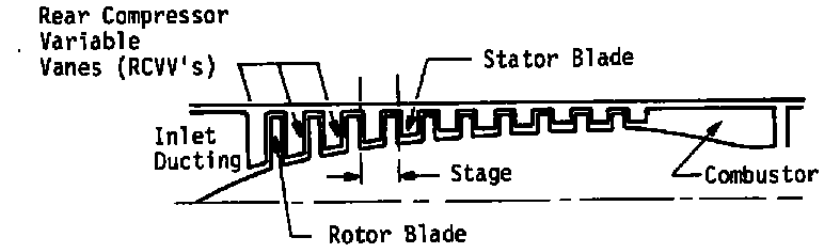

a. Compressor and ducting system

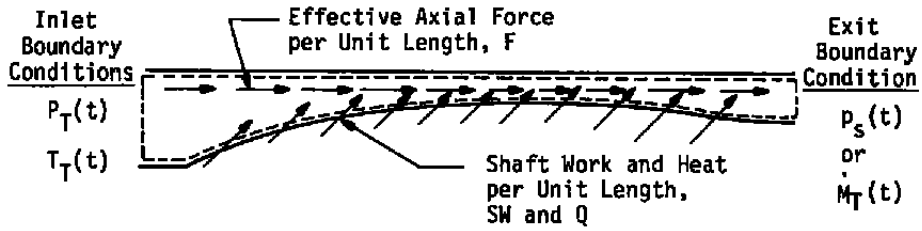

b. Overall control volume

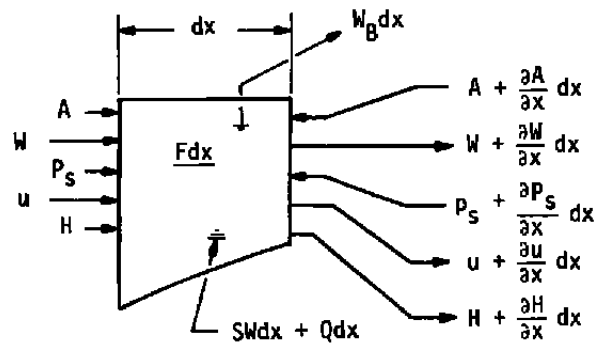

c. Elemental control volume

Figure 6. Physical compression system modeled and control volume concepts.

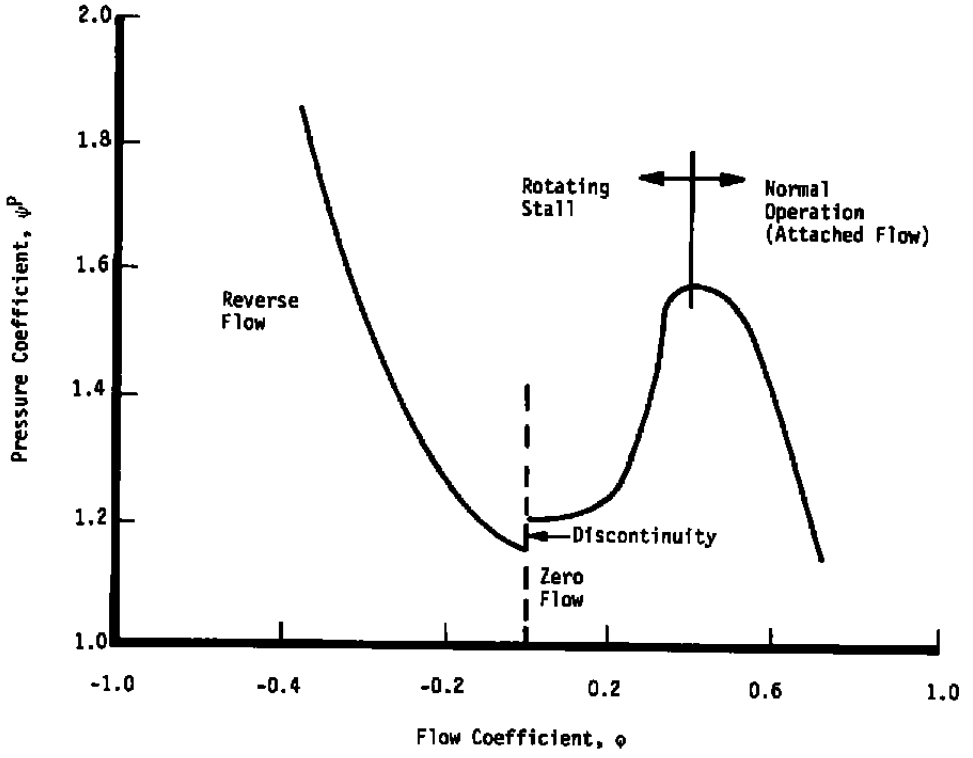

a. Pressure coefficient

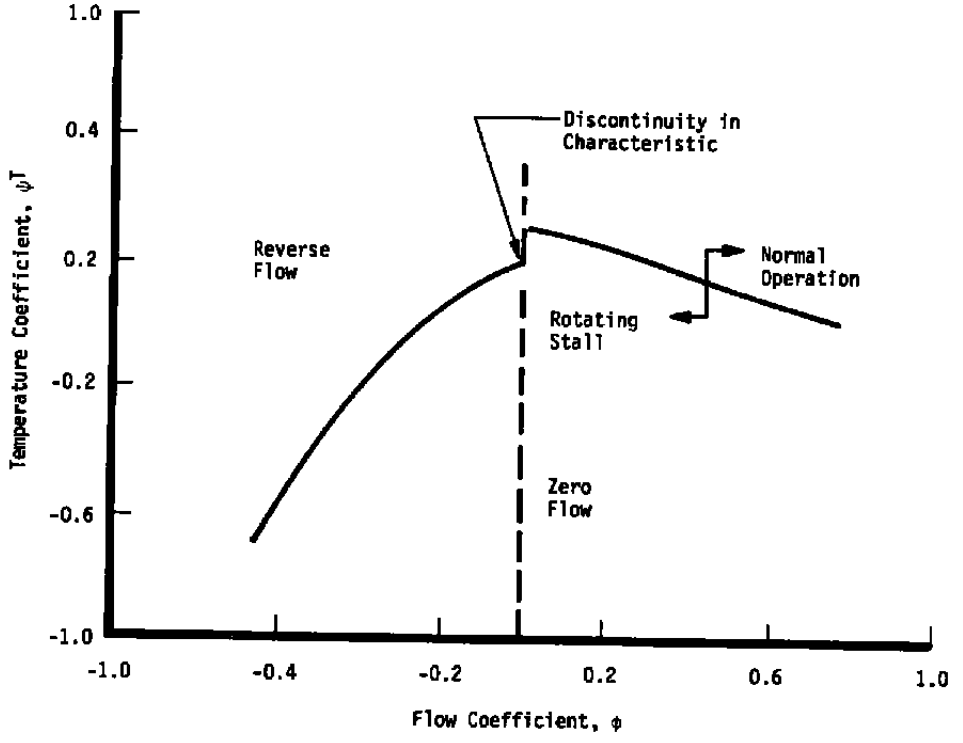

b. Temperature coefficient

Figure 7. Typical stage characteristics.

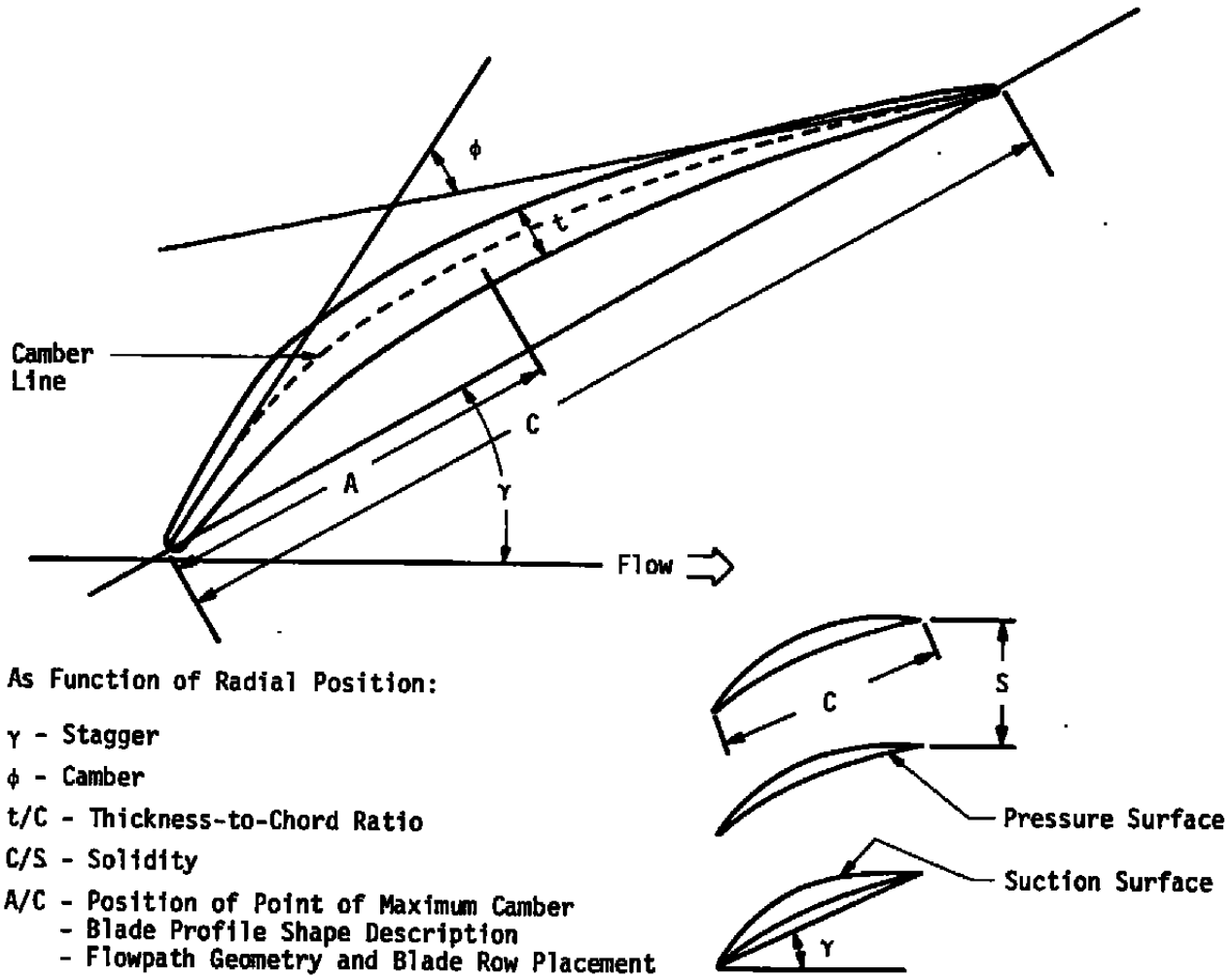

Figure 8. Blade geometry information required for COCODEC.

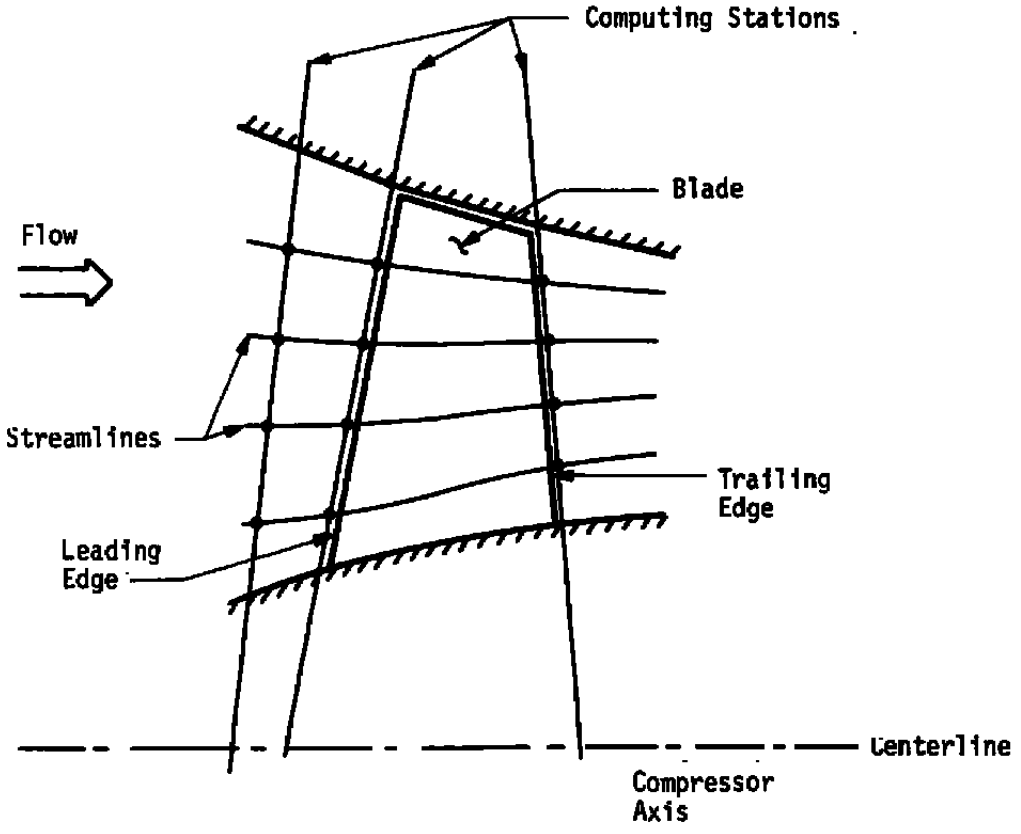

Figure 9. COCODEC computing mesh.

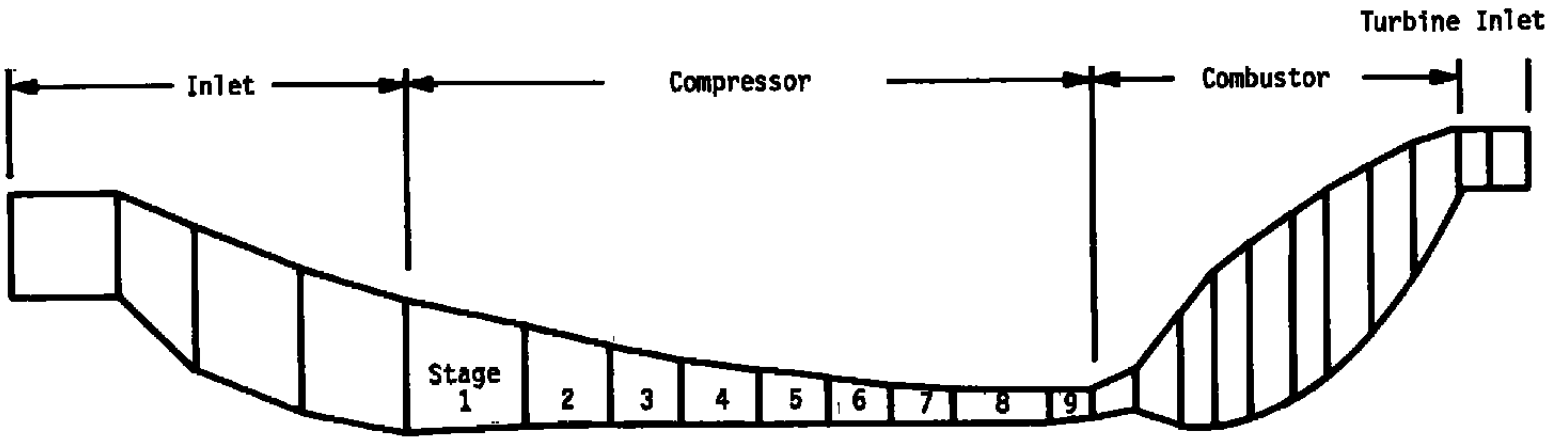

Figure 10. Control volume schematic of nine-stage compressor with representative combustor.

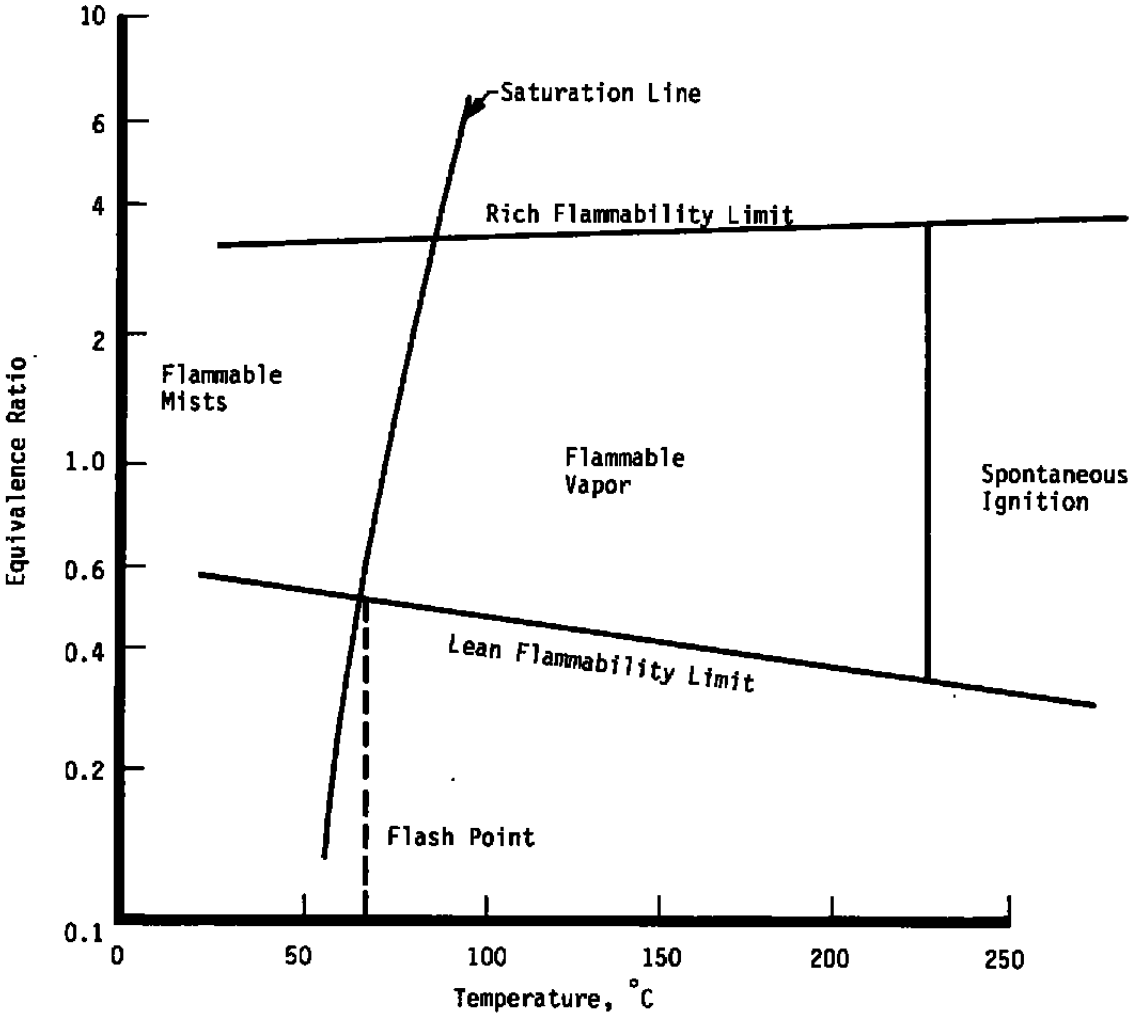

Figure 11. Flammability characteristics for a kerosene-type fuel in air at atmospheric pressure (Ref. 26).

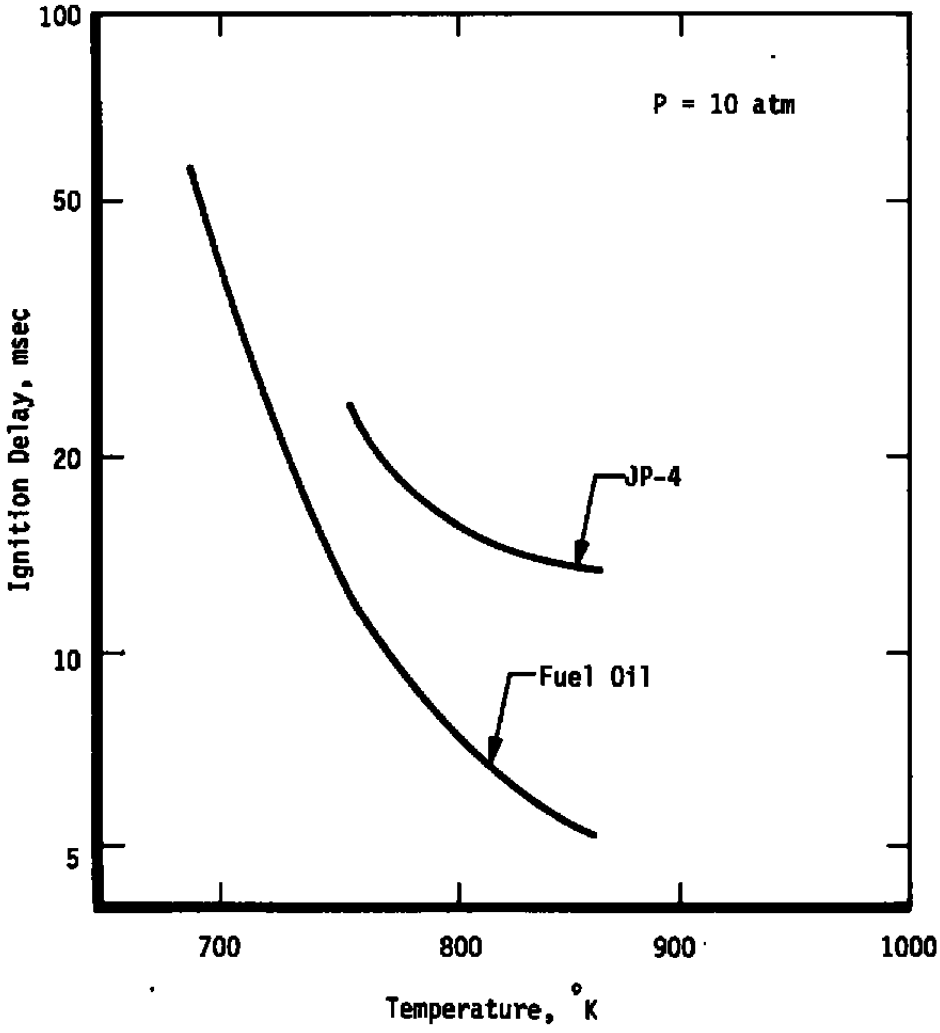

Figure 12. Ignition delay times for practical fuels (Ref. 26).

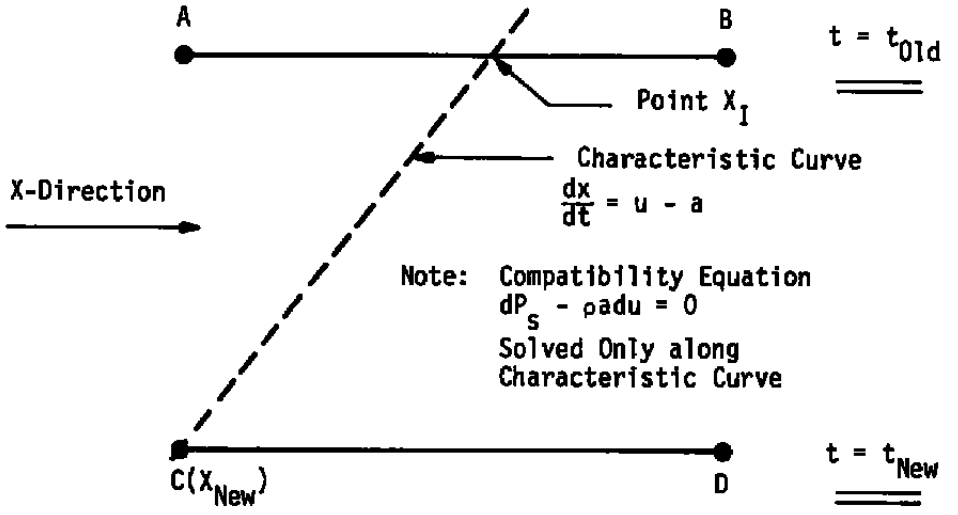

Figure 13. Schematic of inlet characteristic boundary scheme.

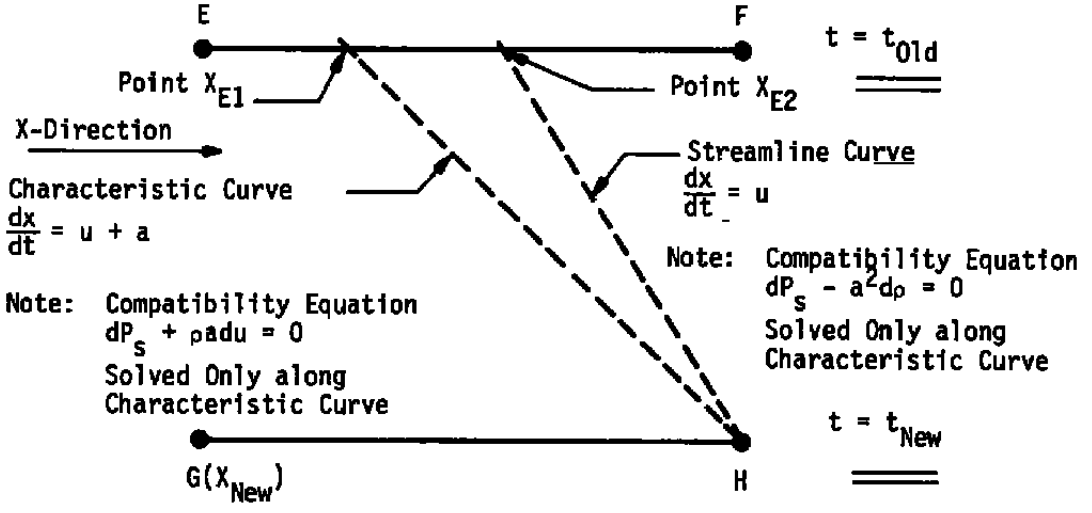

Figure 14. Schematic of exit characteristic boundary scheme.

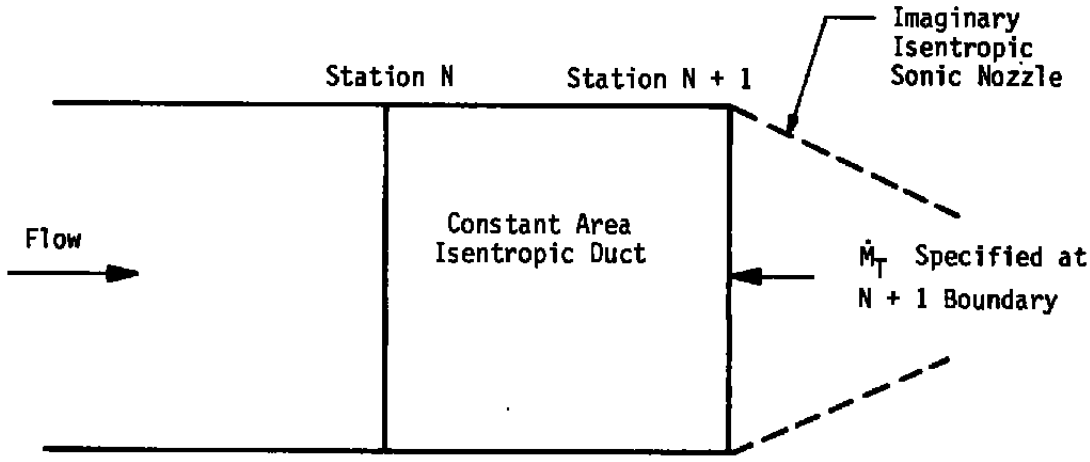

Figure 15. Sonic nozzle exit boundary condition.

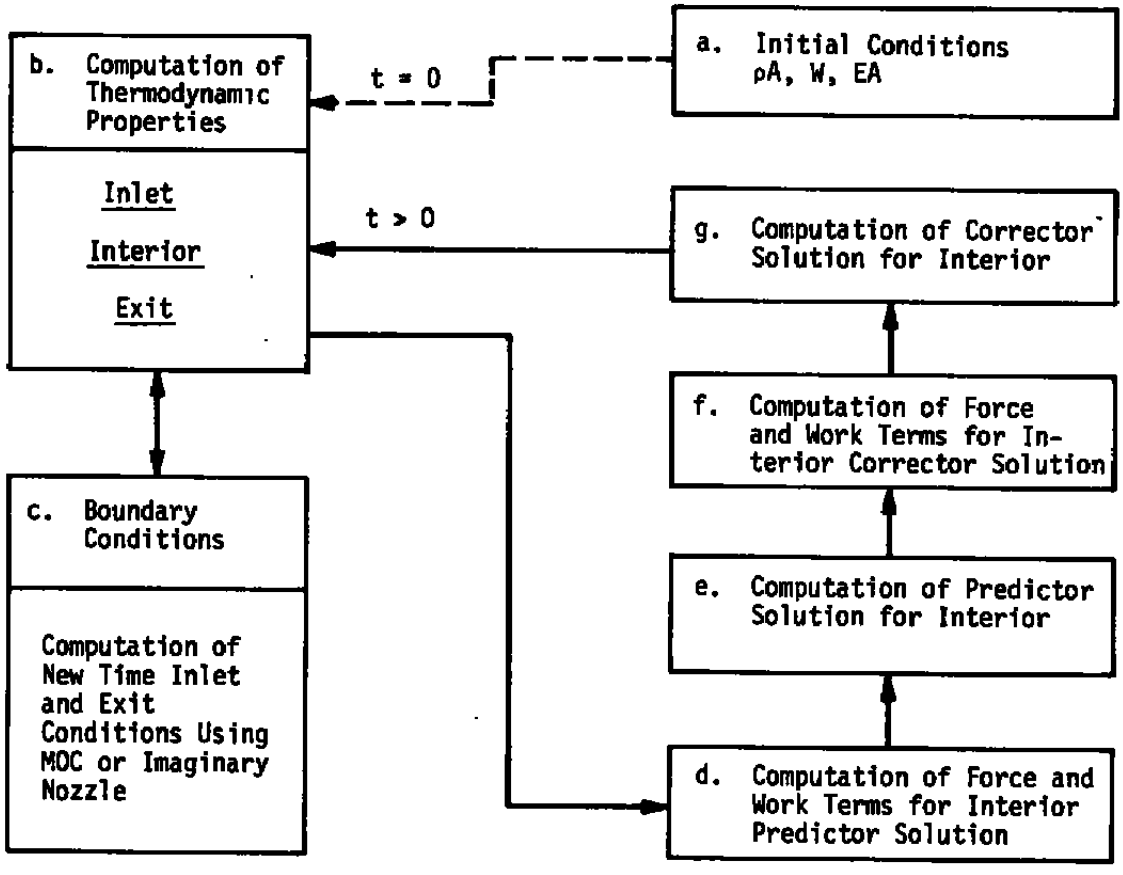

Figure 16. Time-dependent compressor model solution procedure.

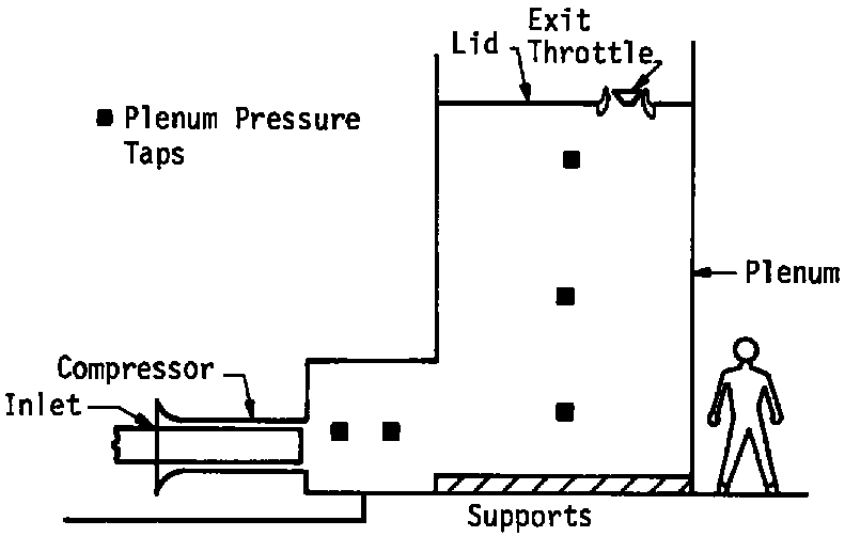

Figure 17. Scale section of compressor/plenum configuration (Ref. 1).

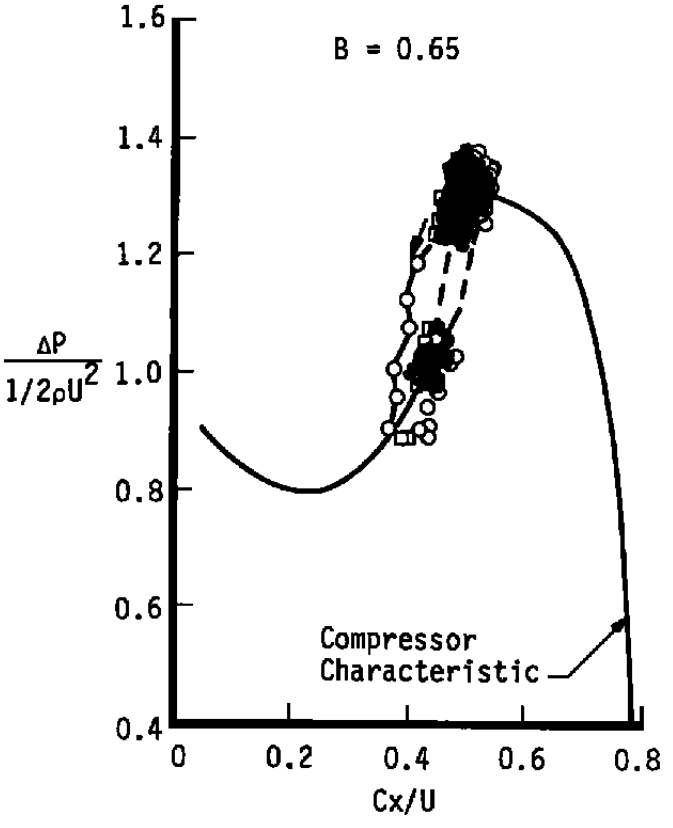

Figure 18. Transient compression system response, B = 0.65 (Ref. 1).

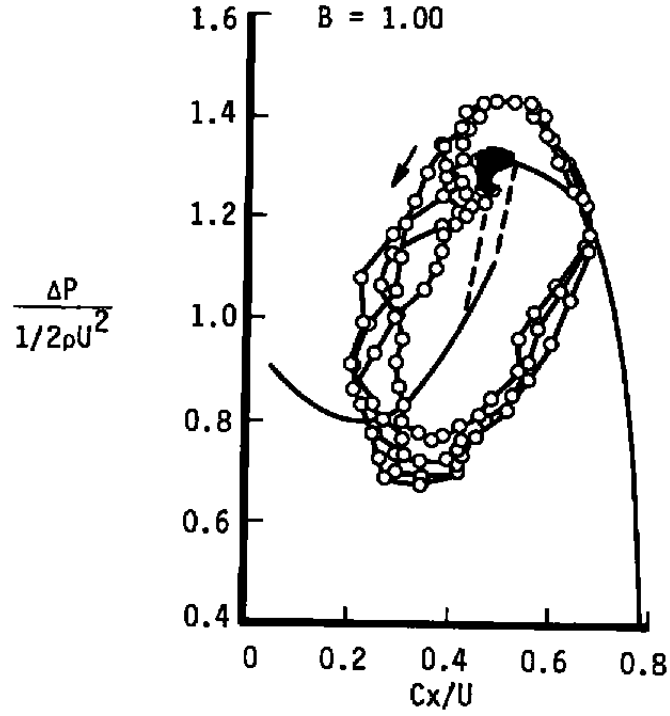

Figure 19. Transient compression system response (low speed, large volume), B = 1.00 (Ref. 1).

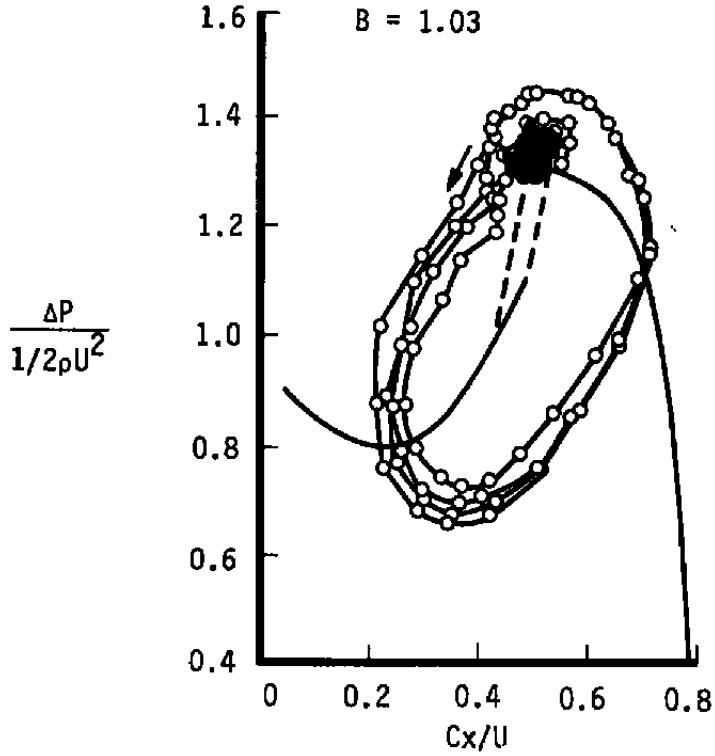

Figure 20. Transient compression system response (high speed, small volume), B = 1.03 (Ref. 1).

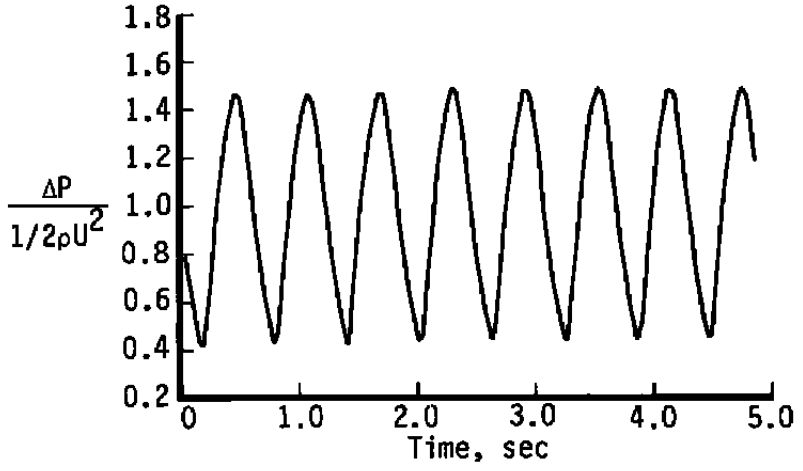

a. Pressure oscilliations during deep surge cycle, B = 1.58

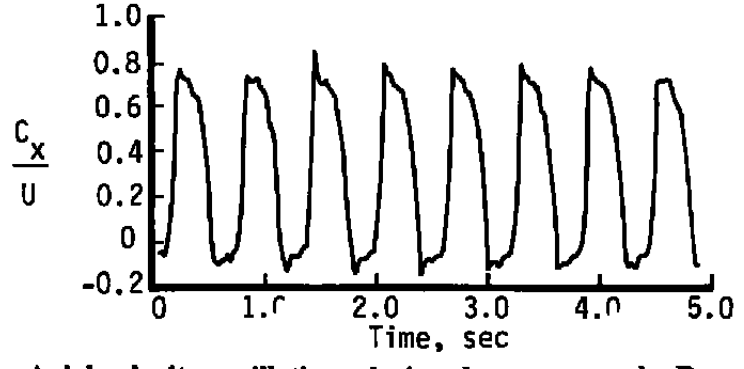

b. Axial velocity oscillations during deep surge cycle, B = 1.58

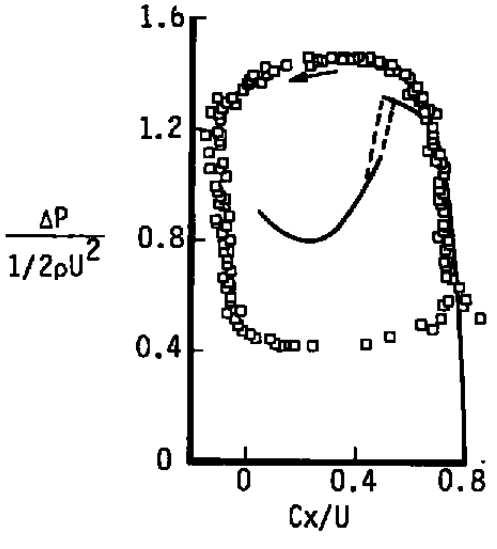

c. Deep surge cycle, B = 1.58

Figure 21. Compression system performance during deep surge cycles (Ref. 1).

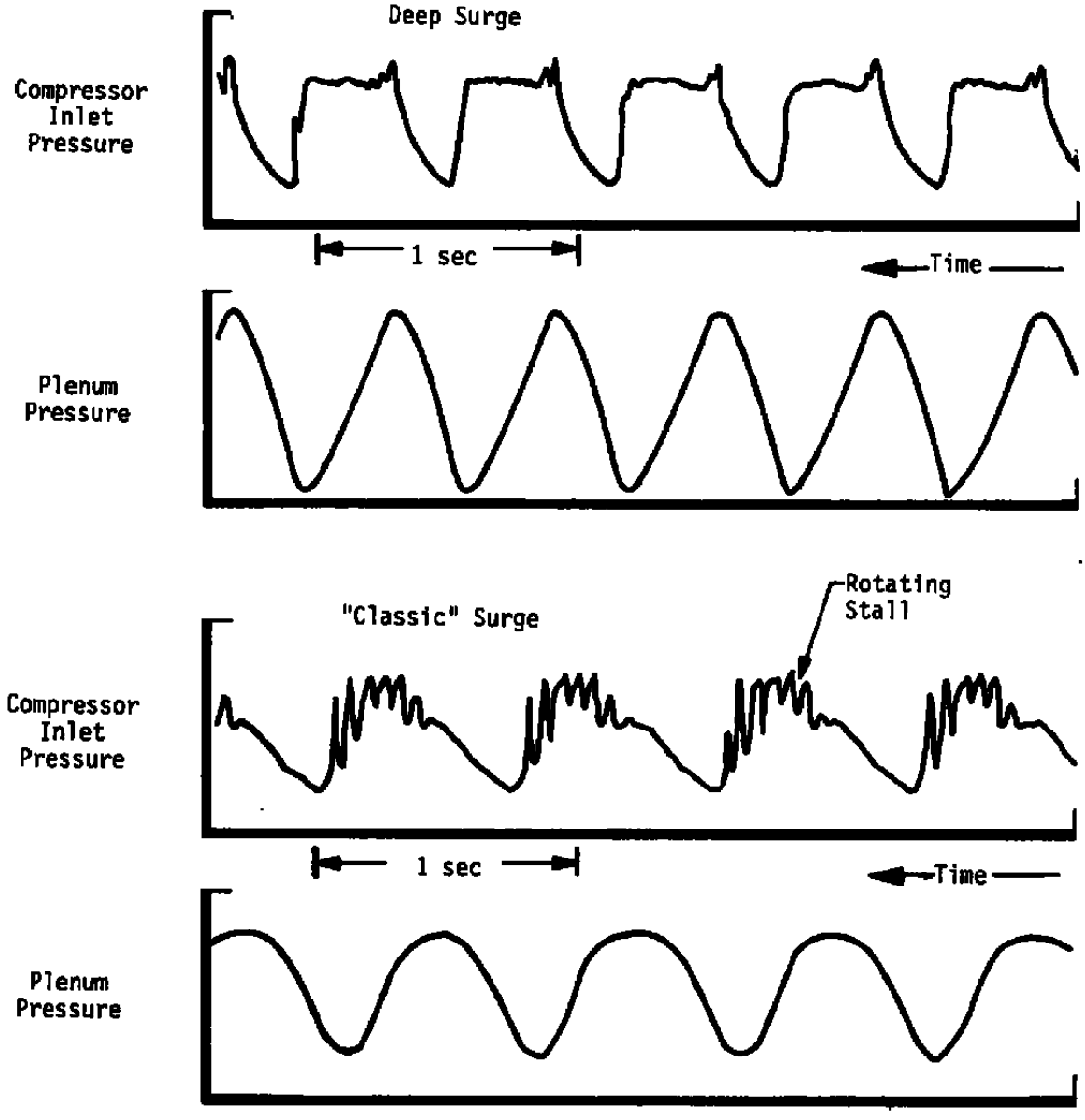

Figure 22. Pressure oscillations during deep surge and classic surge (Ref. 1).

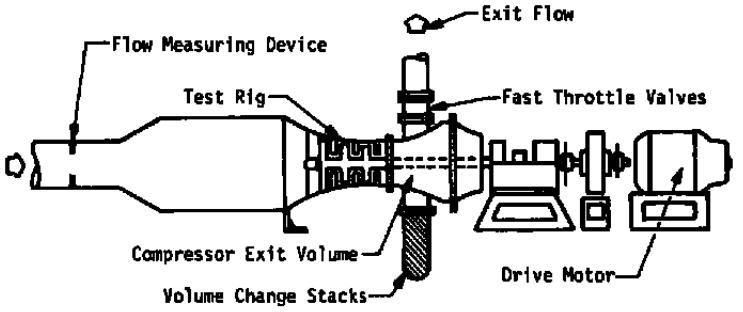

Figure 23. Compressor rig for stall recovery of the high-speed research compressor (Ref. 4).

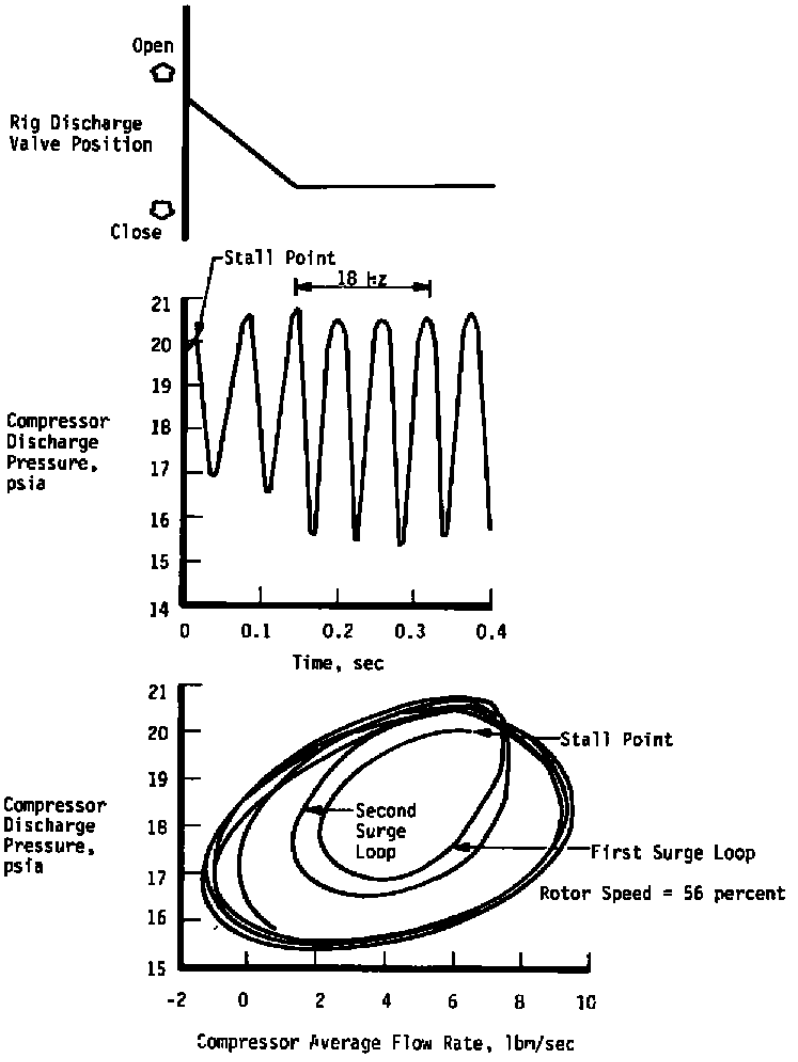

Figure 24. Recoverable stall data for high-speed research compressor rig (Ref. 4).

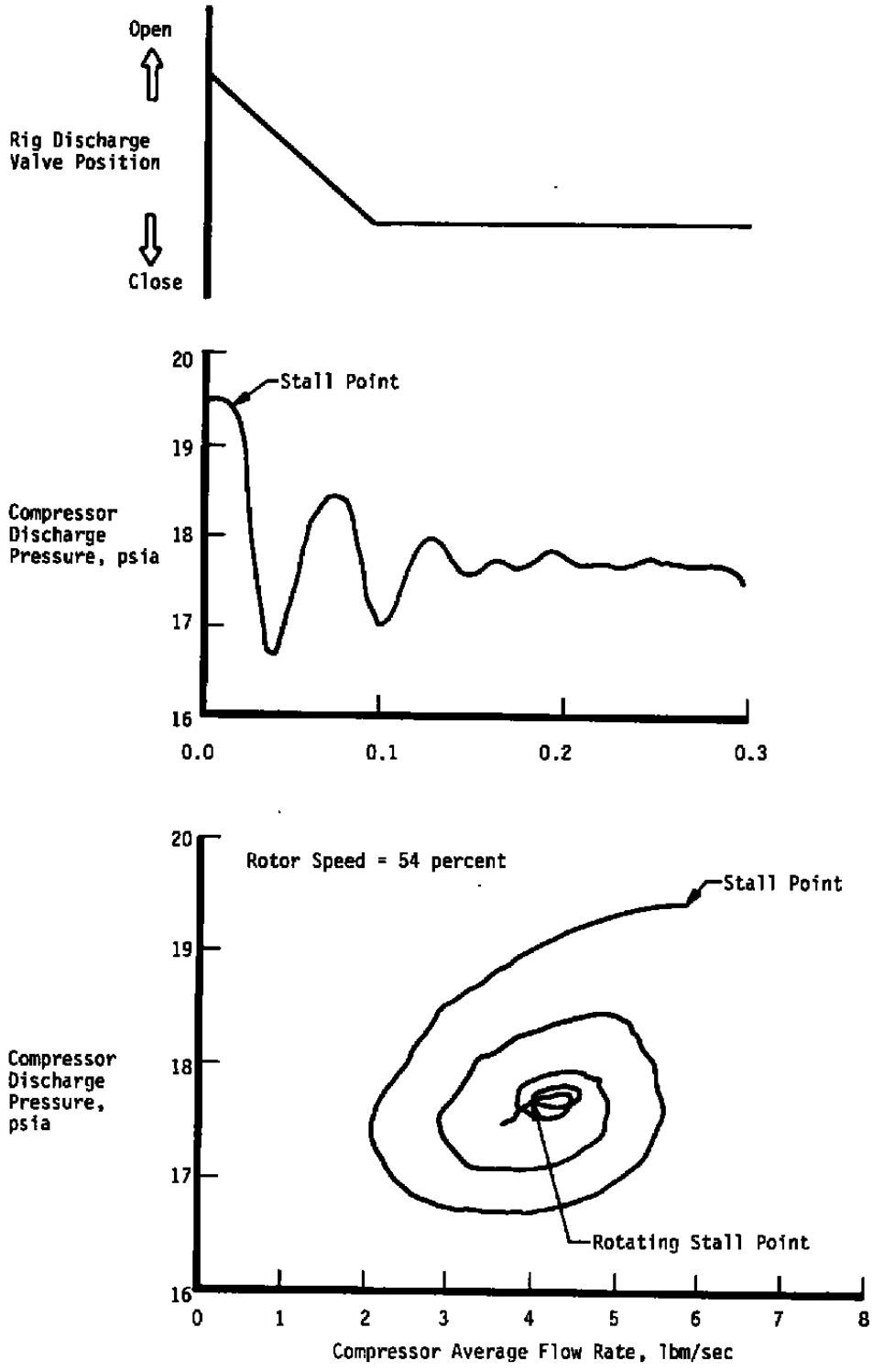

Figure 25. Nonrecoverable stall data for high-speed research compressor rig (Ref. 4).

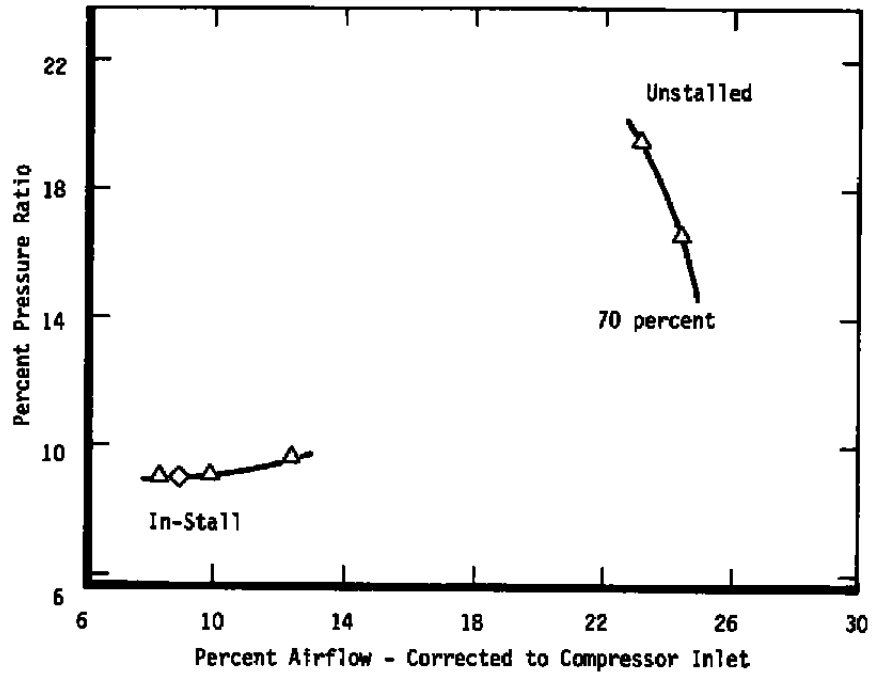

Figure 26. Energy-efficient compressor performance at 70-percent speed.

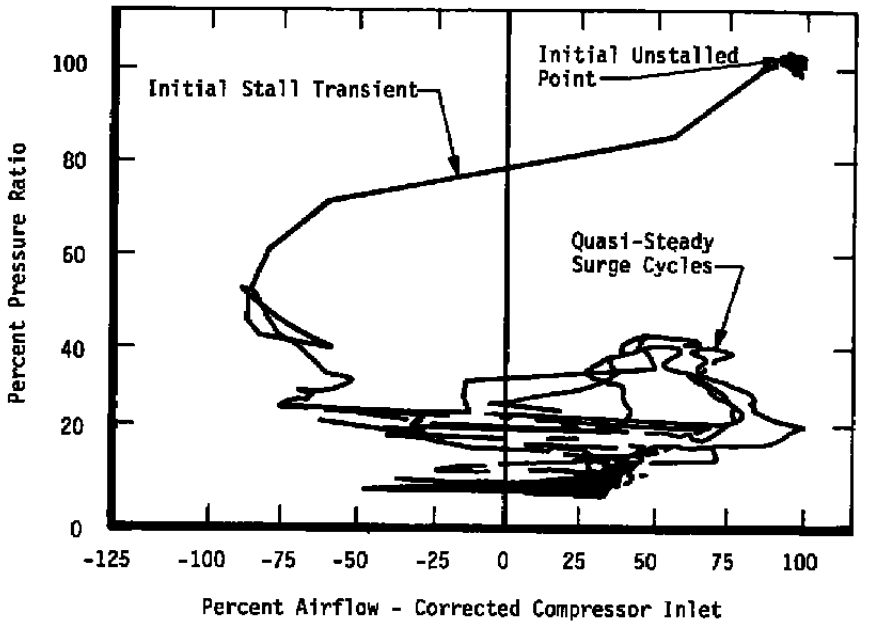

Figure 27. Energy-efficient compressor surge transient at 98.5-percent corrected speed (Ref. 33).

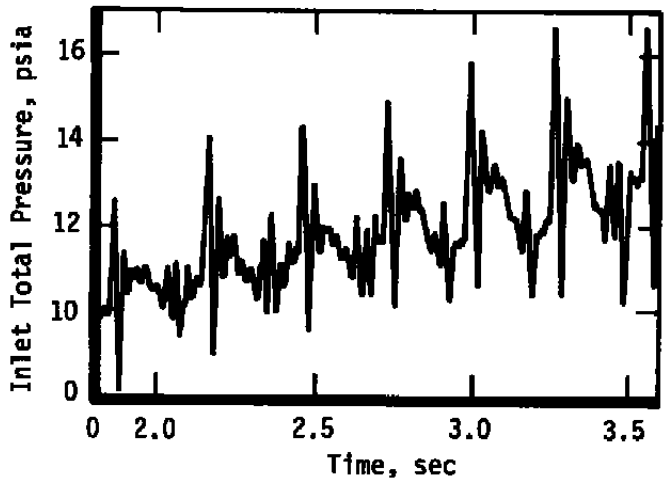

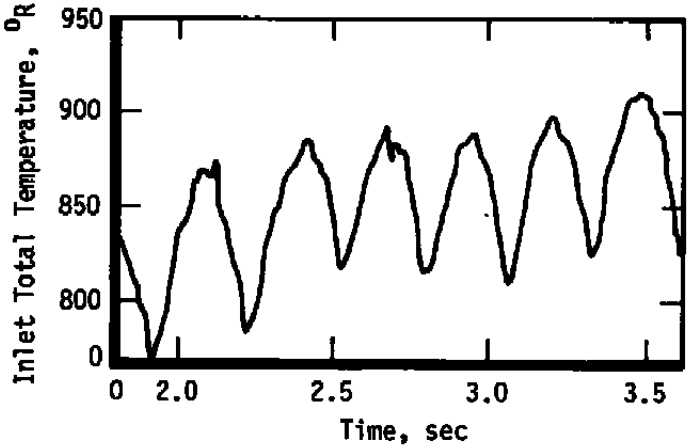

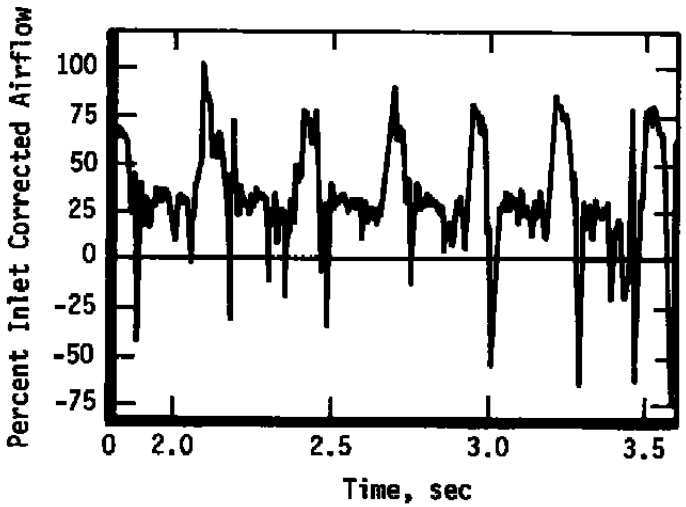

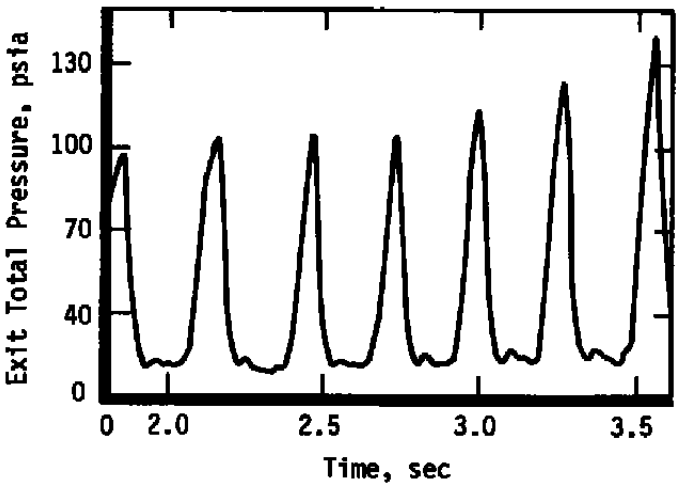

Figure 28. Energy-efficient compressor surge transient at 98.5-percent speed surge cycles (Ref. 33).

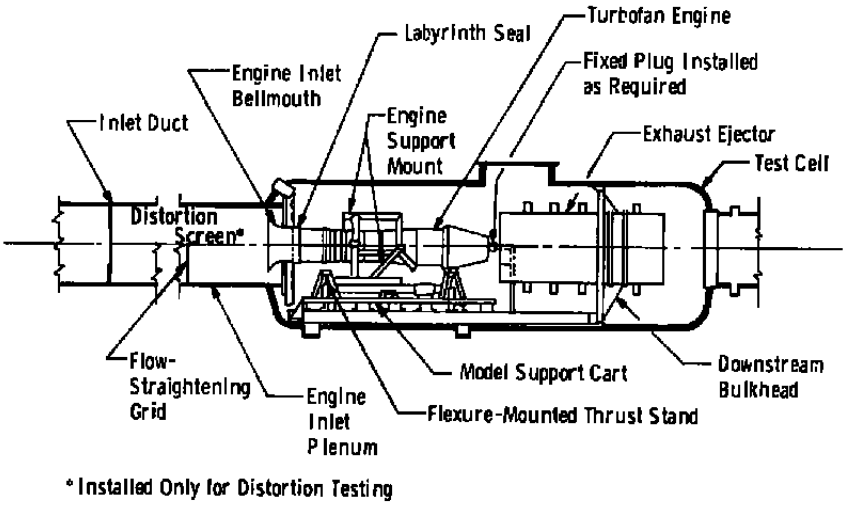

Figure 29. Typical engine installation (Ref. 3).

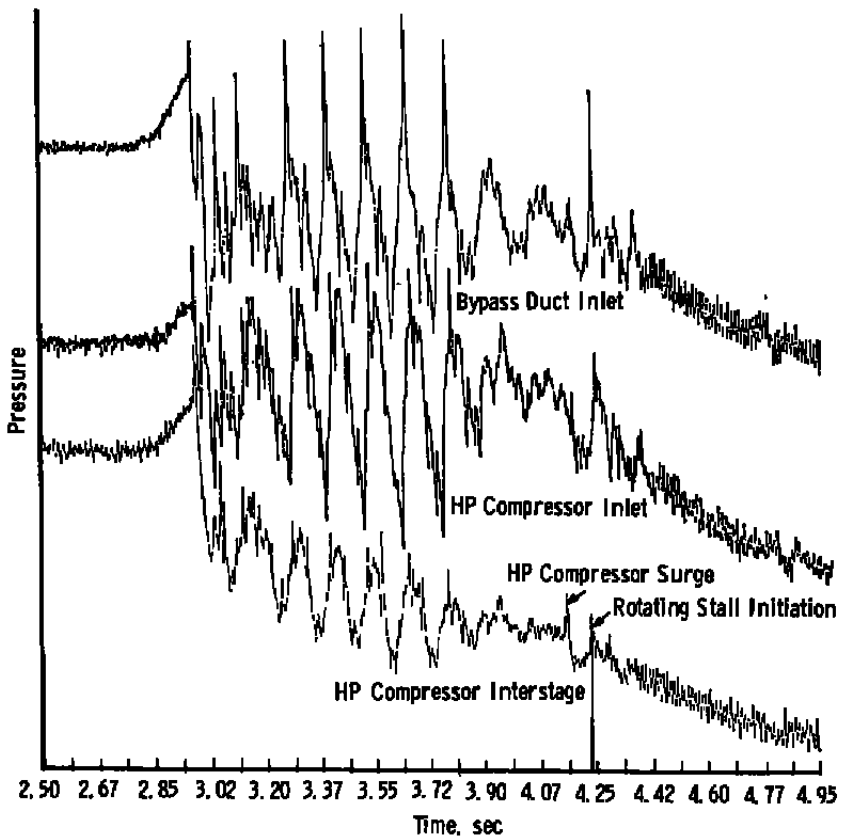

Figure 30. Compressor pressure performance during post-stall events (Ref. 3).

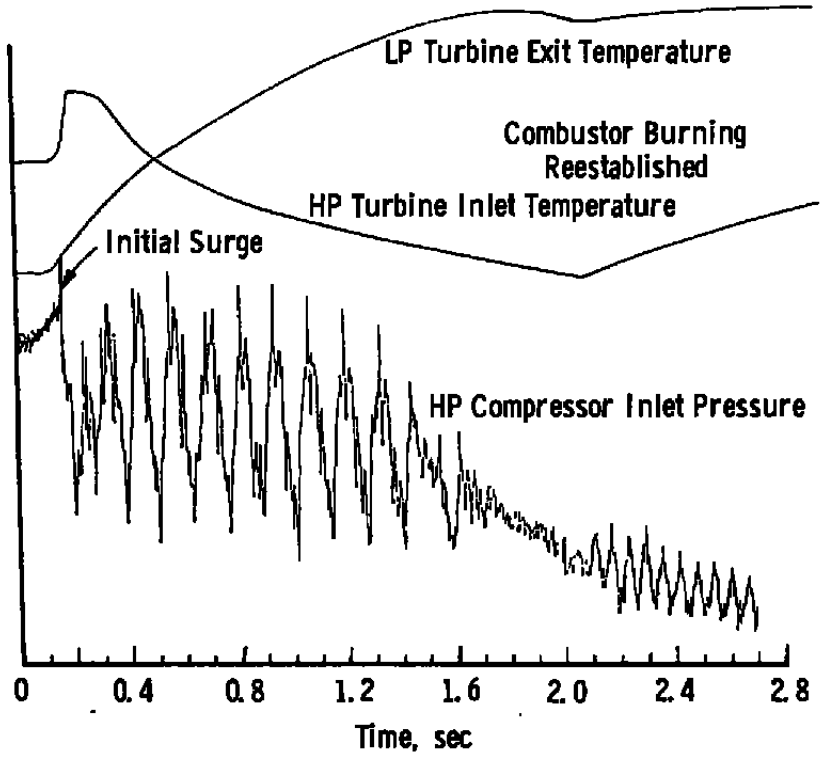

Figure 31. Core engine performance during post-stall events (Ref. 3).

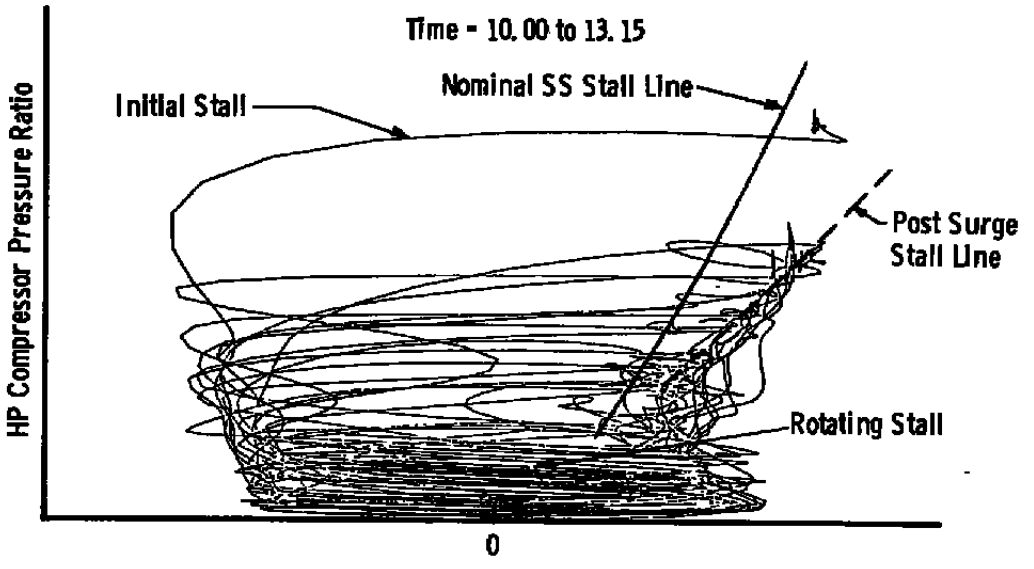

Figure 32. Typical rotating stall trajectories (Ref. 3).

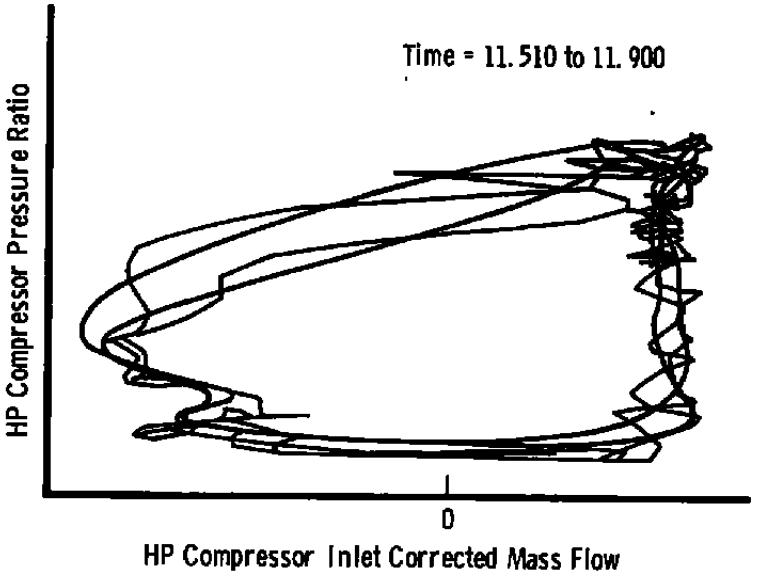

Figure 33. Typical surge cycles (Ref. 3).

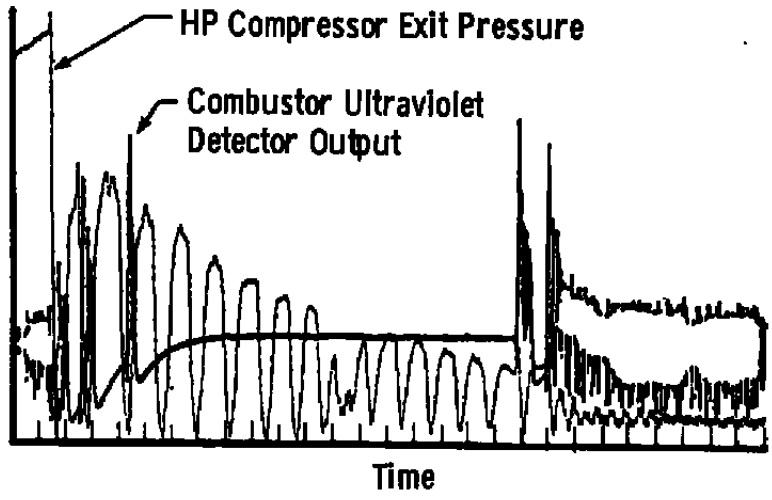

a. Complete combustor blowout

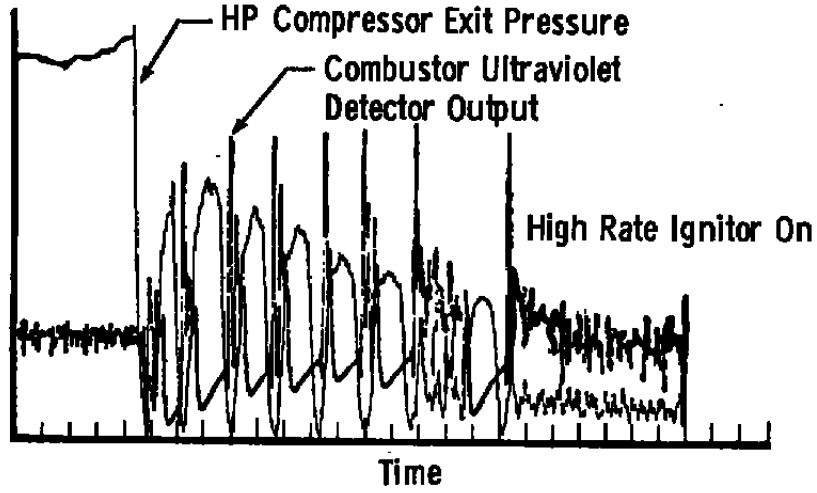

b. Intermittent combustor blowout

Figure 34. Compressor/combustor interactions during post-stall events (Ref. 3).

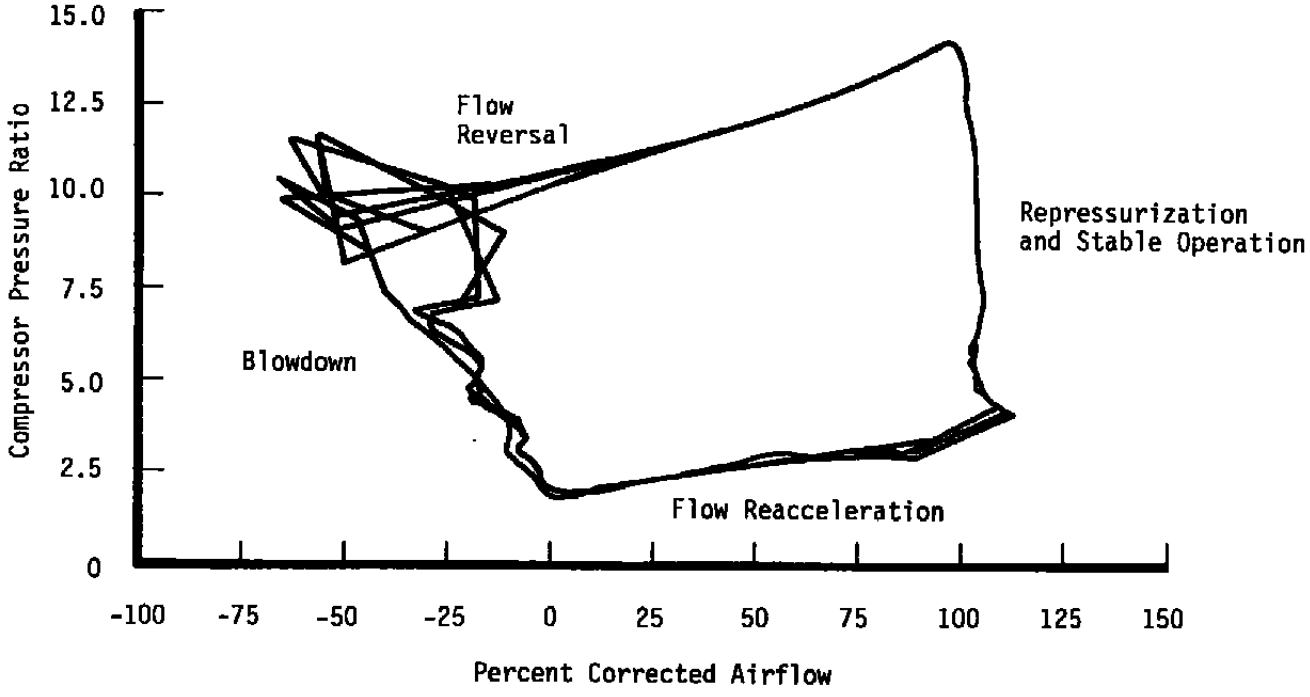

Figure 35. Model compression system performance trajectories during surge at 100-percent speed, no burning in combustor.

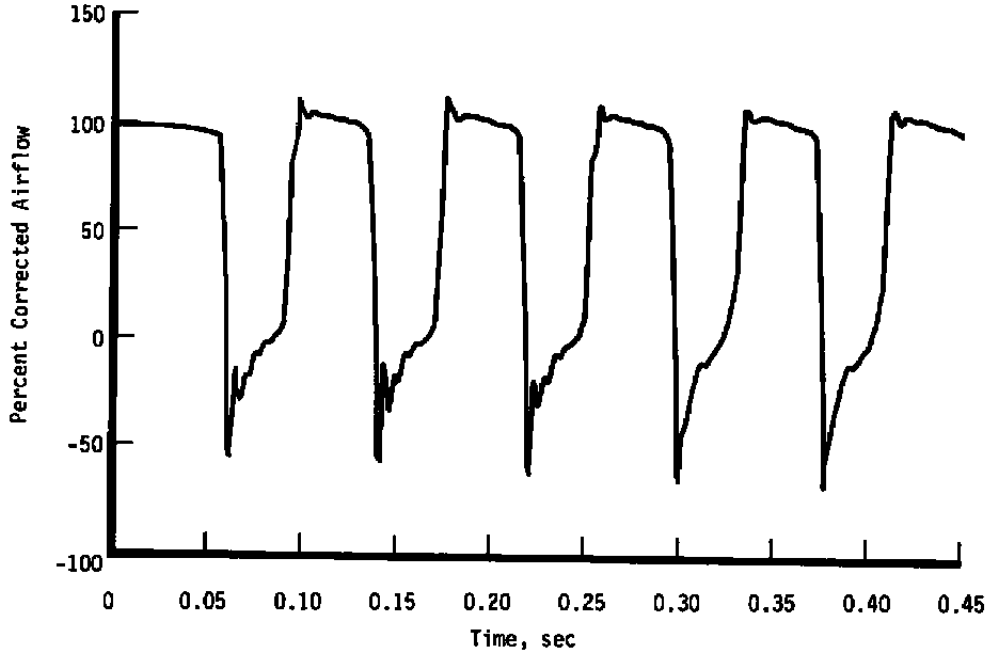

a. Corrected airflow

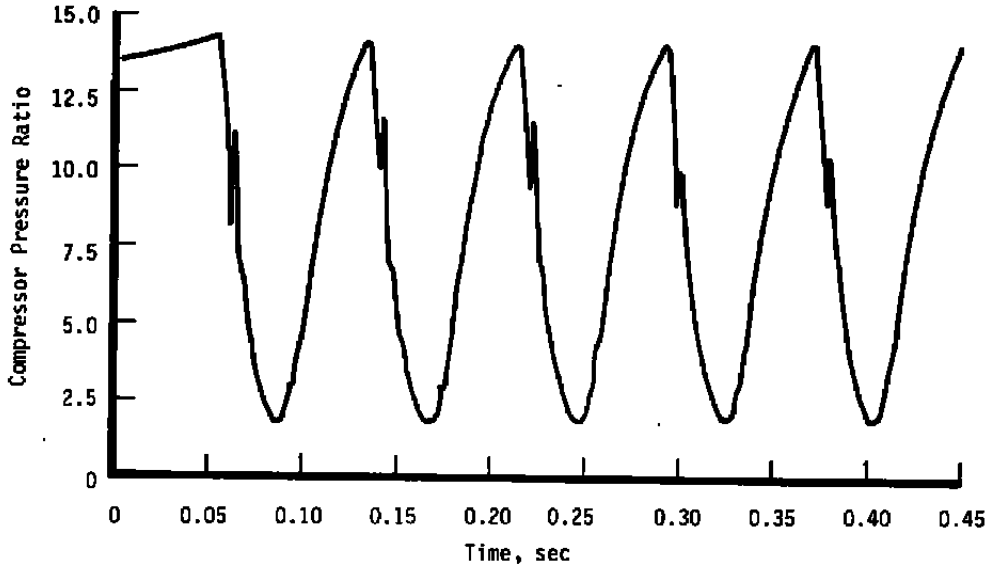

b. Overall pressure ratio

Figure 36. Model compression system performance during surge at 100-percent speed, no burning in combustor.

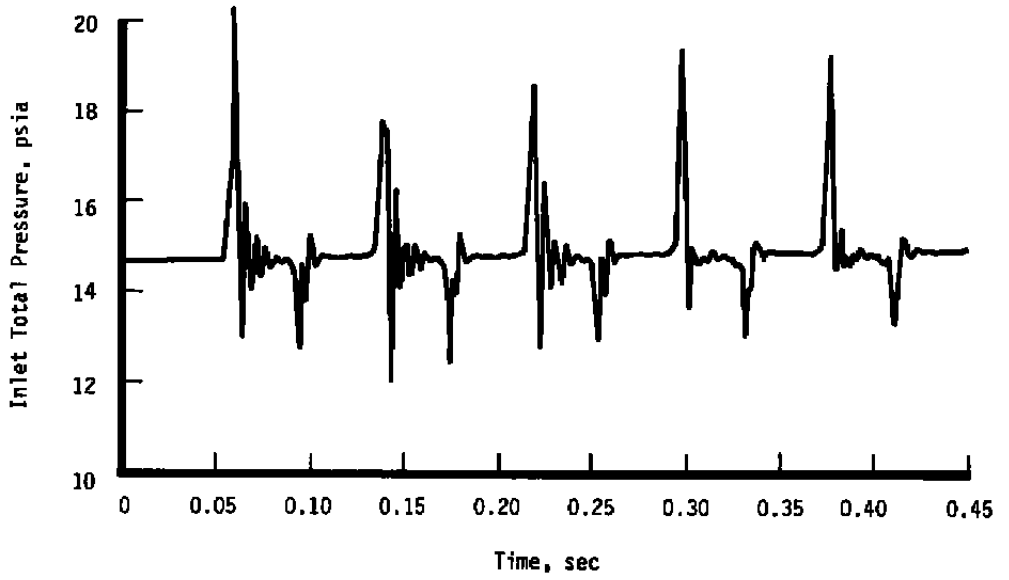

c. Inlet total pressure

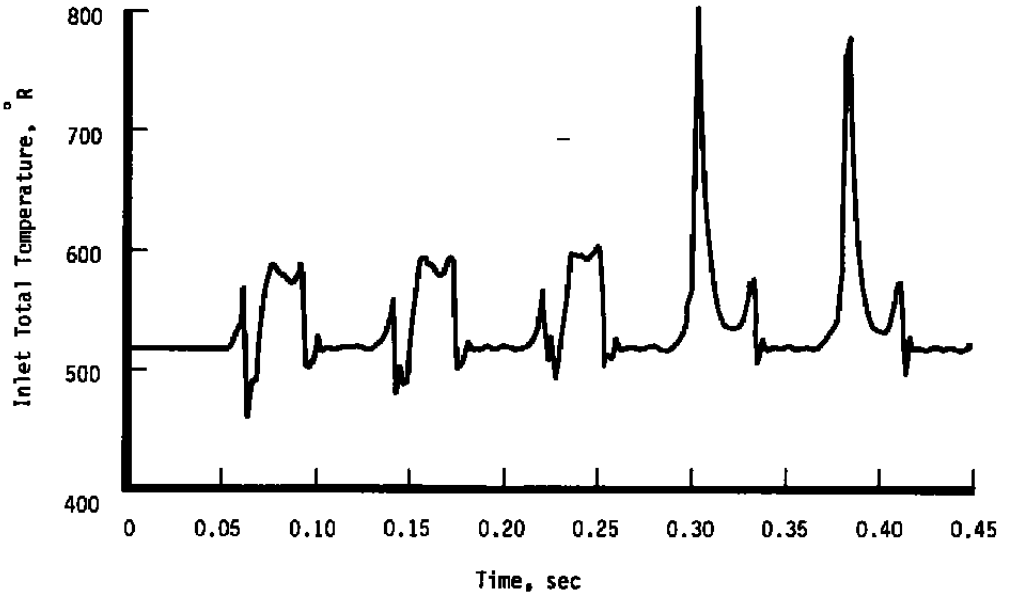

d. Inlet total temperature

Figure 36. Continued.

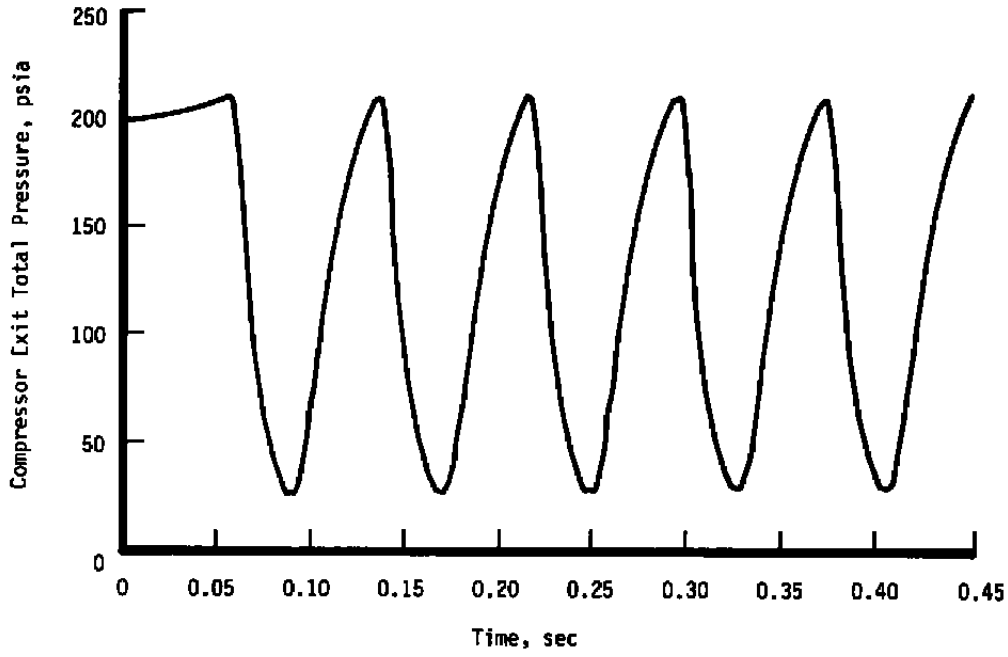

e. Exit total pressure

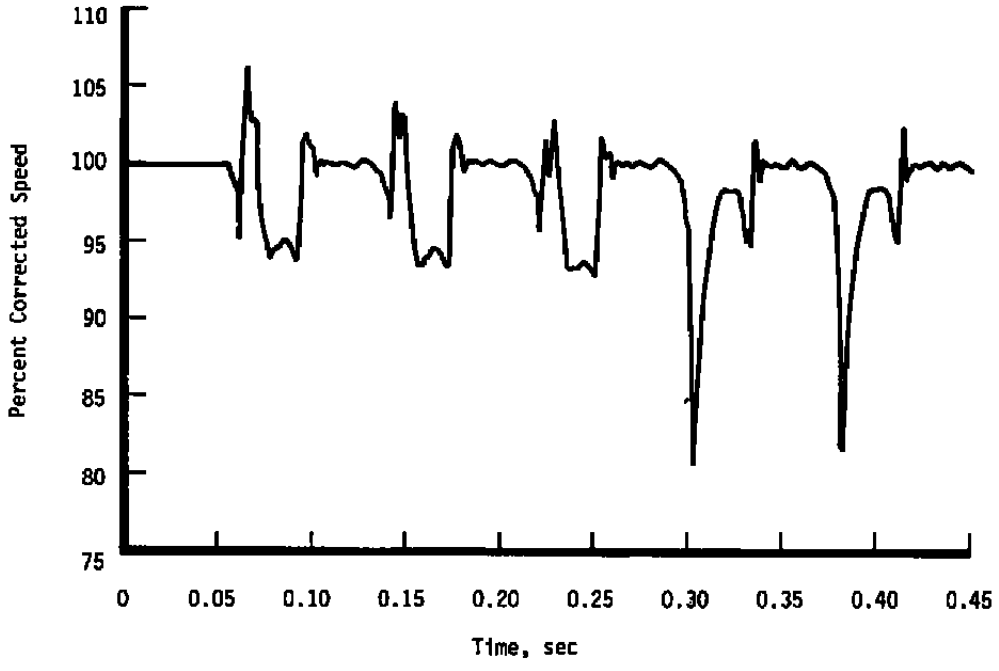

f. Corrected speed

Figure 36. Concluded.

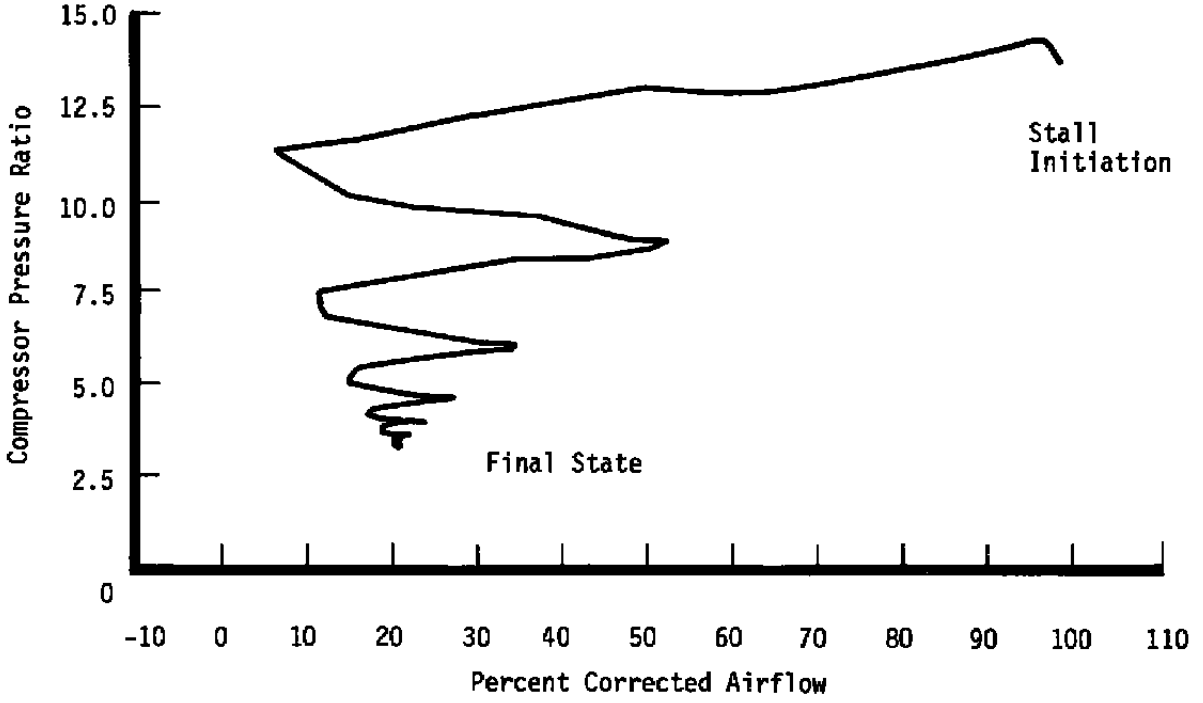

Figure 37. Model compression system performance trajectory during rotating stall at 100-percent speed, no burning in combustor.

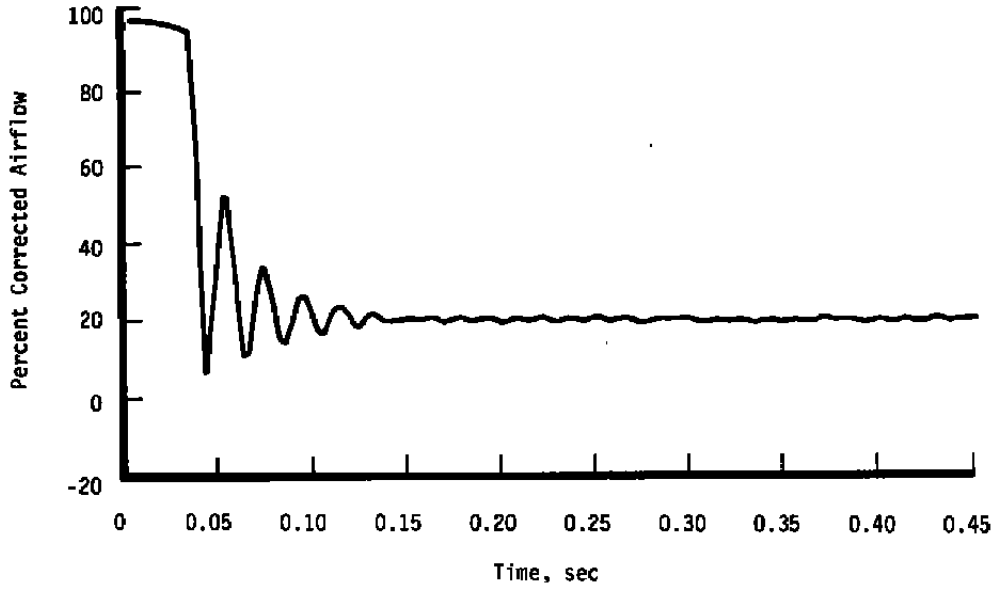

a. Corrected airflow

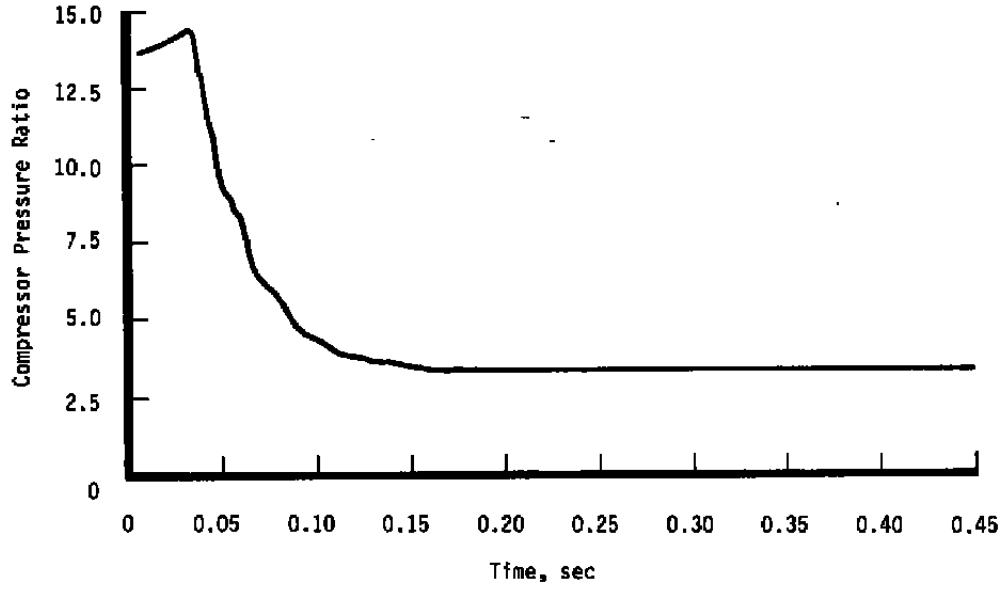

b. Overall pressure ratio

Figure 38. Model compression system performance during rotating stall at 100-percent speed, no burning in combustor.

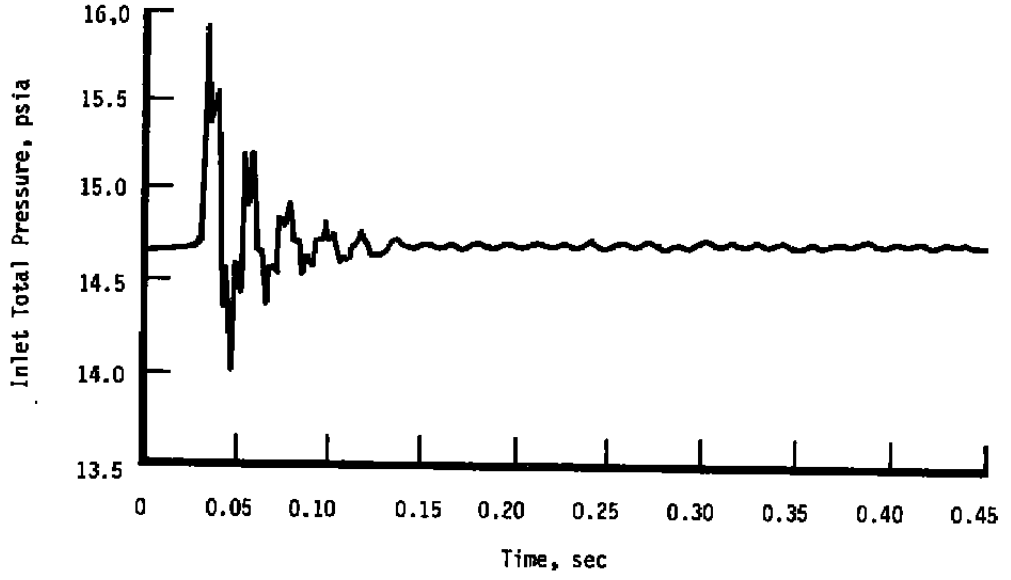

c. Inlet total pressure

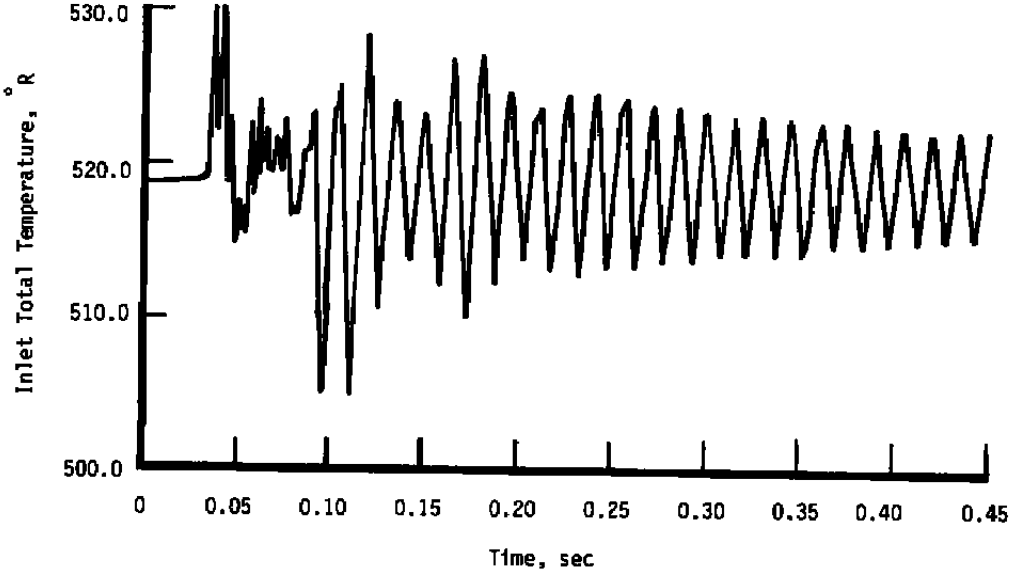

d. Inlet total temperature

Figure 38. Continued.

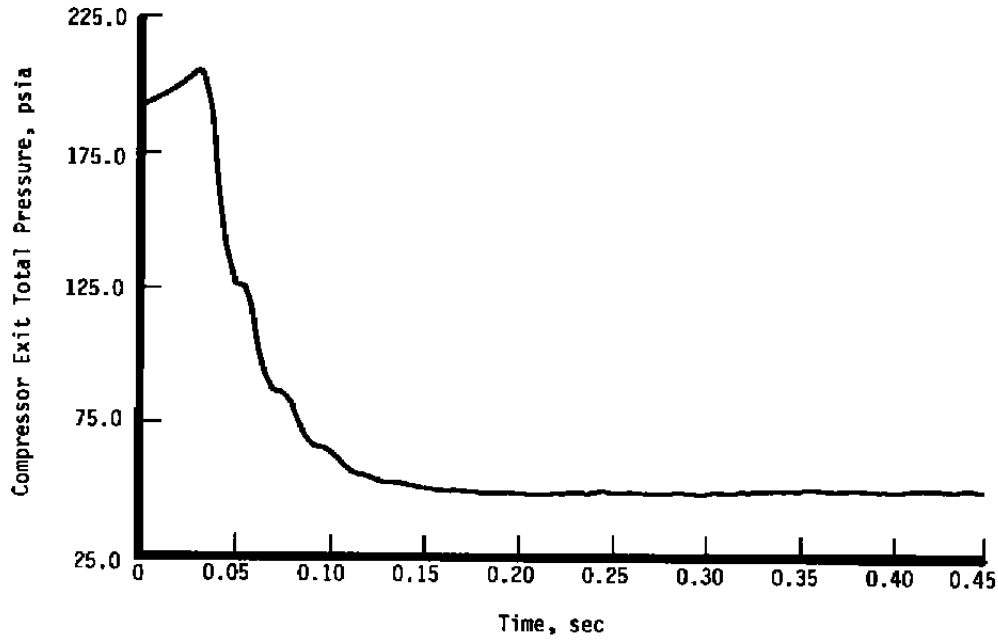

e. Exit total pressure

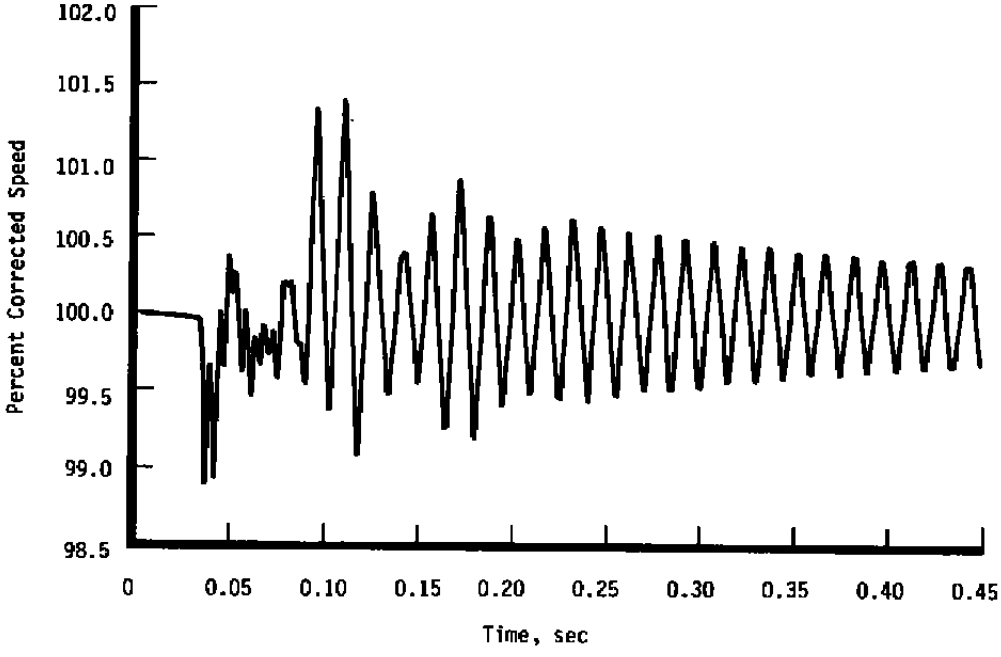

f. Corrected speed

Figure 38. Concluded.

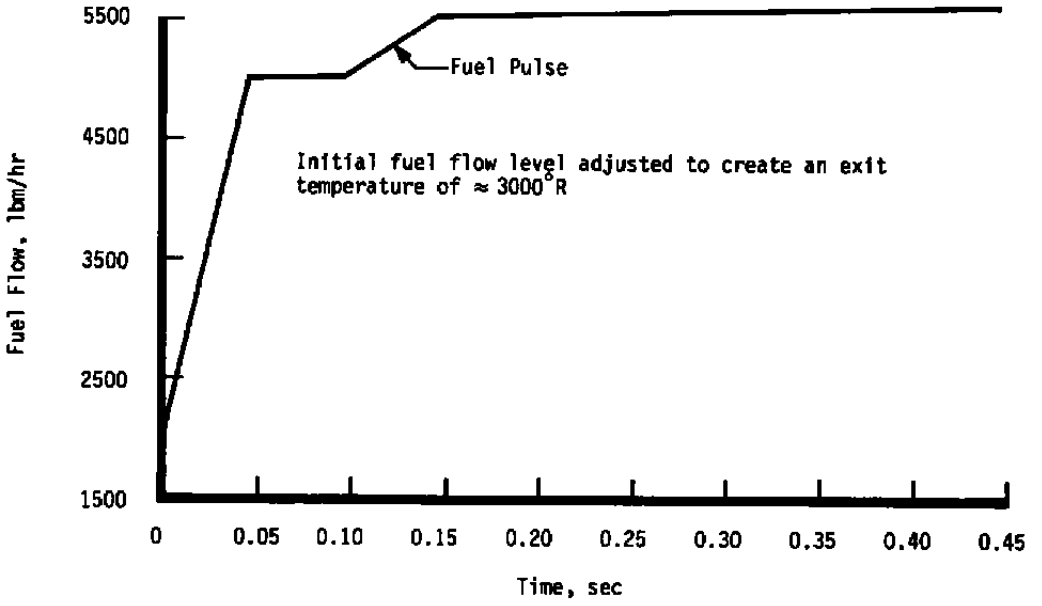

a. Combustor fuel flow

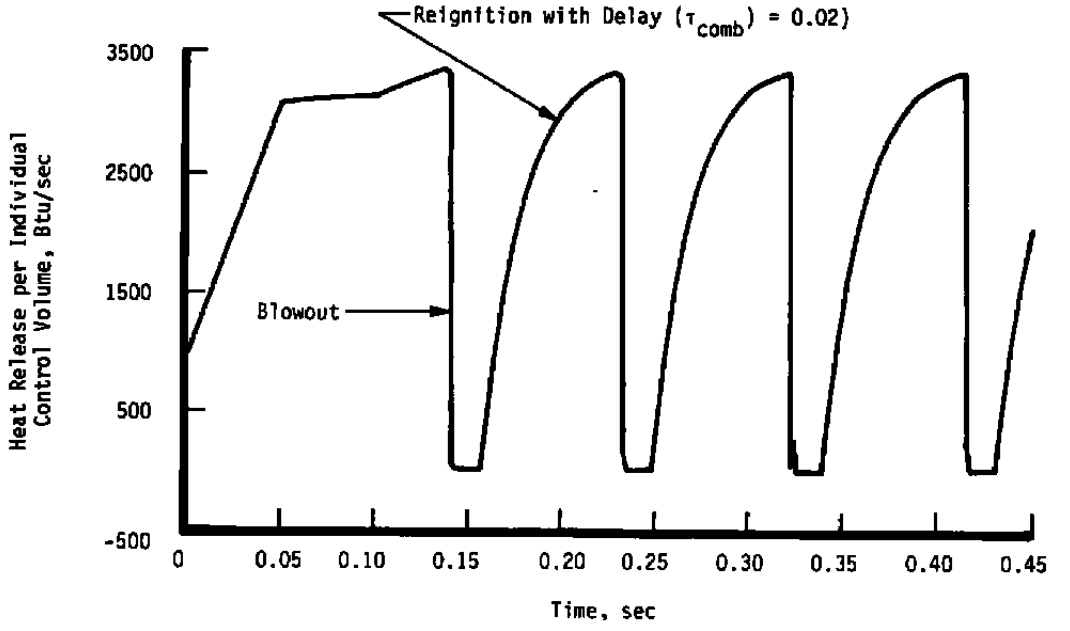

b. Control volume heat release

Figure 39. Model combustor fuel flow and heat release initiating compression system surge.

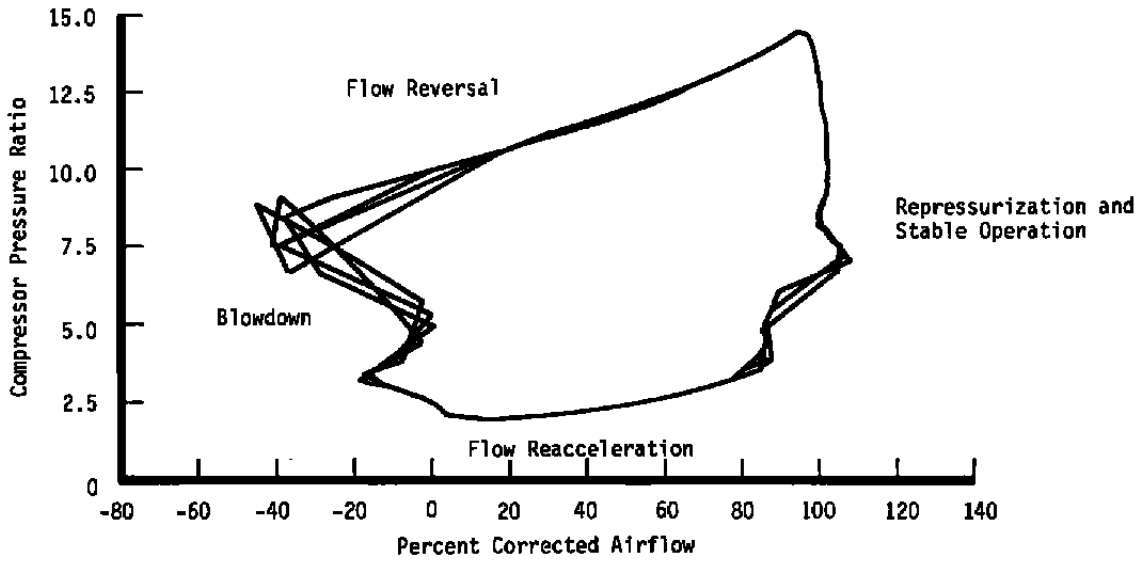

Figure 40. Model compression system performance trajectories during surge at 100-percent speed with heat release in the combustor.

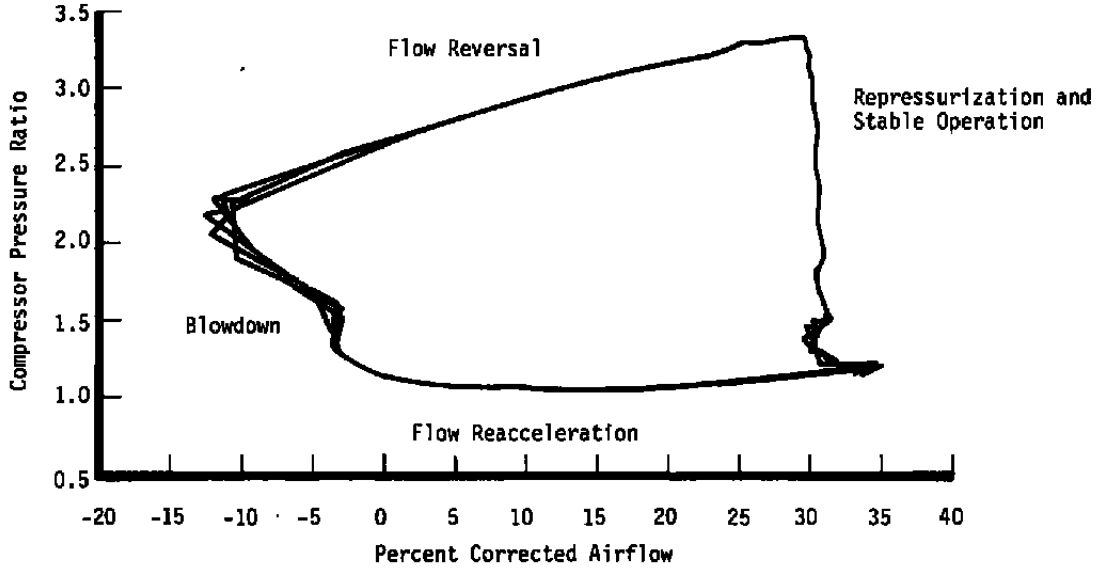

Figure 41. Model compression system performance trajectories during surge at 70-percent speed with combustor blowout and reignition occurring.

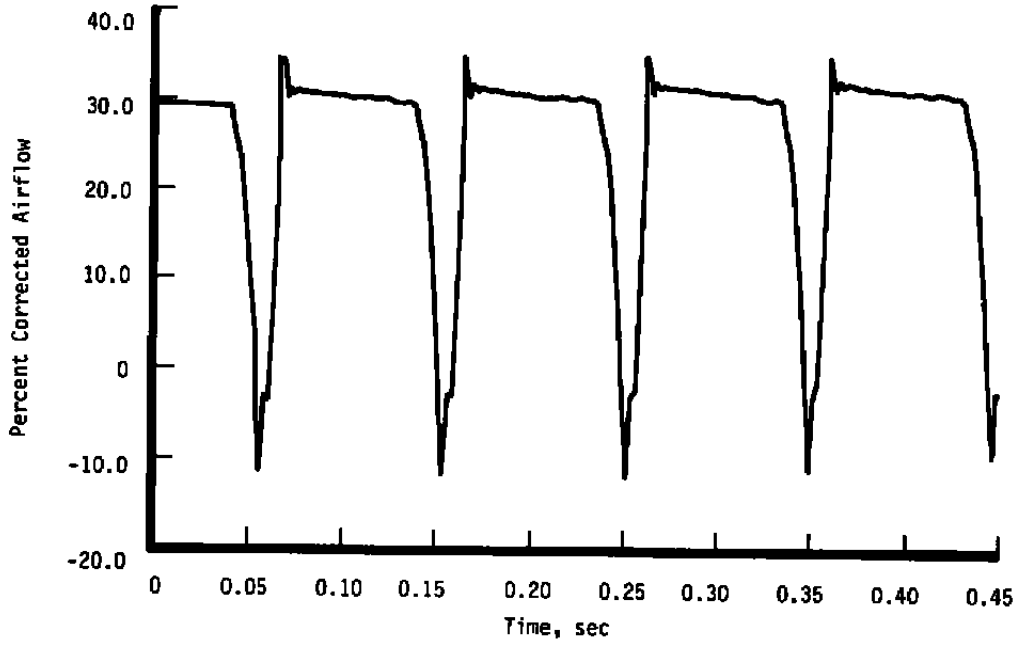

a. Corrected airflow

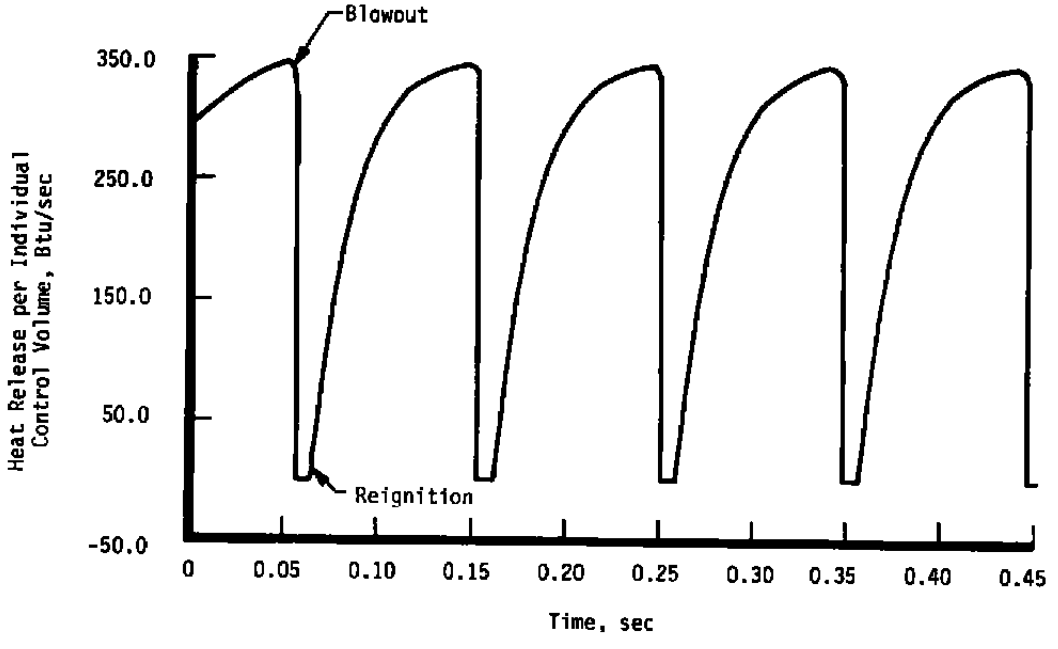

b. Control volume heat release

Figure 42. Combustor/compressor interdependence during surge events.

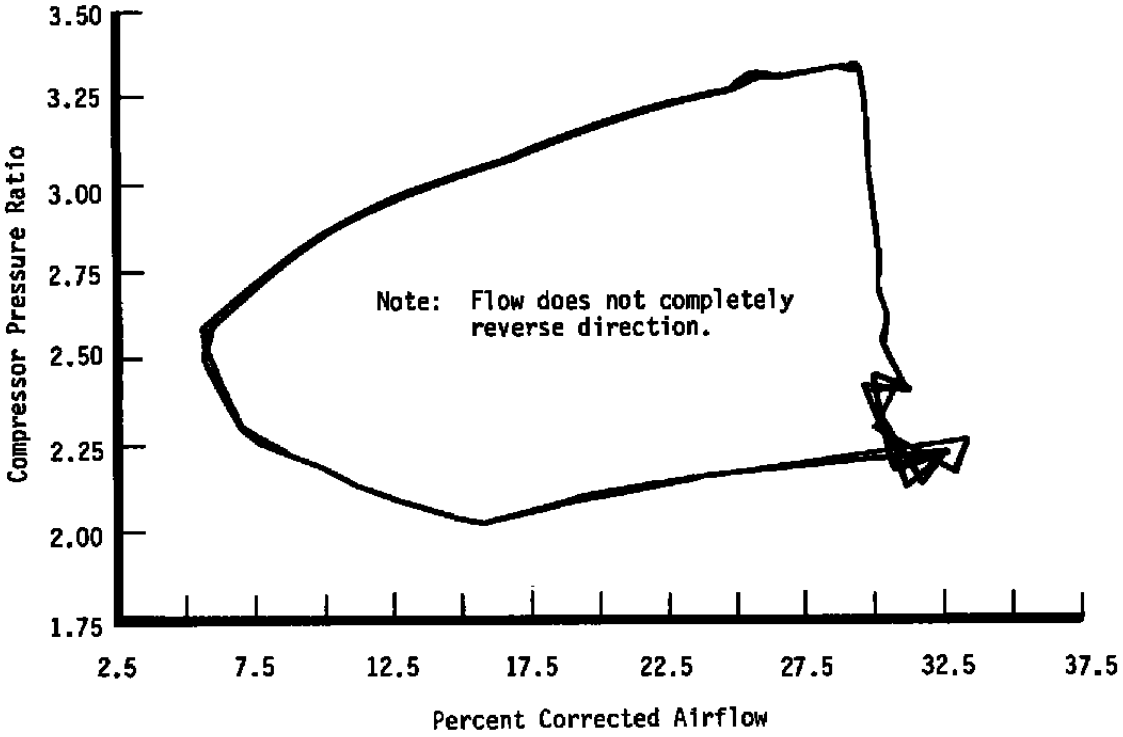

Figure 43. Model compression system performance trajectories during surge at 70-percent speed, continuous combustion in the combustor.

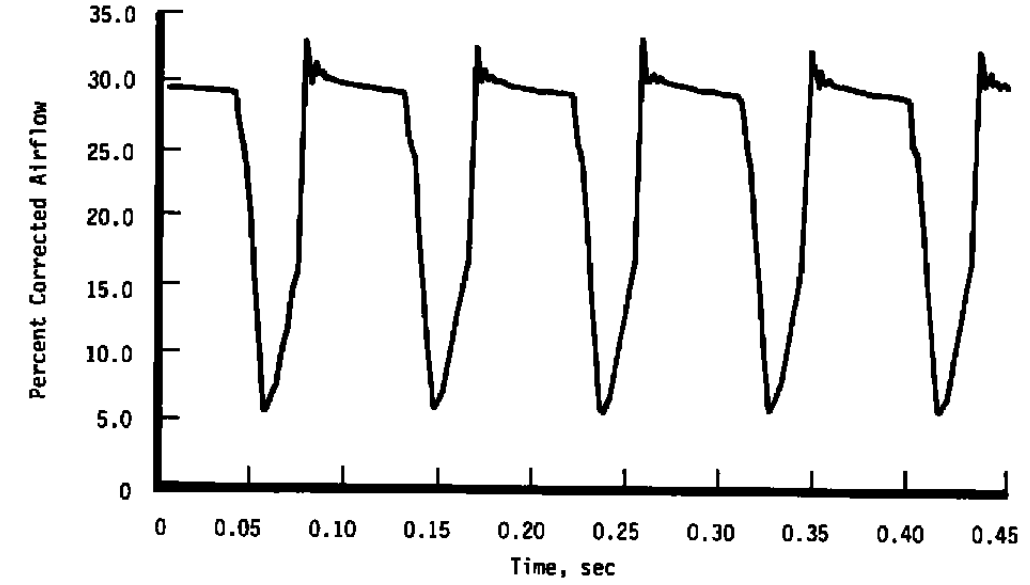

a. Corrected airflow

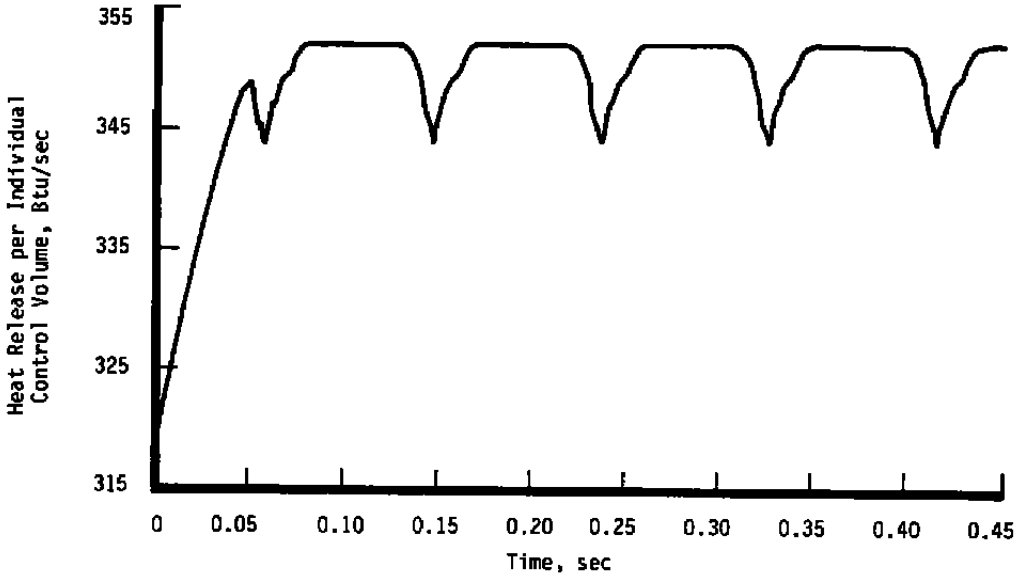

b. Control volume heat release

Figure 44. Model surge cycles with continuous combustion at 70-percent corrected speed.

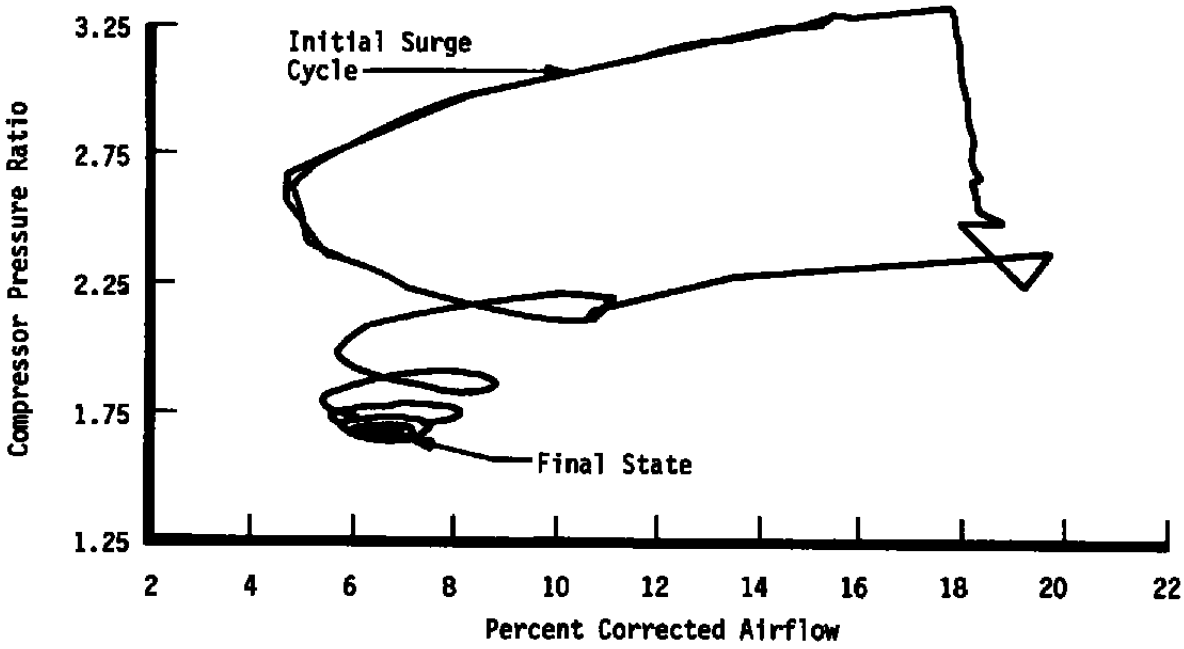

Figure 45. Model compression system performance trajectories during rotating stall at 70-percent speed, continuous combustion in the combustor.

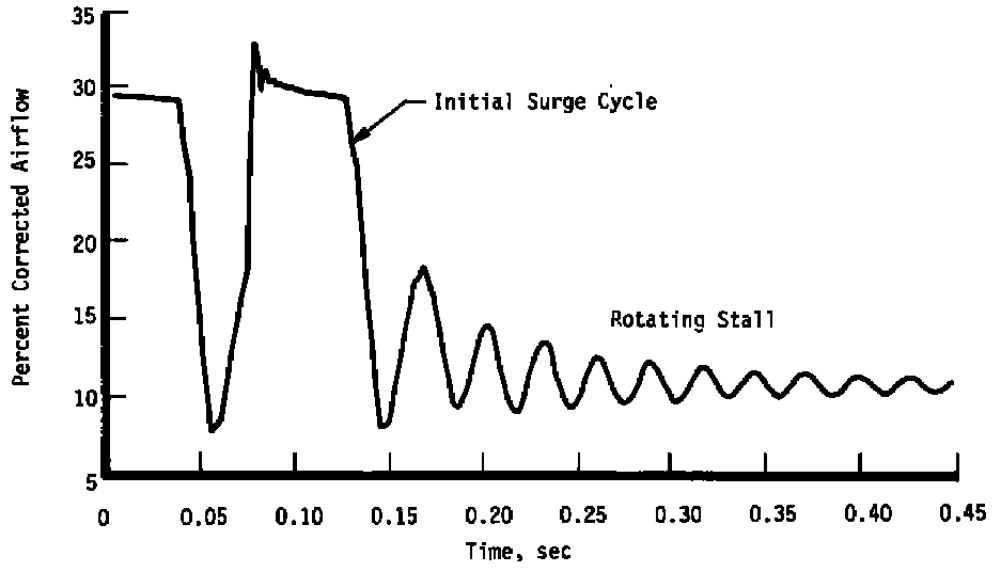

a. Corrected airflow

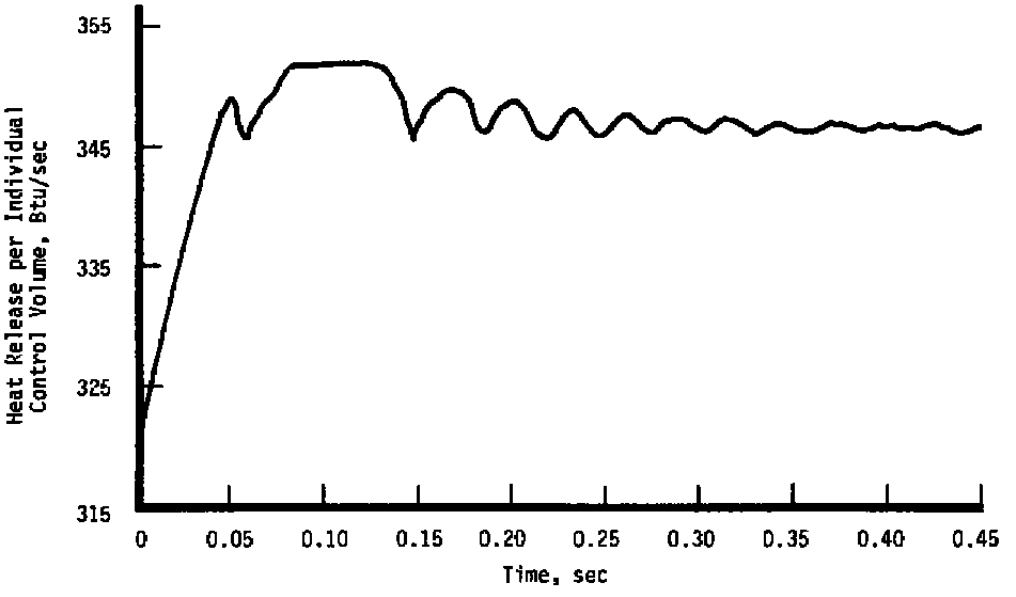

b. Control volume heat release

Figure 46. Model rotating stall with continuous combustion at 70-percent corrected speed.

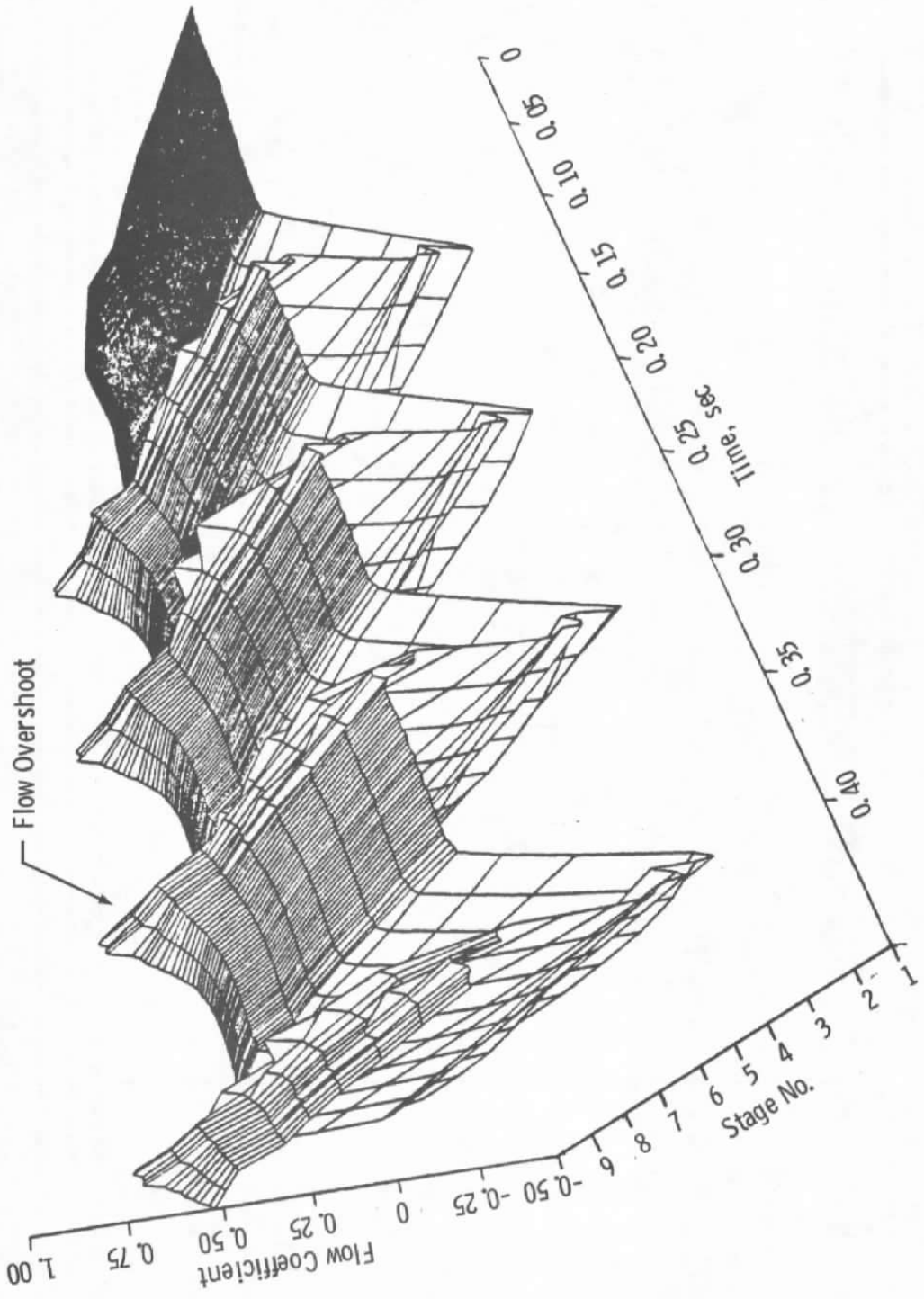

Figure 47. Stage flow coefficient during surge cycles at 100-percent speed.

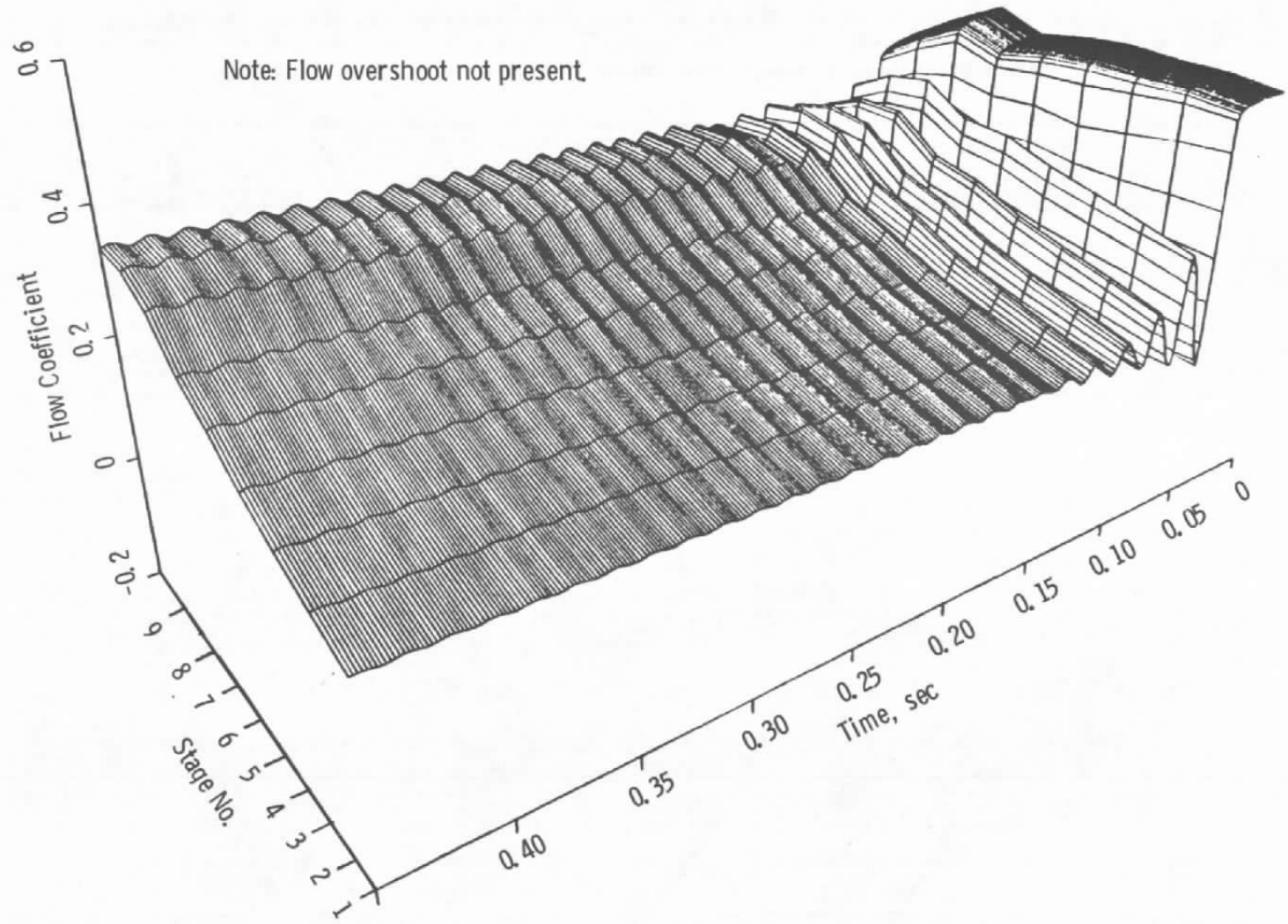

Figure 48. Stage flow coefficient during rotating stall at 70-percent speed.

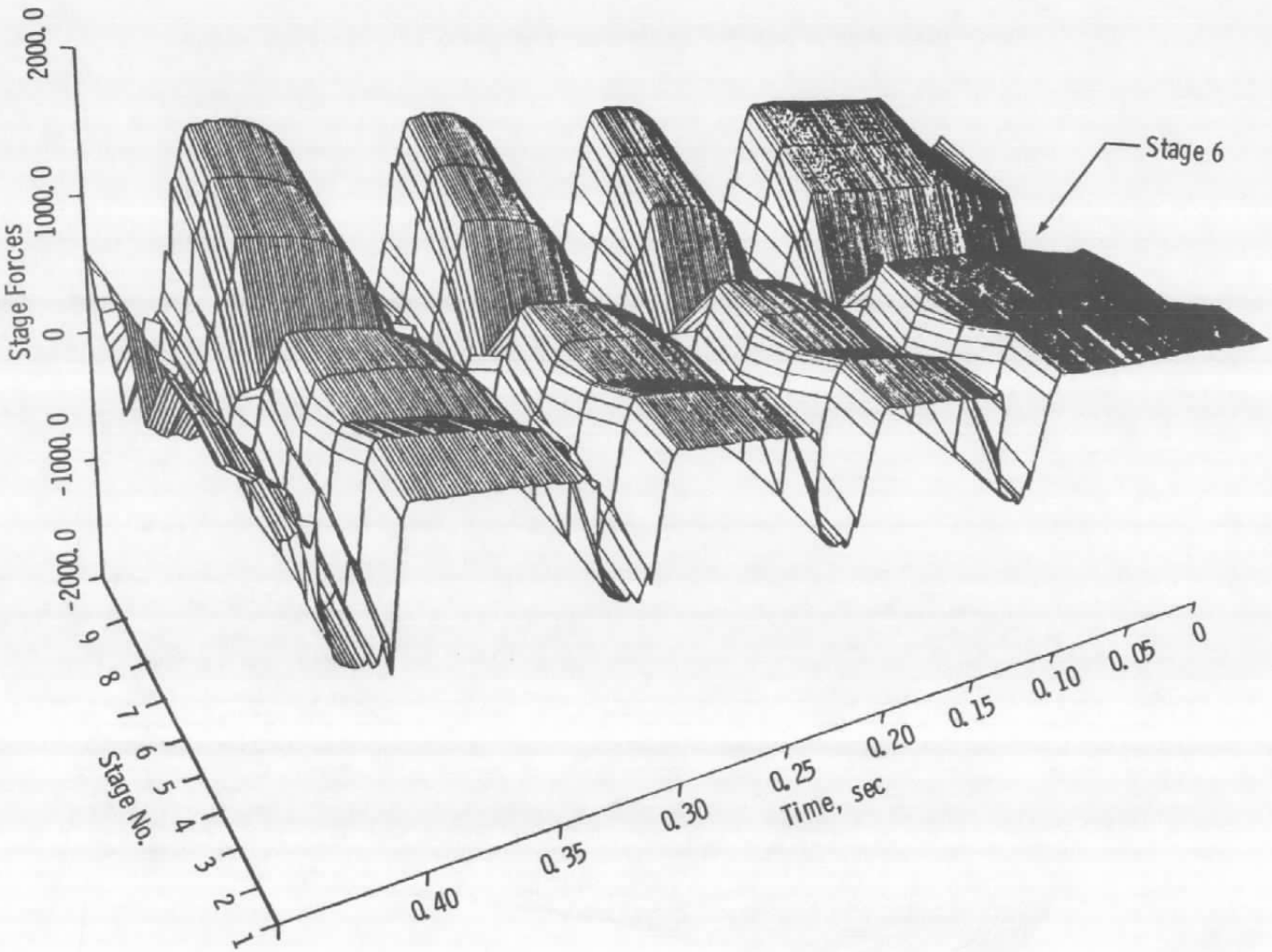

Figure 49. Compressor dynamic stage forces during surge cycles at 100-percent speed.

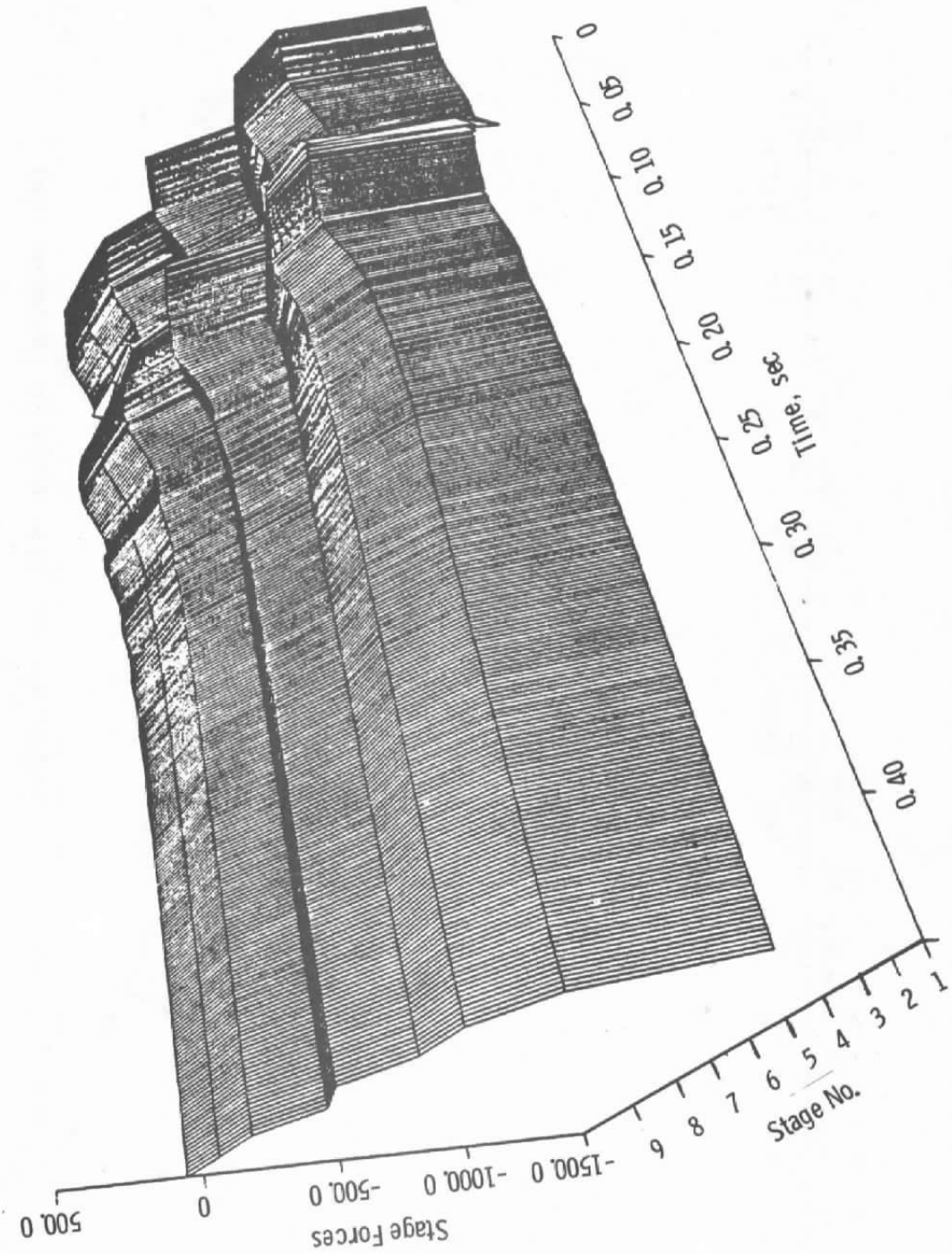

Figure 50. Compressor dynamic stage forces during rotating stall at 70-percent speed.

NOMENCLATURE

A	Area
a	Acoustic velocity
B	Greitzer's "B" parameter [see Eq. (1), p. 11]
c_p	Specific heat at constant pressure
c_v	Specific heat at constant volume
E	Energy function
e	Internal energy
F	Force of compressor blading and cases acting on fluid, including wall pressure area force
F_B	Force of compressor blading
f	Frequency
f	Friction factor
far	Fuel-air ratio
H	Total enthalpy
IMP	Impulse function
k	Coefficient of heat conductivity
L	Compressor length
M	Mach number
$\dot{M}_T$	Mass flow function based on total condition
MOC	Method of characteristics

N	Compressor rotor speed
P	Pressure
PR	Total pressure ratio
Q	Rate of heat addition to control volume
R	Gas constant
SW	Rate of shaft work
T	Temperature
t	Time
TR	Total temperature ratio
U	Generalized notation for Navier-Stokes equations or wheel speed
u	Axial velocity
V	Generalized notation for Navier-Stokes equations or volume
W	Mass flow rate
X	A point along the x-direction
x	Axial coordinate

Greek Symbols

α	Angle of attack
γ	Ratio of specific heats
Δ	A difference
δ	Ratio of compressor entry total pressure to standard day, sea-level-static pressure

ϵ	Energy term in Navier-Stokes equations
η_{ad}	Stage adiabatic efficiency
θ	Angular location, ratio of compressor inlet total temperature to standard day, sea-level-static temperature
λ	Second coefficient of viscosity
μ	First coefficient of viscosity
ϱ	Density
σ	Normal stress
ϕ	Flow coefficient
τ	A time constant
ψ_1,ψ_2,ψ_3	Terms in compatibility equations which account for frictional and energy dissipation terms
ψ^P	Stage pressure coefficient
ψ^T	Stage temperature coefficient (stage loading parameter)

Superscripts

C	Corrector solution
P	Predictor solution

Subscripts

actual	Pertaining to actual measured value
avg	Average value
B	Pertaining to bleed flow

c	Compressor
comb	Pertaining to combustor
core	Pertaining to core engine/high-pressure compressor properties
design	Pertaining to design value
E1	Intersection of characteristic curve with previous time solution, exit boundary
E2	Intersection of streamline curve with previous time solution, exit boundary
entrance	Control volume entrance plane
I	Intersection of characteristic curve with previous time solution, inlet boundary
i	Spatial location
initial	Initial value
ISEN	Pertaining to isentropic flow conditions
max	Maximum value
min	Minimum value
new	New time
old	Old time
P	Plenum
S	Static condition
stall	Value at stall
T	Total conditions
total	Pertaining to total geometric or thermodynamic properties
x	Axial component or direction